Formation and characterisation of electroanalytical junctions

French, Robert

Award date:
2010

Awarding institution:
University of Bath

Formation and Characterisation of Electroanalytical Junctions

Robert William French

A thesis submitted for the degree of Doctor of Philosophy
University of Bath
Department of Chemistry
January 2010

No man is so foolish but he may sometimes give another good counsel, and no man so wise that he may not easily err if he takes no other counsel than his own. He that is taught only by himself has a fool for a master.

Hunter S Thompson

If you are young and you drink a great deal it will spoil your health, slow your mind, make you fat - in other words, turn you into an adult.

P. J. O'Rourke

Abstract

Electrochemical and microscopy techniques are used to form and investigate novel nanojunctions. Initial investigative work is carried out using junction arrays formed via layer-by-layer deposition techniques. In depth studies into novel paired gold junction electrodes formed using simple electrochemical deposition techniques are provided along with subsequent characterisation and application as electrochemical sensors.

The aims of the project are to create a novel method of junction electrode production, which consists of a simple single step deposition technique. These junctions should be easily produced with variable sizes between the electrodes reaching down to the nanometer scale.

The study will include information into effects of gap size within the junction electrodes as well as full characterisation and applications as electrochemical sensors. Finally, a novel multi-phase junction experiment will be demonstrated using paired triple phase boundary ion transfer.

Acknowledgments

There are many people who deserve acknowledgment and thanks for all the help and support given throughout this project.

First, I would like to thank the Innovative Electronic Manufacturing Research Centre (IeMRC) for the financial support of the project. Particular thanks go to Martin Goosey for his continual support and discussions over the past few years.

My thanks also to all those who have worked in the lab with me over the past few years for making this project both achievable and enjoyable. Special thanks must go to Elizabeth Milsom, Stuart MacDonald and Mike Bonné who made the initial confusion of a new project with new equipment so much easier, and for all the entertaining evenings spent outside of work. I would also like to thank Charlie, John, Andrew, Anne and Liza for keeping the lab a pleasurable place to work.

Acknowledgments must also go out to all the people who have helped with my published research papers over the past few years, thanks for your support and input without which this project may not have been as successful as it has been.

Thank you to Misha (Mikhail Yu Vagin) and everyone from the Lomonosov University Moscow, for allowing me to work with you in March 2009, the experience was amazing and one I will never forget.

I would also like to raise a glass to everyone else from the Chemistry Department at Bath, especially to Andy Kirk, Alberto Fattori, Cathy Frankis, Nathan Hollingsworth and Claire Thompson for all the fun and beers over the past few years, you have all been awesome.

A huge thanks to everyone who has kept me sane the past few years from outside the Chemistry Department for their continual support which has helped me complete this project, including the love and support from my family, Mum, Dad, Stephen, Emma as well as Grandparents and Aunts and Uncles.

Thanks to all of my housemates from Bath who over the years have always been there when it was all going wrong and have always seemed to be able to produce the emergency bottle of rum when needed.

And massive shout to all the Gadgets, without your help I think my liver may have survived longer but life just wouldn't be as fun.

Finally and importantly the largest thank you and acknowledgment must go to Frank Marken my supervisor, whose knowledge, support and friendship never ceased to amaze me, without Frank this project would not have been possible and I hope I can one day repay the favour.

There have been so many people to thank over my years at Bath, I wish I could have named all of you here but the list may have ended up longer than my thesis, but thank you all.

Contents

1. Introduction

Contents

Abstract

In this chapter an introduction is given into the background of paired electrode systems similar to those used within the project. A more in-depth review of generator-collector mode electrochemistry and junction fabrication methods is given. The electrochemical theory used within the project is presented and developed. The aims and overall strategy of the project are briefly highlighted discussed.

Chapter 1: Introduction

1.1. Paired Electrode Systems

Paired electrode systems are a rapidly expanding field within electrochemistry. Most systems use two working electrodes, or an array of electrodes, polarised at different potentials. This methodology is often referred to as generator-collector mode electrochemistry.

In generator collector mode one electrode, the generator, drives the reduction or oxidation of a species in solution. The second electrode, the collector, is set to a potential, which will reverse the process occurring at the generator. The effect created by this mode of experimentation is the formation of a steep concentration gradient between the paired electrodes. This large concentration gradient has the advantage of increased flux of material between the two electrodes, and subsequently greatly amplified currents. [1] Further advantages of a generator-collector mode experimentation include

(i) The absence of capacitive current components within the collector signal,

(ii) Enhancements of current responses due to 'feedback' between the paired electrodes. [2]

Generator-collector systems can therefore easily gain both kinetic and mechanistic information about the redox species of interest. [3] Any paired electrode systems therefore allow investigations into the determination of diffusion coefficients via "time-of-flight experiments" originally performed and developed by Anderson and Reiley. [4] A final application and benefit enabled by paired electrode chemistry is to allow redox processes and short lived reaction intermediates from multi-step electrode reactions to be monitored. [2,5]

Within generator-collector mode experimentation the collector efficiency is of highest importance. Collector efficiency is a simple ratio of the current detected at the collector relative to the generator electrode and is a function of the geometry of the electrochemical cell and the rate of mass transport of the species between the electrodes. The higher the collector efficiency the greater the electroanalytical applications of the system. [6]

Classical generator-collector systems include double-channel electrode [7,8], rotating disc electrode [9,10,11] (see Chapter 1.2) and less commonly wall-jet electrode systems. [12] These systems are considered hydrodynamic systems, as the dimensions of the generator and collector electrodes and/or the separation between then are often on the millimetre scale. Therefore stagnant, diffusion-only conditions exist within these dimensions and lead to relatively large transit times between the two electrodes reducing the collector efficiency, introducing the need for 'flow systems' to be combined with the paired electrode configuration. [3] Hydrostatic systems can be created by producing paired electrodes with smaller separation, as lateral diffusion over small distances maintain spontaneously high fluxes between the electrodes, paired electrodes presented within this thesis will be based on hydrostatic generator collector mode systems.

1.2. Current Hydrodynamic Generator-Collector Mode Electrodes

1.2.1. Flow Channel Generator-Collector Electrodes

Electroanalytical sensing via generator-collector mode electrochemistry has gained large interest within many diverse fields of study. The mode works by utilising the fact that the "generator" electrode, where the reaction is initiated, can determine kinetic and/or mechanistic information. Redox active intermediates can then be detected using a second "collector" electrode, which is held in close proximity to the generator. [13]

Several examples of generator-collector based electrodes employed within flow channels have been studied. These studies require two electrodes embedded within an insulating channel through which and electroactive solution can flow.

The simplest arrangements of the electrodes is that of a double channel electrode, in this case flat plane electrodes are placed in series within the flow channel. The electrodes can be positioned on the same channel wall or the more unconventional approach with the electrodes in series on opposite walls of the channel. [7] Both systems have been used to examine the nature of electrolytic processes, and to interrogate the electrode reaction

mechanism without the need for assumptions towards all species in the system having a common diffusion coefficient.

A development upon the double channel electrodes is the double tubular electrodes. These electrodes require an insulating tube as the flow channel with two cylindrical electrodes, in series, embedded within the walls. One advantage of this system is the relative ease of fabrication formed by layering metal sheets or foil between layers of insulating material and then punching or drilling the flow channel through the layers. These systems help provide large amounts of information into different flow rates and flow effects. [8]

1.2.2. Ring-Disc Generator-Collector Electrodes

Ring-disc electrodes consist of a single disc electrode surrounded by a single ring electrode and are gaining support over typical microband and microarray electrodes despite more complex methods of formation. These methods of formation include lithography, [9] deposition of a conducting paint onto the walls of a pulled glass capillary electrode, [10] and vapour deposition, of which there are two types, chemical vapour deposition (CVD) [11] and physical vapour deposition (PVD). [14]

Ring-disc electrodes have two advantages over microband generator-collector electrodes these are their radial symmetry and the fact they contain discs of varying shapes. Radial symmetry simplifies the positioning of the sensor, as there is no preferred axis within the sensing unit. A different shape for the two electrodes allows versatile measurements, due to the difference in the edge to area ratios between the ring and the disc. Additionally to these facts if a micro ring-disc electrode is used all additional advantages of a microelectrode including high signal to noise ratio and enhanced mass transport, are retained. [15]

Ring-disc electrodes in generator-collector mode have been used to study reaction kinetics, [16] where micro ring-disc electrode's have been used to study mass transport effects such as diffusion in scanning probe electrochemical microscopy (SECM) [11] and convection with impinging jet flow. [17]

1.3. Current Hydrostatic Generator-Collector Mode Electrodes

1.3.1. Microband / Microarray Generator–Collector Electrodes

Microelectrode devices or interdigitated arrays composed of at least one pair of parallel electrodes in a side-by-side arrangement can be used to gain generator-collector signals. Unlike rotating ring-disc electrode, discussed above, forced flow conditions are not necessary, as lateral diffusion over small distances maintain spontaneously high fluxes between the electrodes. [18,19]

These electrodes are often used in time-of-flight (TOF) experiments. Time-of-flight experiments are used in many technologies, TOF mass spectrometers and TOF flowmeters for example. Time-of-flight procedure consists of three stages; (i) creation of entities from a generator source, (ii) their subsequent transit through the length of the flight path and (iii) their detection. Initial work into electrochemical time-of-flight using the generator-collector methodology was introduced by Murray et. al. [20] These microband electrodes have also been used in the investigation of diffusing redox species as well as for diffusive electron transport in medias of interest. [21]

Interdigitated Array (IDA) microelectrodes work in a similar way with closely spaced generator-collector electrodes in a side by side configuration, a sensitive (collector efficiencies Ca. 85 %) was developed by Tomcik et. al. [22] using an IDA for the determination of electroactive species capable of quantitative and fast reaction within a generator-collector electrode, where the collector serves as an amperometric detector, as it will be used in this project.

1.3.2. Modified Single Disc Generator-Collector Electrodes

A final type of generator-collector electrode can be formed by chemically attaching molecular probes onto the surface of an electrode. Henstridge et. al [13] were able to measure changes in local pH during a redox reaction by using pH sensitive molecular probes attached to a carbon electrode, this is an example of a zero-gap generator-collector system made using a single macroelectrode as the generator and the molecular pH probe attached to the surface as the collector. This system has allowed highly sensitive monitoring of pH changes at the electrode surface during redox reactions.

Within this project paired gold junction electrodes with a separation of micrometer to nanometer scale, will be used in generator-collector mode allowing for hydrostatic conditions, these junctions will then be used within electroanalysis experiments for several different sensing applications.

1.4. Current Methods of Nanojunction Paired Electrode Fabrication

1.4.1. Mechanical Alignment

In the past few years Garcie et al. [23], have been working on the conductance properties of nanocontacts showing conductance quantization. To do this they devised an experiment in which two nickel wires ended by rounded tips are placed in contact facing each other, a force is applied to the end of the wires until a current flows between the nanocontact formed at the tips when a bias is applied, these wires are then tightly bound within a Teflon tube using a resin giving rigidity to the sample.

Then by inducing a magnetic field along the axis of one wire, and simultaneously an oscillating square current alternates the orientation of the magnetic field in the second wire, a simple oscilloscope on the first wire will show large fluctuations in current representing the fact that the second wire is generating parallel and anti-parallel states of magnetisation giving rise to magnetoresistance. It is easy to see how by adding a thin conduction layer to the surface of one of the metal wires the same method could be applied to bring the wires together once touching the conducting surface could be removed leaving a nanojunction. However several problems exist with this methodology, the first is the approach could easily break apart the tip and cause destruction of the nanojunction, the second is the need to seal the wires in a tube would reduce the ease with which these junctions could be used as a sensor.

Carrara et al. [24], have approached nanojunctions and contacts by depositing monolayer films upon flat graphite electrodes to gain Schottky interfaces, a second electrical contact was then realized by approaching the monolayer film, by a 1-D piezo-electric actuator, with a sharp tip electrode at nanometric distances creating tunnelling barriers, with the

positioning of the electrode controlled by a feedback system. Other groups have used similar methods with AFM probes replacing the piezo-electric actuators. [25] Several problems exist with these junctions and the first is that often the sharp tipped electrode will penetrate into the film. Again, once aligned in this state the monolayer could be removed resulting in a nanojunction.

Nanojunctions have also been made by two hanging mercury drop electrodes (HMDEs) being mounted coaxially, one above the other, in a custom stand. In each electrode a stainless steel rod is driven by a micrometric screw to create a mercury drop of desired size at the tip of a glass capillary, these tips are then aligned using an X-Y-Z micrometer stage [26,27]. A secondary method using HMDE's is to mount the two droplets side by side as shown by John Porter et al. However these junctions have issues with mechanical stability. [28]

A third method is to pull two contacts apart instead of together, this has been demonstrated with metal contacts [29], where the nanowire break shows a few well defined conducting steps. However Versluijs et. al. [30] have demonstrated that by breaking the contact between two $(La_{0.7}Sr_{0.3})MnO_3$ crystals they can gain 20 or more conductance steps occurring close to integral multiples of $G_0 = 2e^2/h$, which is in agreement with Landauer's formula used to compute current in nanoscale devices. To form one of the junctions two crystals (ca. 5 x 3 x 2 mm^3) are placed in mechanical contact and then pulled apart using a relay or piezo crystal, whilst continuously monitoring the resistance of the contact. A small bias voltage of some tens of mV is applied between the electrodes and the current is measured with an I-V converter, the current signal is then fed into an 8-bit digital storage oscilloscope. However these junctions are very temporary, often lasting only fractions of a second, again this is a flaw for commercial sensor applications.

1.4.2. Etching Techniques

Simple photolithography techniques combined with electromigration has allowed Naitoh et. al. [31] to form nanojunctions. This is done by depositing 1000 nm thick resist upon a silicon oxide/silicon wafer, these are then patterned using typical photolithographic methods. A metal layer is then deposited upon this pattern at angle θ_1, +15°, a second lithographic process is run with a mask of slits, ca. 2 μm, orthogonal, to that of the first

layer. A second metal deposition on the opposite side of θ_1, at -15° is deposited due to the resist and angles once lift-off is carried out a metal nanowire between the two metal deposits exists. Next by using electromigration, the atomic motion in a conductor subject to large current density, used to break gold nanowires in a controllable and self-limiting fashion. The breaking process consistently produces two metallic electrodes whose typical separation is about 1 nm. [32] Other groups have used similar methods with varying nanowire fabrication techniques and feedback loops. [33]

A second method of etching nanojunctions is that of focused ion beam (FIB) etching, in this process a metal layer is evaporated onto an insulating layer upon the metal a layer of nitrocellulose and germanium are deposited for the lift of processes later, focused ion beam, in this case 30KeV Ga+ with a beam current of ~20 pA and beam diameter of 10 nm was used to etch a narrow groove within the metal layer, whilst using resistance feedback data to monitor the width of the groove. [34]

1.4.3. Electrochemical Etching and Deposition ELENA

Using a copper nanowire with conductance quantised it is possible to electrochemically etch away the last few atoms in the atomically thin area of the wire resulting in a small nanogap this study was proven by He et. al. [35], using conductance feedback loops to show the step between ballistic electron transport and tunnelling currents, it is then possible to re-deposit some extra copper form solution reducing the gap size. This simple methodology has been adapted and used by many groups. [36,37,38] However many rely on external feedback loops and additional lithographic steps and procedures. The size of the junction electrode's are often very small, often nanowires, making general sensing applications complicated. [39]

1.5. Electrochemical Theory

1.5.1. Electrochemical Equilibrium

Unlike a chemical equilibrium, electrochemical equilibrium contains not only the balance of chemical potentials but also that of charge or electrical energies. A text book example of

an electrochemical equilibrium is that of a solution containing potassium hexacyanoferrate (II), $K_4Fe(CN)_6$, and potassium hexacyanoferrate (III), $K_3Fe(CN)_6$, to this solution an inert wire is added (the electrode), such as platinum.

At the wire surface the equilibrium below (Equation 1.1) is set up between the two ions and the electrons within the metal wire.

Equation 1.1

$$Fe(CN)_6^{3-}[aq] + e^-[m] \rightleftharpoons Fe(CN)_6^{4-}[aq]$$

For ease we can use a simplified model electrochemical reaction equation shown in Equation 1.2

Equation 1.2

$$X^-[aq] + e^-[m] \rightleftharpoons Y^{2-}[aq]$$

The rate at which the oxidised species donates its electrons to the metal is equivalent to the rate at which the reduced species accepts electrons from the metal. However as the process is a transfer of charge, a net electrical charge is induced upon both phases reliant on where the equilibrium lies. Despite this a charge separation will exist and is referred to as the potential difference between the solution and the metal, in other words an electrode potential has been set up between the metal and solution.

By considering the energy levels of the species, observations into how the electrode potential is formed can be made. First, consider the metal which has an electronic structure consisting of electronic conduction 'bands' in which, electrons are free to move about the solid, binding the positive cations together. The energy levels in these bonds form a continuum of levels which are filled up to an energy maximum called the Fermi level. The energy levels associated with the ions within the aqueous phase can be envisaged as discrete levels referred to as unfilled molecular orbitals.

Figure 1.1 shows that prior to electron transfer the Fermi levels in the metal are higher than that of the vacant orbitals in the ions. Therefore, it is energetically favourable for the electrons to move from the metal into the ion and thus reduce the ion. This electron

transfer creates a build up of positive charge upon the metal and an overall negative charge upon the solution phase in close proximity to the metal. Accordingly as Figure 1.1 represents energy levels measured by the number of electrons the Fermi level must be reduced, at the same time the energy levels within the solution phase must be raised. If this is followed to its logical conclusion eventually the Fermi levels and energy levels of the solution phase will eventually reach an average of the original two levels. When this occurs the previously mention dynamic equilibrium is reached where no further net charge change can occur, however at this point there is already a charge separation between the metal and solution phase and the electrode potential has been established upon the metal electrode.

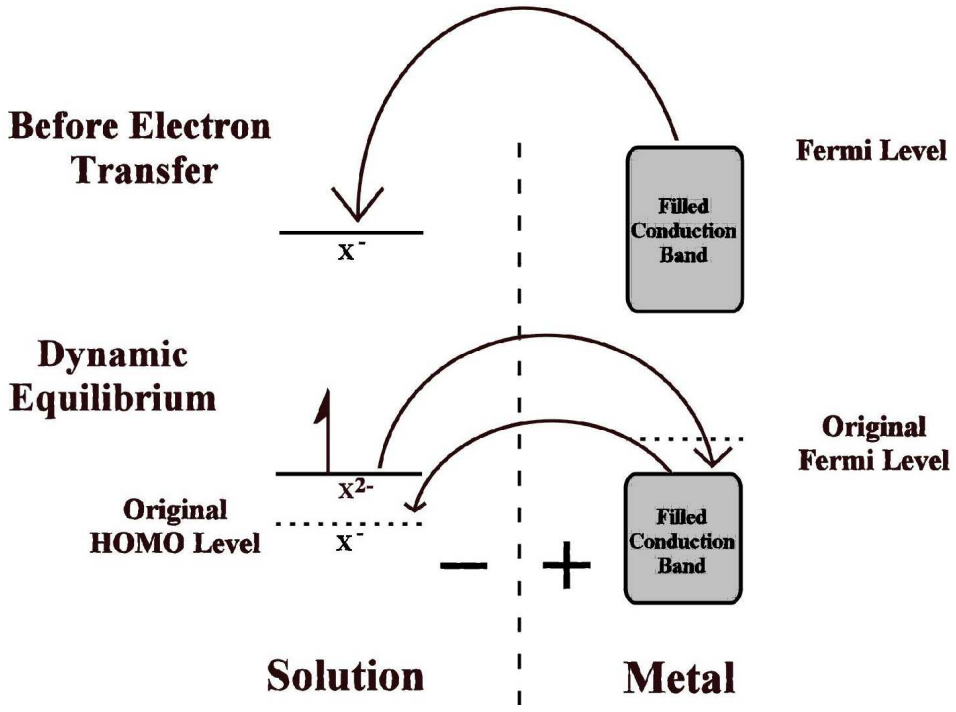

Figure 1.1 The energy levels for a metal wire immersed in solution showing electron movement in both the metal and ions, before electron transfer and at dynamic equilibrium. [40]

1.5.2. The Nernst Equation

Electrochemical equilibrium is the balance of both chemical and electrical energy within a system, this has resulted in an electrochemical potential $\overline{\mu}$, see Equation 1.3, for species *q*.

Equation 1.3

$$\overline{\mu}_q = \mu_q + Z_q F\phi$$

Where Z_q is the charge on molecule *q*, *F* is the Faraday constant (96487 Coulombs mol^{-1}) and ϕ is the potential of the particular phase in which species *q* is found. Thus the electrochemical potential of *q* contains two parts, the chemical potential of the species, μ_q, and the electrical energy is represented by the term $Z_qF\phi$. Due to this, further study of the electrochemical equilibrium is possible as, under conditions of constant temperature and pressure, the electro-chemical potentials of both the reactants and products will be balanced so with reference to Equation 1.2 at equilibrium Equation 1.4 can be written,

Equation 1.4

$$\overline{\mu}_{X^-} + \overline{\mu}_{e^-} = \overline{\mu}_{Y^{2-}}$$

By applying Equation 1.3 to this Equation 1.5 is derived,

Equation 1.5

$$\left(\mu_{X^-} - F\phi_S\right) + \left(\mu_{e^-} - F\phi_M\right) = \left(\mu_{Y^{2-}} - 2F\phi_S\right)$$

Where ϕ_S and ϕ_M are the electrical potential of the solution and metal phases respectively, therefore (ϕ_M - ϕ_S) is the 'driving force' of the electrochemical reaction (the difference between the Fermi level and vacant orbitals) consequently by rearranging Equation 1.5 to Equation 1.6,

Equation 1.6

$$F\left(\phi_M - \phi_S\right) = \mu_{X^-} + \mu_{e^-} - \mu_{Y^{2-}}$$

By then taking Equation 1.7, a law of thermodynamics which can be obtained from the fundamental laws and the definition of chemical potential and combining it with Equation 1.6 the expression Equation 1.8 is formed.

Equation 1.7

$$\mu_q - \mu_q^0 = RT \ln K_c$$

For Equation 1.7 describing species q, μ_q is the standard chemical potential of q, μ^0_q is the energy of one mole of q comparative to the standard concentration, R is the universal gas constant (8.315 J K^{-1} mol^{-1}), T is temperature and Kc the equilibrium constant.

Equation 1.8

$$\phi_M - \phi_S = \frac{\Delta\mu^0}{F} + \frac{RT}{F} \ln\left(\frac{[X^-]}{[Y^{2-}]}\right)$$

Where $\Delta\mu^0 = \mu^0_{X^-} + \mu_{e^-} - \mu^0_{Y^{2-}}$

This can be simplified to the more familiar version of the Nernst equation at constant temperature and pressure, due to the fact that a species gaining an electron is undergoing reduction and the species itself is referred to as the oxidised species (O), where the species losing an electron is undergoing oxidation and is referred to the reduced species (R). Therefore the above reaction can be simplified to Equation 1.9.

Equation 1.9

$$E_e = E^{o'} + \frac{RT}{nF} \ln \frac{[O]}{[R]}$$

In this equation E_e is the equilibrium potential of the electrode which is resultant from the standard electrode potential of the reaction, and $E^{o'}$ is the formal potential. [40]

1.5.3. Nernst Diffusion Layer

Within this project the Nernst diffusion layer approach will play an important role due to the hydrostatic nature of the generator-collector mode employed as well as in the approximation of junctions sizes. The diffusion layer arises from the fact that with any potential step experiment, at a planar electrode, a dependence of the current to the reciprocal square root of time can be observed. Over longer times however due to natural convection the experimentally measured current will tend to an approximate steady state

rather than following the theoretical model which predicts the current converging to zero as predicted by the Cottrell equation.

This observation is consistent with the model shown schematically in Figure 1.2. In this model a bulk solution beyond a critical distance δ from the electrode is completely mixed, via 'natural convection', the movement of solution induced by density differences, resulting in the concentrations of electroactive species being maintained at a constant bulk value.

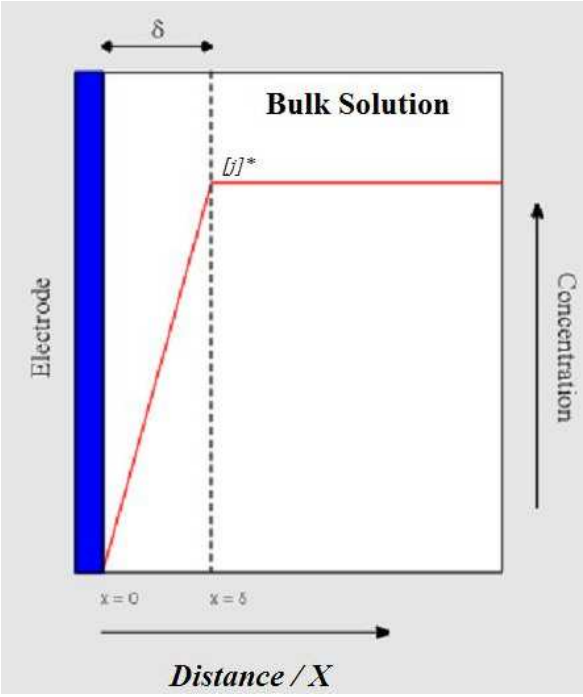

Figure 1.2 The Nernst diffusion layer model. [41]

As X is decreased, (closer to the electrode), natural convection is reduced as a result of the rigidity of the electrode and the operation of frictional forces and therefore cannot compete with the depletion of the redox species. This occurs in δ the region between X = 0 and X = δ and is commonly known as the diffusion layer, as this is the only region where diffusional transport occurs due to the fact it is the only region where concentration changes happen.

From Fick's first law the steady state diffusional flux is

Equation 1.10

$$j = D\left(\frac{\partial c}{\partial x}\right)_j = \frac{D[j]^*}{\delta}$$

Therefore the corresponding current can be written as

Equation 1.11

$$I_{ss} = \frac{nFADc^*}{\delta}$$

It is important to remember that this is a simplified model for the Nernst diffusion layer as the boundary between stagnant zone of diffusion and that of well mixed bulk solution is gradual. However the oversimplified model is a useful tool with experimental studies showing the diffusion layer at conventional electrodes to be in the order of tens to hundreds of micrometers.

1.6. Electrochemical Equipment

1.6.1. Potentiostat

It is possible to run voltammetric studies using only two electrodes, one as the *working electrode* (WE), the interface of interest under study, and the second employed as a *reference electrode* (RE), a standard to compare against, however this creates two problems.

The first is that current may be drawn through the reference electrode inducing chemical changes within the system. This will alter $(\phi_M - \phi_S)_{WE}$ in accordance with the Nernst equation.

The second problem is the magnitude of the *IR* term within Equation 1.12, which reflects the electrical resistance of the bulk solution between the reference and working electrodes

in this case *E* effects *IR* with unknown changes as well as altering $(\phi_M - \phi_S)_{RE}$ resulting in an uncontrolled signal. [40]

Equation 1.12 $$E = (\phi_M - \phi_S)_{WE} + IR - (\phi_M - \phi_S)_{RE}$$

Within this project electrochemical data will be gained using a three electrode cell, containing a reference, a working electrode and a *counter electrode* (CE), to pass the same current as that induced to flow through the working electrode are two separate electrodes, and a potentiostat, Autolab PGSTAT30 bipotentiostat system (EcoChemie, Netherlands). The potentiostat works by imposing a fixed potential, *E*, between the working electrode and the reference electrode, in this study a saturated calomel electrode (SCE) will be used and introduced in the next section. Reliant on the fact that the potentiostat draws negligible current through the reference electrode Equation 1.12 can be considered to be simplified to Equation 1.13.

Equation 1.13 $$E = (\phi_M - \phi_S)_{WE} - (\phi_M - \phi_S)_{RE}$$

Therefore as the reference is providing a constant value of $(\phi_M - \phi_S)_{RE}$ any changes of *E* are represented by the working electrode.

The third electrode, the counter electrode, is needed due to the fact that the imposition of the potential drop on the working electrode-solution interface, typically causes current flow, this is the aim of the study, to investigate the current through the working electrode-solution interface as a function of a controlled potential applied. The counter electrode serves to pass the same current as that induced to flow through the working electrode. Accordingly the potentiostat drives the counter electrode to whatever voltage is required to pass this current.

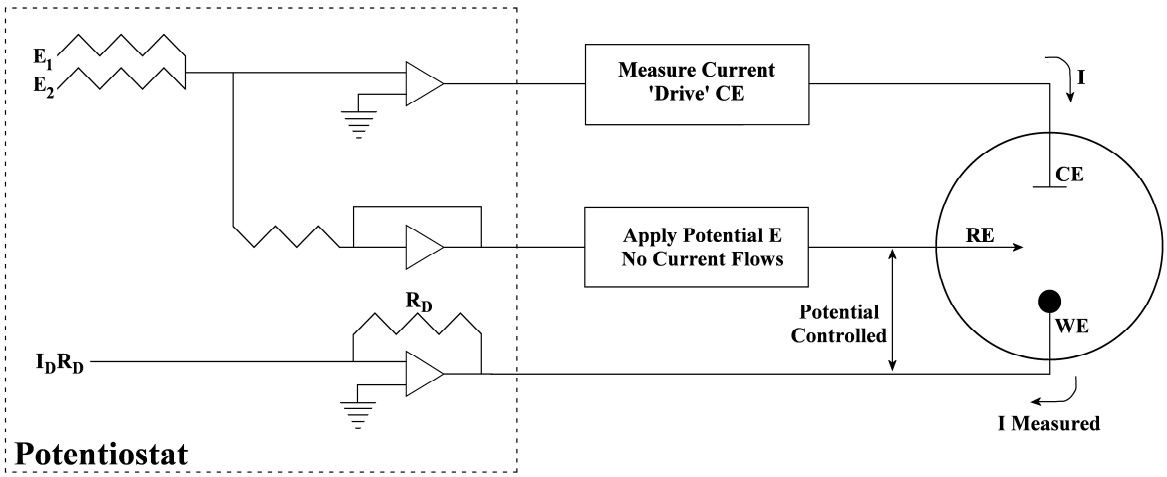

Figure 1.3 Schematic drawing showing a simplified circuit of a potentiostat. E1 and E2 represent applied input.

In this study a duel potentiostat will be used for the majority of experimentation, although they may contain alternative circuitry the roles of the three electrodes and the general theory behind each is the same as shown above.

1.6.2. Saturated Calomel Electrode

Within this study the reference electrode of choice is the saturated calomel electrode (SCE), the electrode consists of a column of mercury in contact with insoluble di-mercury (I) chloride (historically known as 'calomel'), both are then in contact with saturated aqueous potassium chloride.

The potential determining equilibrium $(\phi_M - \phi_S)_{RE}$ is formed at the triple phase boundary between the mercury, the di-mercury (I) chloride and the aqueous chloride solution.

Equation 1.14

$$\tfrac{1}{2} Hg_2Cl_2(s) + e^-(m) \rightleftharpoons Hg(l) + Cl^-(aq)$$

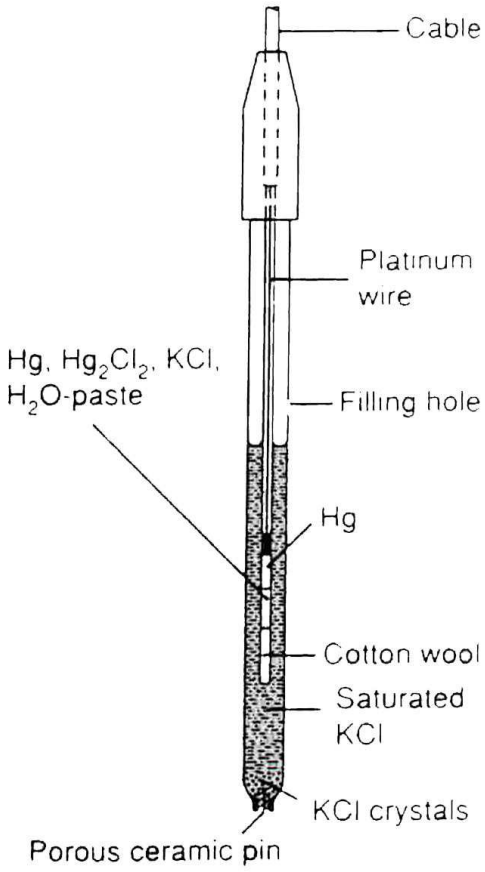

Figure 1.4 A saturated calomel reference electrode, (SCE). [42]

1.7. Voltammetric Techniques

1.7.1. Experimental Considerations

Electrochemistry is the study of electron transfer reactions between electrodes and reactant molecules typically in the solution phase. The three main techniques used in the study of these reactions are, linear sweep voltammetry, cyclic voltammetry and potential step chronoamperometry. The most common experimental set up is a three electrode cell (Figure 1.5), with second working electrode removed. As described before, within the cell is, a working electrode, reference electrode and counter electrode placed in a solution of the redox system under investigation and an inert background electrolyte. It is often

necessary to purge the reaction of oxygen using argon and the experiment is controlled electronically using a potentiostat (Figure 1.3) and personal computer for data recording.

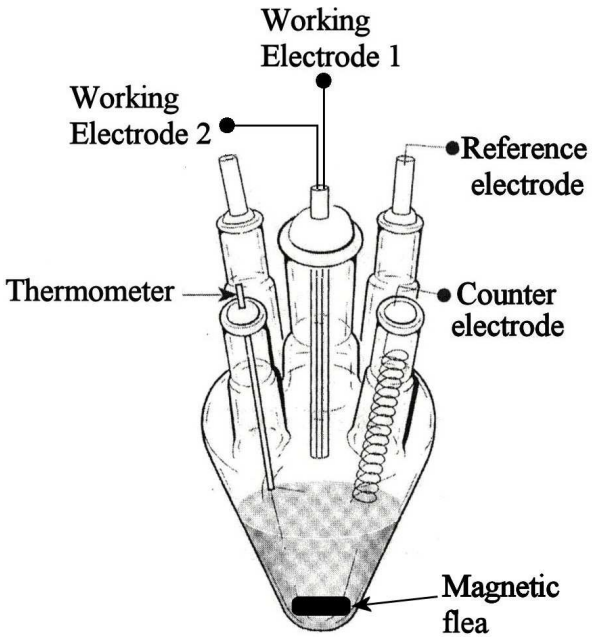

Figure 1.5 Demonstrating a typical electrochemical cell. [43]

1.7.2. Voltammetry

Linear sweep voltammetry and cyclic voltammetry quickly and easily provide large amounts thermodynamic and kinetic information about any system under investigation. The experiments are conducted in a three electrode cell with a stationary solution of electrolyte, ensuring that diffusion is the only method of transport for the active species to reach the electrode. Linear Sweep voltammetry changes the potential of the working electrode from a set value, E1 to E2, usually from a situation where electron transfer does not occur to one where it is driven rapidly. As the change in potential is set over a specific time, measurements of the change in current, over both, a potential and time range can be gained. Cyclic voltammetry is an extension of linear sweep voltammetry so that once E2 is reached, the direction of the sweep is reversed and the electrode potential scanned back to E1.

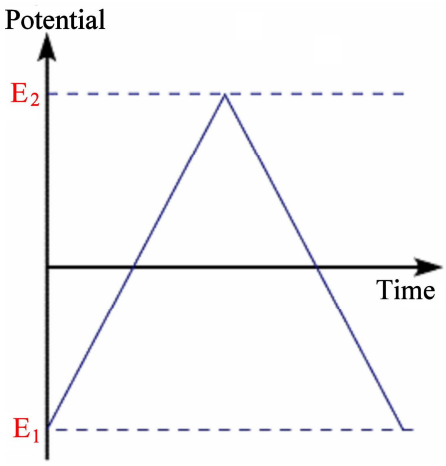

Figure 1.6 Variation of potential with time during a cyclic voltammetry experiment.

1.7.3. Voltammetric Response

The basic shape of the current response for a cyclic voltammetry experiment is shown below as well along with the basic redox reaction occurring, (Equation 1.15).

Equation 1.15 $O + e^- \rightarrow R$

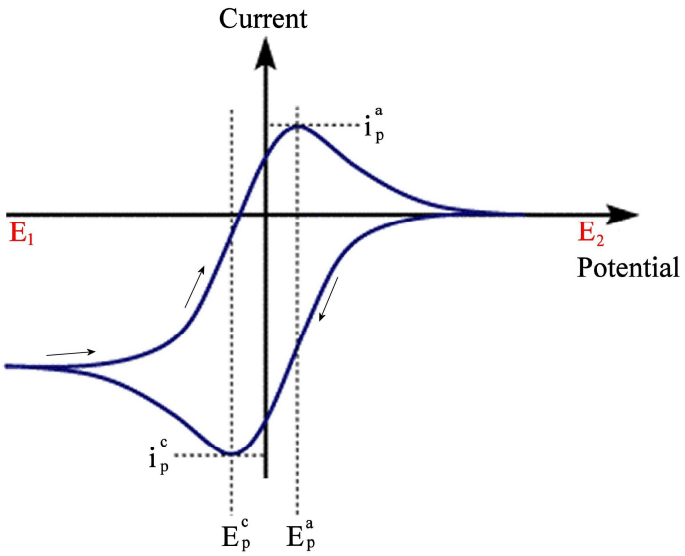

Figure 1.7 Cyclic voltammogram for reversible one electron reduction and oxidation.

At the start of the experiment the solution contains only the oxidised form of the redox couple (O) (see Equation 1.15) and initially no current is passed since the potential applied

is not great enough to induce electron transfer. As the redox potential for species O is reached, a current starts to pass which rises approximately exponentially with potential (time). As the species O is converted to R concentration gradients are set up for O and R and diffusion occurs along these gradients.

At the reduction peak the redox potential is sufficient to reduce almost all O that reaches the electrode surface. Although the equation states that the electrochemical rate constant, k_{red}, should continue to increase with increasing potential, the current flowing reflects both the k_{red} and the surface concentration of O, which is being steadily consumed and only replenished from the bulk by diffusion. After the peak current, the current detected is controlled by how much O can diffuse up to the electrode surface and so a fall in current is seen because as the experiment continues the depletion zone of O around the electrode becomes thicker increasing diffusion times.

Once the potential cycle is reversed, in cyclic voltammetry a current response in the opposite sense to the forward scan as R is converted back to O, assuming the reaction is fully reversible, is observed. For a fully reversible reaction the anodic and cathodic peak potentials are separated by $2.218\ \frac{RT}{nF}$ which in this case ~ 57 mV (25 ^{o}C) independent of scan rate. However for any system, reversible or not, the peak currents are directly proportional to the concentration of O and also the square root of scan rate. [44]

1.8. Electrodeposition

1.8.1. Kinetics and Mechanism of Electrodeposition

When an electrode is placed in an electrochemical cell with a flowing current the potential will remove the initial equilibrium, where the difference between the equilibrium potential (E) and the potential as a result of a current flowing (E(I)) is called the overpotential (η).

Equation 1.16 $$\eta = E(I) - E$$

For large negative overpotentials, the cathodic current density, *i,* (*i* = I/A where A is the surface area) increases exponentially, as the rate determining step is the rate charge transfer,

Equation 1.17 $$i = -i_0 e^{-\alpha n f \eta}$$

For large positive overpotential values, (anodic processes) the exponential relationship is given in Equation 1.18,

Equation 1.18 $$i = i_0 e^{(1-\alpha) n f \eta}$$

where α is the transfer coefficient, i_0 is the exchange current density and *n* is the number of electrons,

Equation 1.19 $$f = \frac{F}{RT}$$

Where F is the Faraday constant, R the gas constant and T the absolute temperature.

These relationships show that even a small change in the overpotential produces a large shift in current density. When the deposition reaction has a limiting factor, the transport of M^{z+} ions, a limiting or maximum current density is reached

Equation 1.20 $$i_L = \frac{nFD}{\delta} C_b$$

Where D is the diffusion coefficient of M^{z+}, C_b is the bulk concentration of M^{z+} in solution, δ is the diffusion layer thickness, n the number of electrons involved and F is the Faraday constant.

The overpotential is very important in electrodeposition as the type and quality of deposit depends upon relative values of the corresponding current density and the limiting current. [44]

1.8.2. Voltammetry of Electrodeposition

Voltammetry for the electrodeposition of gold from an alkaline cyanide bath is shown in Figure 1.8.

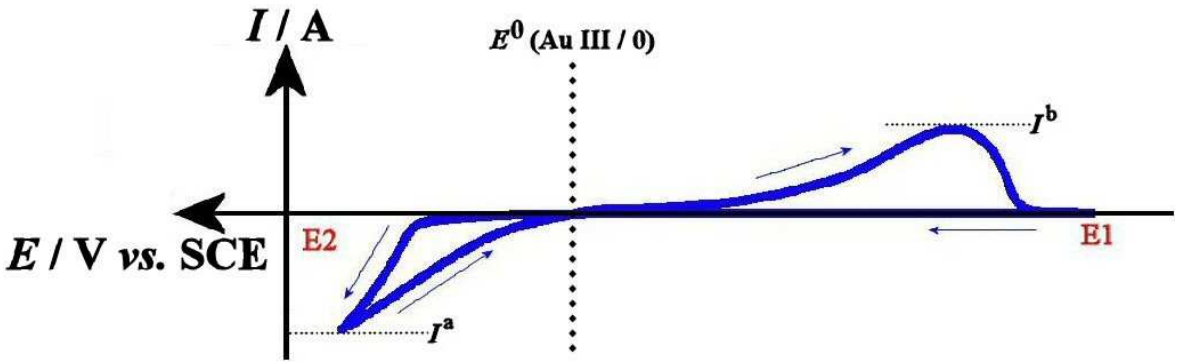

Figure 1.8 Typical cyclic voltammogram of electrodeposition of gold, onto 1 cm^2 of ITO, from an alkaline cyanide bath held at 55 °C with continuous agitation.

Initially at E1, the solution contains only the oxidised form of the metal ion, as with previous redox reactions in solution, initially no current is passed, as the potential applied is not great enough to induce electron transfer. At the reversible potential of the metal, (in the case of gold under conditions used within this project E^0(Au III/ 0) equals ca. –0.85 vs. SCE), a current immediately starts to flow, rising rapidly with potential (time) shown by current I^a.

Two distinct mechanisms for gold deposition occur during deposition from the alkaline cyanide bath. At lower currents or less negative potentials the first step is the chemical absorption of the [$Au(CN)_2^-$] complex (Equation 1.21).

Equation 1.21

$$\left[Au\left(CN\right)_2\right]^-\left[aq\right] \rightarrow \left(AuCN\right)\left[ad\right] + CN^-$$

Next the electron transfer step can then occur (Equation 1.22), this is the rate limiting step.

Equation 1.22 $$(AuCN)[ad] + e^- \rightarrow (Au^0CN)^-[ad]$$

The chemical desorption and crystallization is considered the final step in deposition (Equation 1.23).

Equation 1.23 $$(Au^oCN)^-[ad] \rightleftharpoons Au[lattice] + CN^-$$

The equilibria of the reduced absorbed species and deposited gold depends on the crystal orientation of the substrate and the presence of impurities, which affect the nucleation rate.

The second mechanism is the direct electroreduction of the gold cyanide ion at the electrode surface, this process occurs at more negative potentials, where a second gradient with more negative currents exists. [44]

Once the potential reaches E2 the cycle is reversed, the current becomes more positive and peaks at I^b, as the oxidised metal ion is re-formed, assuming the reaction is fully reversible. This is electrodissolution or 'stripping' and we see a removal of gold from the electrode surface.

1.9. Electrodeposition of Gold

1.9.1. Typical Deposition Baths

Gold was one of the first metals known to man and has been used for centuries, early work with the electrodeposition of gold is credited to Brungatelli in 1805. Due to the fact that it has the third best electrical and thermal conductivity at room temperature, electrodeposited gold has gained favour in the electronics industry. Other favourable properties of gold are its ductility and wear resistance, combined with its relative inertness and poor catalytic properties the high cost of gold can be justified and helps explain the steady increase of its use in industry.

The most important ion for electrodeposition of gold is gold (I) cyanide complex ($[Au(CN)_2]^-$). The stability of the complex is reflected in the shift of reduction potential from 1.71 V for Au (I) (aquo complex) to –0.611 V for the cyanide complex, due to this many plating baths are cyanide based. There are three main classifications: (i) the alkaline cyanide bath, (ii) acidic buffered cyanide baths and (iii) neutral buffered cyanide baths.

For this project many different plating baths were tested. However the work in this project has been carried out within alkaline cyanide baths. These baths operate at a high pH with an excess of free cyanide. In this project potassium cyanide is used as a source of free cyanide, as the cyanide released will not effect cyanide concentrations of the bath, thus preventing any Nernstian shifts in reduction potential. Excess cyanide also permits the use of gold anodes for the replenishment of the metal deposited from the bath Equation 1.25. Free cyanide also helps reduce any codeposition of some metals due to the fact that their cyanide complexes stability shifts their reduction potentials to values more negative than those used in gold deposition.

Equation 1.24 Cathodic equation $$\left[Au(CN)_2\right]^- + e^- \rightarrow Au + 2CN^-$$

Equation 1.25 Anodic equation $$Au + 2CN^- \rightarrow \left[Au(CN)_2\right]^- + e^-$$

With sufficient agitation and adequate gold content the cathodic current efficiency for the deposition of gold from an alkaline cyanide bath can be as high as 90 to 100 %. [44]

Several problems do exist with alkaline cyanide baths, such as their incompatibility with polymers such as photoresists due to their high pH and high cyanide concentrations. Health and safety implications are also a major issue as the bath is at a pH > 8.5 the equilibrium of Equation 1.26 is shifted to the right and free cyanide is stable in the bath leading to the health risk of accidental cyanide ingestion.

Equation 1.26 $$HCN[g] \rightarrow H^+ + CN^- \qquad pKa = 8.06$$

However the advantages of the cyanide bath and given the fact that the deposition process is both reversible and forms smooth deposits outweigh any disadvantages. [43]

In this project we hope to demonstrate a new method of producing cheap and robust paired electrode systems formed via new ELENA fabrication techniques with no pre or post lithographic stages required. The junctions will be formed via gold deposition and contain simple methodologies to alter the spacing between electrodes.

1.10. Reference

[1] D. Menshykau, F. J. Del Campo, F. X. Muñoz, R.G. Compton, *Sensors and Actuators B. Chemical*, 138, **2009**, 362-367.

[2] L. Rassaei, R.W. French, R.G. Compton, F. Marken, *Analyst*, 134, **2009**, 887-892.

[3] M.C. Henstridge, G.G. Wildgoose, R.G. Compton, *Langmuir*, 26, **2010**, 1340-1346.

[4] T.R.L.C. Paixão, E.M.Richter, J.G.A. Brito-Neto, M. Bertotti, *Electrochemistry Communications*, 8, **2006**, 9-14.

[5] B. Fosset, C. Amatore, J. Bartelt, A. Michael, R. Wightman, *Analytical Chemistry*, 63, **1991**, 306-314.

[6] W.J. Aldbury, M.L. Hitchman, "Ring-Disc Electrodes." *Clarendon Press Oxford*, **1971.**

[7] R.G. Compton, B.A. Coles, J.J. Gooding, A.C. Fisher, T.I. Cox, *Journal of Physical Chemistry*, 98, **1994**, 2446-2451.

[8] M. Thompson, R.G. Compton, *Journal of Electroanalytical Chemistry*, 583, **2005**, 318-326.

[9] Y. Chen, A. Pepin, *Electrophoresis*, 22, **2001**, 187-207.

[10] J.V. Macpherson, P.R. Unwin, *Analytical Chemistry,* 70, **1998**, 2914-2921.

[11] G. Zhao, D.M. Giolando and J.R. Kirchhoff, *Analytical Chemistry***,** 67**, 1995**, 1491-1495.

[12] A. Lindgren, F-D. Munteanu, I.G. Gazaryan, T. Ruzgas, L. Gorton, *Journal of Electroanalytical Chemistry*, 458, **1998**, 113-120.

[13] M.C. Henstridge, G.G. Wildgoose, R.G. Compton, *Journal of Physical Chemistry C*, 113, **2009**, 14285-14289.

[14] P. Liljeroth, C. Johans, C.J. Slevin, B.M. Quinn and K. Kontturi, *Analytical Chemistry,* 74, **2002**, 1972-1978.

[15] S.L.R. Harvey, K.H. Parker, D. O'Hare, *Journal of Electroanalytical Chemistry*, 610, **2007**, 122-130.

[16] W.J. Albery, M.L. Hitchman, "Ring Disc Electrodes", *Oxford University Press*, **1971**.

[17] M.A. Ghanem, M. Thompson, R.G. Compton, B.A. Coles, S. Harvey, K.H. Parker, D. O'Hare, F. Marken, *Journal of Physical Chemistry B,* 110, **2006**, 17589-17594.

[18] B. Fosset, C.A. Amatore, J.E. Bartelt, A.C. Michael, R.M. Wightman, *Analytical Chemsistry*, 63, **1991**, 306-314.

[19] B. Fosset, C.A. Amatore, J.E. Bartelt, R.M.M. Wightman, *Analytical Chemistry*, 63, **1991**, 1403-1408.

[20] B.J. Feldman, S.W. Feldberg, R.W. Murray, *Journal of Physical Chemistry*, 91, **1987**, 6558-6560.

[21] C.A. Amatore, C. Sella, L. Thouin, *Journal of Electroanalytical Chemistry*, 593, **2006**, 194-202.

[22] P. Tomcik, S. Jursa, S. Mesaros, D. Bustin, *Journal of Electroanalytical Chemistry*, 423, **1997**, 115-118.

[23] N. Garcia, M. Munoz, Y.W. Zhao, *Physics Review letters*, 82, **1999**, 2923-2926.

[24] S. Carrara, V. Bavastrello, M.K. Ram, C. Nicolini, *Thin Solid Films*, 510, **2006**, 229-234.

[25] T. Morita, S. Lindsay, *Journals of the American Chemical Society*, 129, **2007**, 7262-7263.

[26] R.L. York, P.T. Nguyen, K. Slowinski, *Journal of the American Chemical Society*, 125, **2003**, 5948-5953.

[27] R.L. York, D. Nacionales, K. Slowinski, Chemical Physics, 319, **2005**, 235-242.

[28] J.D. Porter, A.S. Zinn, *Journal of Physical Chemistry*, 97, **1993**, 1190-1203.

[29] C.J. Muller, J.M. van Ruitenbeek, L.J. de Jongh, *Physics Review Letters*, 69, **1992**, 140-143

[30] J.J. Versluijs, M. Bari, F. Ott, J.M.D. Coey, A. Revcolevschi, *Journal of Magnetism and Magnetic Materials*, 211, **2000**, 212-216.

[31] Y. Naitoh, M. Horikawa, T. Yatabe, T. Funaki, H. Abe, T.T. Liang, Y. Suzuki, T. Shimizu, Y. Kawanishi, W. Mizutani, *Nanotechnology*, 17, **2006**, 2406-2410.

[32] H. Park, A.K.L. Lim, A.P. Alivisatos, J. Park, P.L. McEuen, Applied Physics Letters, 75, **1999**, 301-303.

[33] J. Dong, B.A. Parviz, Nanotechnology, 17, **2006**, 5124-5130.

[34] M. Yoshida, M. Nakayama, J. Yanagisawa, F. Wakaya, T. Kaito, K. Gamo, *Microelectronic Engineering*, 57-58, **2001**, 877-882

[35] C.Z. Li, H.X. He, N.J. Tao, *Applied Physics Letters*, 77, **2000**, 3995-3997.

[36] Y.V. Kervennic, H.S.J. Van der Zant, A.F. Morpurgo, L. Gurevich, L.P. Kouwenhoven, *Applied Physics Letters*, 80, **2002**, 321-323.

[37] A.F. Morpurgo, C.M. Marcus, D.B. Robinson, *Applied Physics Letters*, 74, **1999**, 2084-2086

[38] F. Chen, Q. Qing, L. Ren, Z.Y. Wu, Z.F. Liu, *Applied Physics Letters*, 86, **2005**, 123105.

[39] S. Carrara, J. Riley, V. Bavastrello, E. Stura, C. Nicolini, *Sensors and Actuators B: Chemical*, 105, **2005**, 542-548.

[40] R.G. Compton, C.E. Banks, "Understanding Voltammetry", *World Scientific Publishing*, **2007**.

[41] P.R. Roberge, http://www.corrosion-doctors.org/Corrosion-Kinetics/Overpotential-concentration.htm, **1999**.

[42] Van London Company, http://www.vl-pc.com/default/index.cfm/continuing-education/practical-ph-theory-and-use/, **2009**.

[43] A.M. Bond, R.G. Compton, D.A. Fiedler, G. Inzelt, H. Kahlert, S. Komorsky-Lovric, H. Lohse, M. Lovric, F. Marken, A. Neudeck, U. Retter, Z. Stojek, F. Scholz (ed.), "Electroanalytical Methods, Guide to Experiments and Applications", *Springer*, **2005**.

[44] M. Schlesinger, M. Paunovic (ed.), "Modern Electroplating, fourth edition", *Wiley-Interscience Publication*, **2000**.

2. Sub-Monolayer Gold Particle Junction Arrays

Contents

Abstract

In this chapter initial concepts about nanojunction technology will be investigated using assemblies of gold nanoparticles and poly-(diallyldimethylammonium chloride) (PDDAC), formed using layer-by-layer deposition across a 40 μm gap between two tin-doped indium oxide (ITO) conducting surfaces. Both electron microscopy and voltammetric characterisation are used to demonstrate the sub-monolayer formation and laterally insulating characteristics. The removal of the organic PDDAC allows for "clean" gold-gold junctions arrays to be formed, which are electrically conducting. Investigations into the effect of humidity, as well as dithiols, upon both resistance and capacitive currents are described.

Publication

R.W. French, E.V. Milsom, A.V. Moskalenko, S.N. Gordeev, F. Marken, *Sensors and Actuators B*, 129, **2008**, 947-952.

Chapter 2: Sub-Monolayer Gold Particle Junction Arrays.

2.1. Introduction

Nanoparticle arrays or films can be considered as nanojunction arrays when considering the gaps between the deposited particles rather than the particles themselves. The simplicity of formation of the nanoparticle arrays often based on drop-cast [1,2] or the more versatile layer-by-layer [3,4] deposition process, has attracted interest for nanoparticle arrays. Taking into account nanoparticle array uses in both analytical [5,6] and gas sensing [7,8], makes them an interesting starting point for research into nanojunctions, as they also form a bridge between the normal applications of nanojunctions (eg. crossed wire sensors [9]) and the more chemisresistive effects in sensor applications that have been predominantly investigated using junction arrays. [10]

In this chapter the basic ideas of nanojunctions and their applications are introduced using a nanoparticle array formed by the versatile layer-by-layer deposition techniques. Layer-by-layer allows a suitable metal nanoparticle, in the case of this project gold, to be combined with a suitable binder molecule, e.g. silk [11] and dendrimer [12,13] binders have been used however within this chapter we will concentrate on thiols [14] and poly-cationic binders. [15]

Exploratory work with the thin self-assembled films is discussed and the formation of a sub-monolayer film of gold nanoparticles bound together with a poly-cationic binder, poly-(diallyldimethylammonium chloride) (PDDAC) is investigated. It is shown that, when deposited in a layer-by-layer manner, films with clusters of nanoparticles are formed, which only gradually inter-connect after many deposition cycles. The extremely low electrical conductivity of these sub-monolayer films can be improved after chemical (UV-ozonolysis) removal of the organic (PDDAC) binder components. Films then become very sensitive to humidity and to vapours. The response to dithiols is demonstrated and the re-usability of probes after surface ozonolysis allows the effect of different vapours to be compared quantitatively.

2.2. Experimental

2.2.1. Reagents

Chemical reagents such as 70 % phosphoric acid, sodium hydroxide, potassium hydroxide, tartaric acid, oxalic acid, hexanethiol, butanethiol, ethylenedithiol, butylenedithiol, octylenedithiol, poly-(diallyldimethylammonium chloride) of very low molecular weight ($M_W < 10^5$, 35 wt.% in water) (Sigma Aldrich), gold nanoparticles (Sigma Gold Colloids nominal 20 nm diameter, mean 17-23 nm, monodisperse, approx 0.01 % as $HAuCl_4$ in water) were obtained commercially and used without further purification. Demineralised and filtered water was taken from an Elga purification unit, with a resistivity not less than 18 MOhm cm. Pureshield argon (BOC) was employed in controlled atmosphere experiments. If not stated otherwise, the temperature during experiments was 22 +/- 2 ^oC and the relative humidity ca. 60 %.

2.2.2. Instrumentation

For electrochemical and conductivity measurements an Autolab PGSTAT30 bipotentiostat system (EcoChemie, Netherlands) was employed. In electrochemical experiments a conventional three-electrode cell with platinum counter and saturated calomel reference (SCE, Radiometer, Copenhagen) were utilised. Conductivity measurements were conducted in two-electrode mode. In controlled humidity experiments a HMP50 temperature and relative humidity probe (Campbell Scientific) was employed connected to the external potential input of the Autolab system. The humidity chamber was controlled with water saturated air and with solid potassium hydroxide (relative humidity range 10 % to 100 % [16]). A tube furnace (Elite, UK) was employed for thermal treatment and a room temperature UV-ozonolysis cleaner (Bioforce, USA) was used for mild chemical cleaning. Field emission gun scanning electron microscopy (FEGSEM) images were obtained using a Leo 1530 FEGSEM system. Samples were gold sputter coated prior to imaging. Lithography procedures were carried out using standard procedures as described below.

2.2.3. Lithography of Tin-Doped Indium Oxide Film Electrodes

Tin-doped indium oxide (ITO, 15 Ohm/square, Image Optics, Basildon, UK) coated glass slides were washed in ethanol and demineralised water, covered with PRP positive photoresist spray (RS components, UK) and left to dry in the dark for a minimum of 24 hours. Ultra Violet exposure was carried out with a positive electrode mask (see Figure 2.1B, Vision Graphics, UK) under a UV light source for 20 minutes. The electrodes were then carefully developed in aqueous 0.175 M potassium hydroxide solution at ca. 20 °C leaving a resist layer on unexposed areas. ITO etching was carried out in 1 wt.% tartaric acid and 3 wt.% oxalic acid solution at 35 °C for approximately 20 minutes. [17] The photoresist was then removed using acetone, the slides were once again thoroughly rinsed, for final cleaning electrodes were placed into a tube furnace (Elite, UK) for half an hour at 500 °C in air.

2.2.4. Layer-by-Layer Assembly of Sub-Monolayer Gold-PDDAC Films

The layer-by-layer assembly of the gold nanoparticle - poly(diallyldimethylammonium chloride) (PDDAC) films consisted of a sequence of liquid immersion steps with: (i) an aqueous PDDAC solution (3 wt.% in water) for 60 seconds followed by rinsing with distilled water, (ii) dipping into 20 nm diameter gold colloid (ca. 0.01 % in $HAuCl_4$, Sigma-Aldrich) for 10 minutes followed by rinsing with distilled water and drying in air. This completed a single deposition cycle of the gold nanoparticle - PDDAC film. The process was then repeated until the necessary number of layers was achieved. The colour of the deposit is initially red but turns dark green (see Figure 2.1A) in subsequent deposition cycles due to gold nanoparticle surface plasmon interactions. [18]

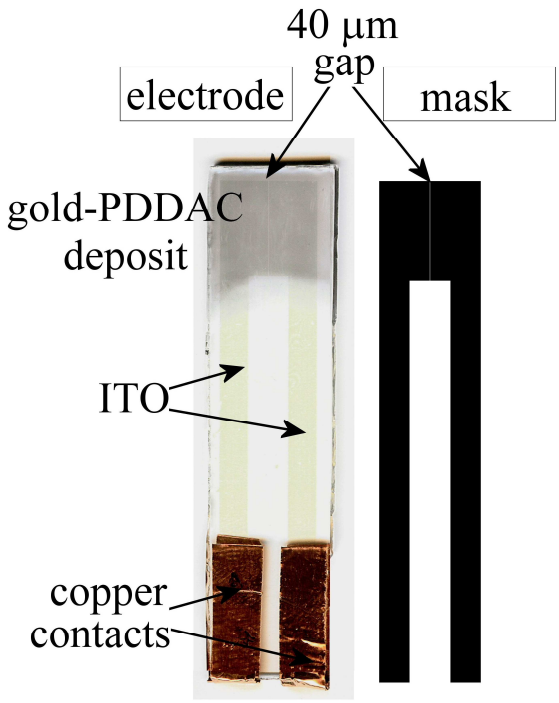

Figure 2.1 (A) Photographic image of a gold-PDDAC coated (16 deposition cycles) ITO electrode with a 40 µm inter-electrode gap and copper contacts. (B) Mask used to produce the patterned ITO electrode in a lithographic process.

2.3. Results and Discussion

2.3.1. Formation and Morphology of Sub-Monolayer Gold Nanoparticle - PDDAC Assemblies on Patterned Tin-Doped Indium Oxide (ITO) Substrates

The formation of layered structures based on the layer-by-layer deposition of gold nanoparticles with suitable binder systems have been explored in several previous studies. [19,20,21] Interesting thin film nanocomposite structures with novel electronic and electrochemical properties can be obtained. [22] In this chapter 20 nm diameter gold nanoparticles are employed and are bound to a ITO-coated glass substrate with the help of poly-(diallyldimethylammonium chloride) (or PDDAC) in a cyclic aqueous deposition process (see experimental).

Initially, the gold nanoparticle assembly process is investigated. The formation of the gold film deposit is readily monitored with cyclic voltammetry in aqueous 0.1 M phosphate

buffer (pH 7) solution. Under these conditions the gold surface is known to exhibit a surface oxidation response (at ca. 0.8 V vs. SCE) and the associated re-reduction response (at ca. 0.4 V vs. SCE) as shown in Figure 2.2A. The gold surface signal is observed immediately after the first deposition cycle and in each subsequent deposition cycle the gold surface response is increased (see Figure 2.2B). It can be concluded that a highly regular layer-by-layer growth occurs. Under these conditions a planar macroscopic gold surface shows typically a 1 mC cm^{-2} oxidation/re-reduction charge. Therefore from the charge for the 10-layer deposit it can be calculated that approximately 10 % electrode coverage has been reached (see plot in Figure 2.2B). The colour of the gold coating develops from red in the initial cycle into dark green in subsequent deposition cycles. This colour change is due to the surface plasmon interaction of individual gold nanoparticles. [23]

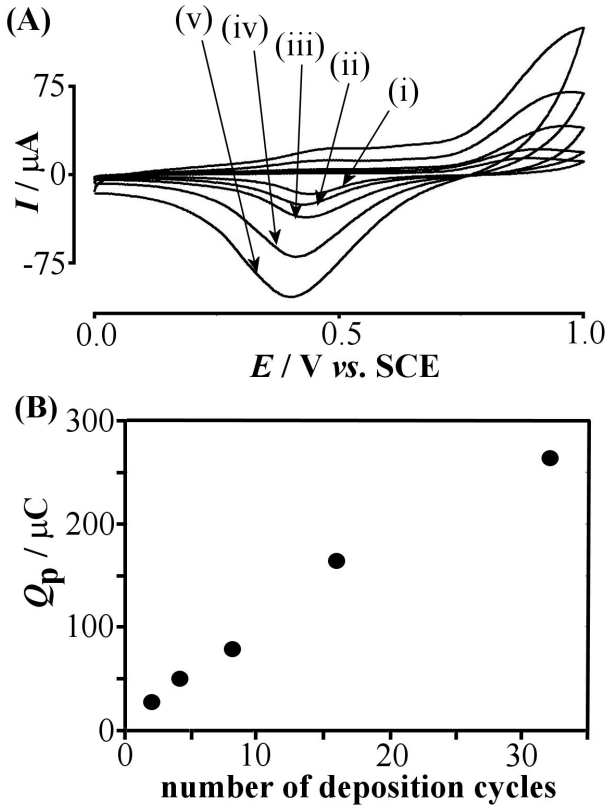

Figure 2.2 (A) Cyclic voltammograms (scan rate 0.1 Vs^{-1}) for the surface oxidation and re-reduction for a gold nanoparticle - PDDAC modified ITO electrode (area 1 cm^2) with (i) 2, (ii) 4, (iii) 8, (iv) 16, and (v) 32 deposition cycles in aqueous 0.1 M phosphate buffer pH 7.2 (B) Plot of the charge under the voltammetric reduction peak for the gold-PDDAC film as a function of the number of deposition layers.

Next, the gold nanoparticle-PDDAC film deposits were investigated by electron microscopy. Figure 2.3 confirms the presence of gold nanoparticles of ca. 20 nm diameter. The deposition conditions result in sub-monolayer films of nanoparticles with a density consistent with the estimate obtained from the charge observed in cyclic voltammograms. The approximate surface coverage for the 10-layer deposit (see Figure 2.3B) is ca. 5×10^{10} particles cm^{-2}. Surprisingly, the continued deposition of gold nanoparticles does not lead to a smooth and homogeneous coverage of the surface. Figure 2.3B and Figure 2.3C clearly demonstrate that cluster formation is preferred and the formation of junctions is very rare. This can be attributed to the deposition process in which PDDAC is adhering to the gold nanoparticles and this causes a preferential deposition of the next gold nanoparticles onto existing clusters rather than onto the bare ITO surface.

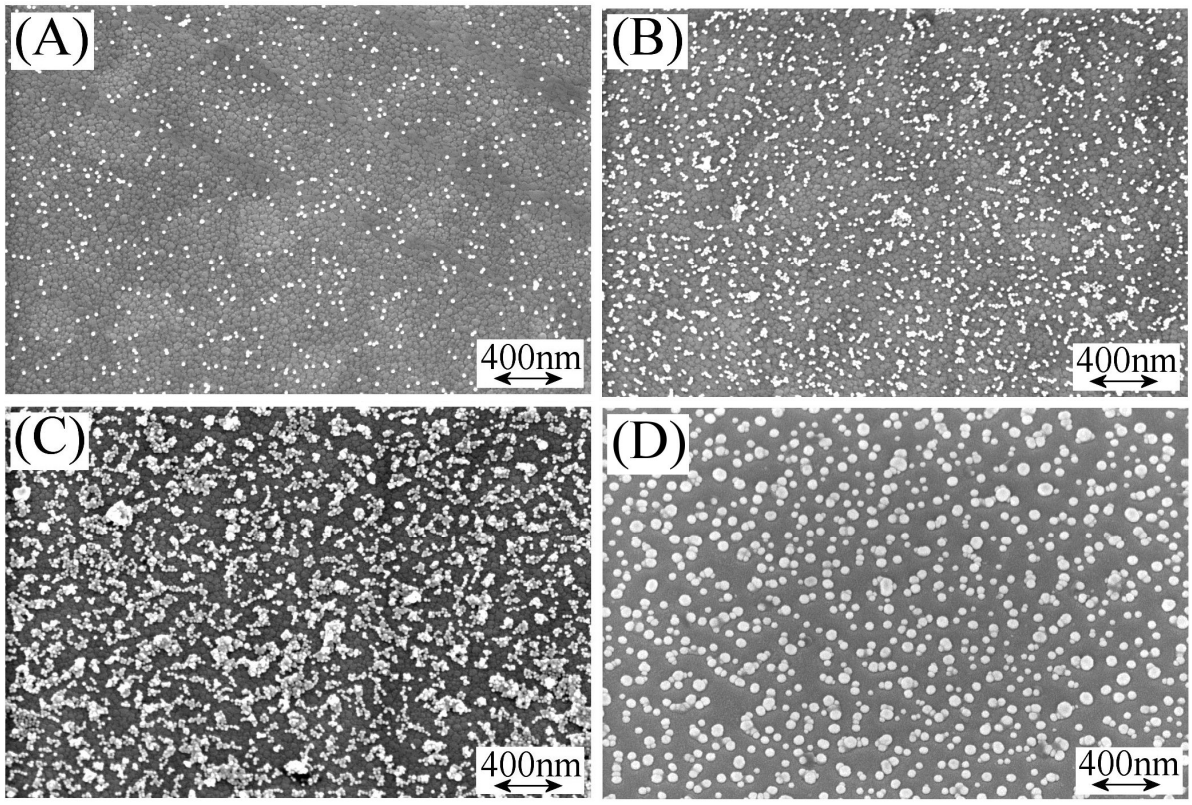

Figure 2.3 FEGSEM images showing (A) 1-layer gold nanoparticle - PDDAC film, (B) 10-layer film, (C) 40-layer film, and (D) 10-layer film heat treated at 500 ^{o}C for 30 minutes.

In order to clean and modify the gold nanoparticle decorated surfaces two strategies were employed and compared. A thermal treatment in air (500 ^{o}C for 30 minutes) which is known to remove all volatile and combustible organic components from the surface [24]

and a room temperature UV-ozonolysis process [25] are investigated. The thermal treatment caused a colour change of the gold deposit from green to the original red, which is indicative of the presence of individual particles rather than of clusters of gold nanoparticles. FEGSEM imaging reveals that partial sintering of gold nanoparticles, forming individual particles, occurs under these conditions. Figure 2.3D shows that bigger particles have formed when compared to Figure 2.3B. In contrast, a 30 minute UV-ozonolysis treatment at room temperature did not cause any colour modification or any FEGSEM-visible changes in the nanoparticle deposit appearance. It is assumed that the room temperature UV-ozonolysis process only removes organics (by oxidation to volatile oxides) without attacking the inorganic components of the film.

2.3.2. Electrochemical Characterisation of Sub-Monolayer Gold Nanoparticle - PDDAC Assemblies and Ozone Treated Gold Nanoparticle Assemblies on Patterned Tin-Doped Indium Oxide (ITO) Substrates

In order to characterize the effect of clustering on the electrical conductivity of gold nanoparticle - PDDAC films a patterned ITO electrode was employed. Figure 2.1 shows the design with two ITO regions separated by a 40 μm gap. The gold-PDDAC film was deposited across the gap and conductivity data recorded as a function of film thickness. Figure 2.4A shows typical 2-probe measurement cyclic voltammograms, run in atmospheric conditions, indicating highly resistive behaviour (curve i). The analysis of this data was based on the assumption that the slope in the signal is indicating resistance (given by $\frac{\Delta U}{\Delta I}$). In addition a capacitive current component is observed (see curve ii) which is analysed by calculating the apparent capacitance (given by the capacitive current divided by the scan rate [26]). The reason for the capacitive currents is explained below.

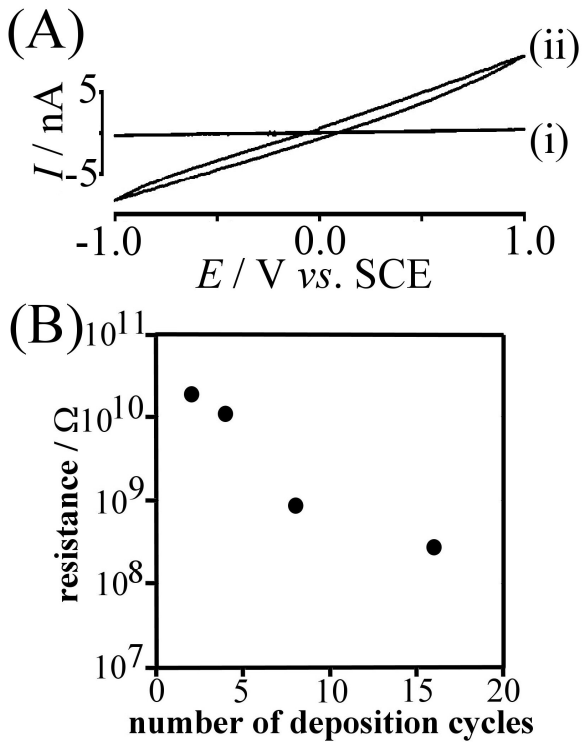

Figure 2.4 (A) 2-probe measurement cyclic voltammograms carried out in atmospheric conditions (scan rate 0.02 Vs^{-1}) obtained for a 16-layer gold-PDDAC film on a 40 µm gap electrode obtained in two-electrode mode. (i) Before UV-ozonolysis cleaning and (ii) after UV ozonolysis treatment. (B) Plot of the apparent resistance of gold nanoparticle - PDDAC film deposits as a function of the number of deposition cycles. Data for 0-layer deposit is much more resistive and not included.

The conductivity of gold-PDDAC film deposits was extremely low and not measurable even after up to 40 deposition cycles. However, UV-ozonolysis of the gold nanoparticle deposit did result in measurable current responses. A plot of the resistance versus the number of deposition cycles is shown in Figure 2.4B demonstrating an approximately logarithmic dependence of the resistance on deposition cycles. The reason for this kind of dependence is in part due to electrical conductivity in sub-monolayer deposits (vide infra) but also due to ionic conductivity as is shown next.

The conductivity measurements for UV-ozonolysis cleaned gold nanoparticle films were repeated and an effect was observed in different environments (ambient air, argon, vacuum). The conductivity was observed to drop significantly under vacuum or dry argon conditions (although, the conductivity never dropt to zero) and is therefore particularly

sensitive to the level of ambient humidity. It has been shown recently that chemiresistor-type devices can be sensitive to humidity depending on the gold-capping agent and depending on the type of vapour detected. [27] In these devices both resistance and capacitive responses are observed in the presence of elevated humidity levels. [28] A series of experiments were conducted under controlled humidity conditions with the results shown in Figure 2.5.

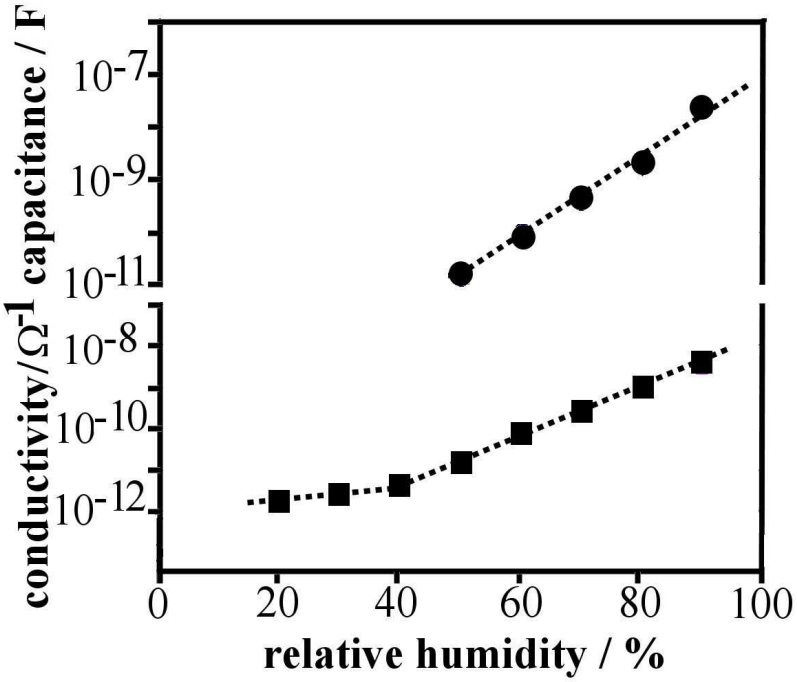

Figure 2.5. **Plot of the apparent capacitance and conductivity (obtained from cyclic voltammograms at a 40 µm ITO gap electrode) of a 16 deposition cycle gold nanoparticle deposit (after UV ozonolysis) in air with controlled humidity (T = 20 °C).**

It can be observed that both the conductivity of the probe and the apparent capacitive currents are strongly humidity dependent, and increase with humidity. The apparent capacitive current is significant at humidity levels higher than 50 % and it can be explained with the formation of an extremely thin film of water on the sub-monolayer gold nanoparticle film modified substrate (see Figure 2.6). In the conductivity data it can be seen that the onset of the "liquid-like" properties (which equates to lateral ion conduction) of the water film occurs at ca. 40 % relative humidity. The dependency of both capacitance and conductivity on the humidity are logarithmic in good approximation.

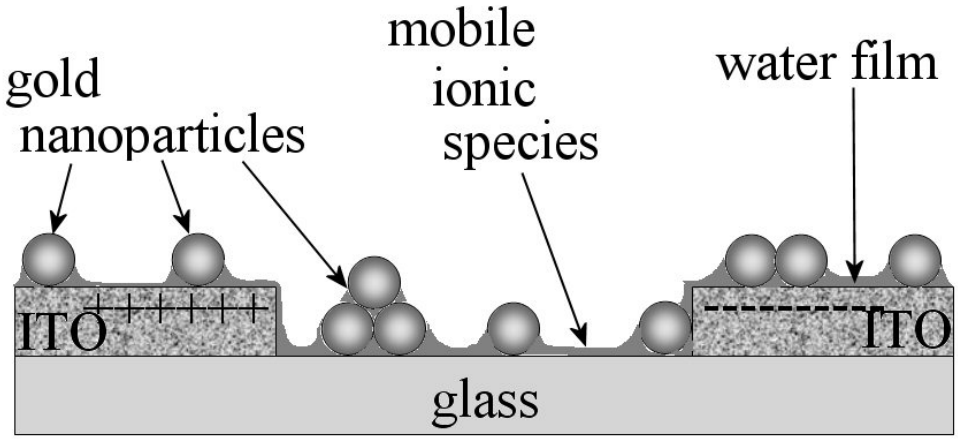

Figure 2.6. **Schematic drawing of the gold nanoparticle deposit within the ITO gap electrode system and a thin film of water forming an ionically conducting film allowing the charging of the two ITO electrode and therefore allowing a capacitive current component.**

The presence of the liquid water film allows electrical conductivity and capacitive current contributions to be explained. The gold nanoparticle may also contribute to this effect by acting as a scaffold supporting the liquid film. It has to be pointed out that the measured or apparent capacitance is not the real capacitance of the two ITO electrodes but only a fraction of this. The apparent capacitance increase becomes more significant as the thickness of the water film is gradually increasing with relative humidity and this is connected with the water film on the ITO film gradually making a larger electrode area accessible.

2.3.3. Electrochemical Characterisation of Sub-Monolayer Gold Nanoparticle Assemblies on Patterned Tin-Doped Indium Oxide (ITO) Substrates Exposed to Dithiol Vapours

The electrical conductivity of the gold nanoparticle film deposit after UV-ozonolysis cleaning and in a very dry environment (vacuum, argon) is typically 1.5×10^{-10} Ω^{-1} for a 16 deposition cycle gold nanoparticle film. This is two orders of magnitude lower when compared to the conductivity observed in ambient air (ca. 60 % relative humidity). However, this level of conductivity is significant and a function of the number of deposition cycles. This electrical conductivity is believed to arise from electron tunnelling events along random pathways across the 40 μm gap between the two ITO electrodes. In

order to explore this finding in more detail the UV-ozonolysis cleaned conductivity probes were exposed to differently contaminated vapour atmospheres. Dithiols resulted in immediate and significant changes in electrical conductivity (at 0 % humidity) and these changes were reversed after UV-ozonolysis. Below the effect of some dithiols are explored in more detail.

Figure 2.7 shows that a systematic decrease in conductivity occurs after exposure of the probe to ethylenedithiol, butylenedithiol, and octylenedithiol with an approximately logarithmic dependency on the number of carbon atoms. Only one probe was employed and UV-ozonolysis cleaned between experiments. The systematic decrease in conductivity is consistent with impeded electron tunnelling across random junction networks. However, the slope (or decay factor) of the plot in Figure 2.7 is inconsistent with the expected behaviour for a single junction (expected slope ca. 0.87 $Å^{-1}$ [29], observed slope ca. 0.06 $Å^{-1}$). In a network of junctions the current will flow along the path of lowest resistance and therefore the effect of the dithiol is probably reduced to a statistically averaged value favouring the more conducting junctions. It is unlikely that all junctions are fully responsive (fully covered in dithiol) and therefore the slope is reduced.

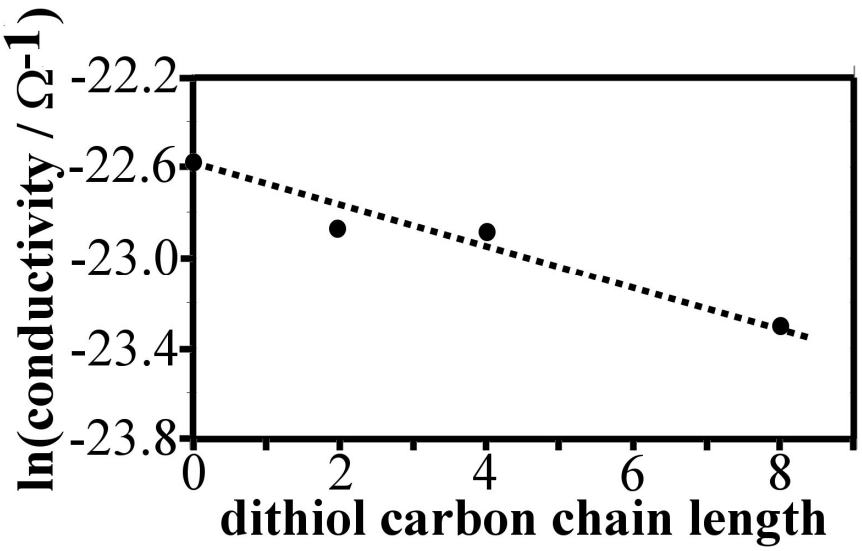

Figure 2.7. **Plot of the conductivity measured for a 16 deposition cycle gold nanoparticle film (UV ozonolysis cleaned) across a 40 µm gap as a function of the number of carbon atoms in the alkyl chain of dithiols.**

2.4. Conclusions

The formation of a nanojunction network between two ITO electrodes with a 40 μm gap has been demonstrated, giving some insight into the uses of nanojunction technology. The layer-by-layer deposition process allows gold nanoparticles to be assembled and the resistivity of the resulting probe to be tuned. The electrical properties of the probe after UV ozonolysis cleaning have been demonstrated to depend on humidity and on specific adsorption from the gas phase onto the gold particles. In future, this kind of probe could offer low cost and highly versatile sensor films. However to further this project a single nanojunction is need rather than an array, the next chapter will discuss formation methodologies of these single junctions.

2.5. References

[1] W.P. Wuelfing, R.W. Murray, *Journal of Physical Chemistry B*, 106, **2002**, 3139-3145.

[2] J.P. Choi, M.M. Coble, M.R. Branham, J.M. DeSimone, R.W. Murray, *Journal of Physical Chemistry C*, 111, **2007**, 3778-3785.

[3] F.N. Crespilho, F.C. Nart, O.N. Oliveira, C.M.A. Brett, *Electrochimica Acta*, 52, **2007**, 4649-4653.

[4] A. Escorcia, A.A. Dhirani, *Journal of Electroanalytical Chemistry*, 601, **2007**, 260-268.

[5] W.P. McConnell, J.P. Novak, L.C. Brousseau, R.R. Fuierer, R.C. Tenent, D.L. Feldheim, *Journal of Physical Chemistry B*, 104, **2000**, 8925-8930.

[6] L. Han, D.R. Daniel, M.M. Maye, C.J. Zhong, *Analytical Chemistry*, 73, **2001**, 4441-4449.

[7] S.D. Evans, S.R. Johnson, Y.L.L. Cheng, T.H. Shen, *Journal of Materials Chemistry*, 10, **2000**, 183-188.

[8] H. Wohltjen, A.W. Snow, *Analytical Chemistry*, 70, **1998**, 2856-2859.

[9] Z.H. Zhong, D.L. Wang, Y. Cui, M.W. Bockrath, C.M. Lieber, *Science*, 302, **2003**, 1377-1379.

[10] A. Kolmakov, M. Moskovits, *Annual Review of Material Research*, 34, **2004**, 151-180.

[11] A. Singh, S. Hede, M. Sastry, *Small*, 3, **2007,** 466-473.

[12] Y. Joseph, N. Krasteva, I. Besnard, B. Guse, M. Rosenberger, U. Wild, A. Knop-Gericke, R. Schlogl, R. Krustev, A. Yasuda, T. Vossmeyer, *Faraday Discussions*, 125, **2004**, 77-97.

[13] N. Krasteva, Y. Fogel, R.E. Bauer, K. Mullen, N. Matsuzawa, A. Yasuda, T. Vossmeyer, *Advance Functional Materials*, 17, **2007**, 881-888.

[14] Y. Joseph, B. Guse, A. Yasuda, T. Vossmeyer, *Sensors and Actuators B-Chemical*, 98, **2004**, 188-195.

[15] W. Zhao, J.J. Xu, H.Y. Chen, *Frontiers in Bioscience*, 10, **2005**, 1060-1069.

[16] D.R. Lide, ed., "CRC Handbook of Chemistry and Physics, 74th edition", *CRC Press*, **1993-1994**, p. 15-25.

[17] T.H. Tsai, Y.F. Wu, *Journal of the Electrochemical Society*, 153, **2006**, C86-C90.

[18] Z.Y. Zhong, K.B. Male, J.H.T. Luong, *Analytical Letters*, 36, **2003**, 3097-3118.

[19] K.J. McKenzie, F. Marken, *Langmuir*, 19, **2003**, 4327-4331.

[20] E.V. Milsom, H.R. Perrott, L.M. Peter, F. Marken, *Langmuir*, 21, **2005**, 9482-9487.

[21] M. Amiri, S. Shahrokhian, F. Marken, *Electroanalysis*, 19, **2007**, 1032-1038.

[22] E.V. Milsom, J. Novak, M. Oyama, F. Marken, *Electrochemical Communication*, 9, **2007**, 436-442.

[23] K.C. Grabar, R.G. Freeman, M.B. Hommer, M.J. Natani, *Analytical Chemistry*, 67, **1995**, 735-743.

[24] E.V. Milsom, J. Novak, S.J. Green, X.H. Zhang, S.J. Stott, R.J. Mortimer, K. Edler, F. Marken, *Journal of Solid State Electrochemistry*, 11, **2007**, 1109-1117.

[25] T. Goto, H. Inokawa, M. Nagase, Y. Ono, K. Sumitomo, K. Torimitsu, *Japanese Journals of Applied Physics Part 1*, 46, **2007**, 1731-1733.

[26] F. Scholz, ed., "Electroanalytical Methods", *Springer*, **2005**, p. 38.

[27] P.F. Pang, J.L. Guo, S.H. Wu, Q.Y. Cai, *Sensors and Actuators B-Chemical*, 114, **2006**, 799-803.

[28] P.F. Pang, Z.D. Guo, Q.Y. Cai, *Talanta*, 65, **2005**, 1343-1348.

[29] E. Tran, C. Grave, G.M. Whitesides, M.A. Rampi, *Electrochimca Acta*, 50, **2005**, 4850-4856.

3. Paired Gold Junction Electrode Formation

Contents

Abstract

Within this chapter simultaneous bipotentiostatic methodology used to produce paired gold junction electrodes is introduced, including initial developmental methodologies attempted. In-depth details into the formation of paired electrodes with gap sizes ranging from 5 μm to 300 nm via a simultaneous electrodeposition growth method are given. The resulting junctions are tested using alizarin red S with considerations into sensitivity and the reversibility of electron transfer.

Publicised

R.W. French, S.N. Gordeev, P.R. Raithby, F. Marken, *Journal of Electroanalytical Chemistry*, 632, **2009**, 206-210.

Chapter 3: Paired Gold Junction Electrode Formation

3.1. Introduction

Bipotentiostat controlled electrochemical probes with a generator electrode and a collector electrode, configured to allow fast inter-diffusion of reagents, are of considerable importance in analytical measurements. The positioning of two electrodes is commonly achieved by lithography [1] or, with the help of nanopositioner systems. [2] An alternative approach based on a simultaneous metal deposition process was pioneered by Porter et. al. [3] for hanging mercury drop electrodes (HMDE's). In this chapter, a novel method for forming these types of junctions using the simultaneous deposition of gold will be discussed.

The principle and applications of generator-collector mode sensing were developed in particular by J. W. Albery [4] using rotating disc electrodes with numerous new techniques following including double-band channel electrodes [5], micro-electrode arrays [6] and interdigitated microband arrays [7], SECM probe techniques [8], and micro-ring-disc electrodes [9] as described in Chapter 1.2 and Chapter 1.3. Bringing two electrodes into close distance allows fast processes to be probed and short-lived intermediates to be studied.

Emerging areas of application of closely spaced electrodes are in molecular electronics [10], sensors and biosensors [11], and single molecule devices. [12] New techniques for the formation of nanojunctions have been developed such as "break junctions" [13] and electro-migration. [14] Electro-deposition and electro-dissolution offer versatile methods for nanostructure formation [15] and a range of techniques have been reported for nanojunction electrodeposition. [16,17,18,19]

The formation of paired gold junction electrodes is achievable by simultaneously growing deposits upon two adjacent platinum electrodes under bipotentiostatic potential control. The two gold deposits were demonstrated to grow towards each other until a small gap was formed and a feedback current between the two working electrodes causes automatic

termination of the deposition. In this chapter, the development of the simultaneous gold growth used to create nanogap junctions is shown and evidence that varying the electrodeposition potential can conveniently control the gap size in junction electrodes is presented.

3.2. Experimental

3.2.1. Chemical Reagents

Potassium hydroxide, potassium gold (I) dicyanide, potassium cyanide, monobasic potassium phosphate, dibasic potassium phosphate, potassium carbonate, poly-(diallyldimethylammonium chloride) or PDDAC (molecular weight < 100 kDalton), and alizarin red S, were obtained commercially (Sigma - Aldrich) and used without further purification. Demineralised and filtered water with not less than 18 MOhm cm resistivity was taken from an Elga purification unit. Pureshield argon (BOC) was employed to de-aerate solutions prior to experiments.

3.2.2. Instrumentation

For electrochemical measurements and electro-deposition experiments an Autolab PGSTAT30 bipotentiostat system (EcoChemie, Netherlands) was employed. In electrodeposition experiments a conventional three-electrode cell with a gold counter and saturated calomel reference (SCE, Radiometer, Copenhagen) were utilised, for electrochemical experiments, a platinum counter was implemented opposed to gold. Scanning electron microscopy (SEM) images for gold sputter-coated samples were obtained using a JEOL JSM6480LV system. All experiments were conducted under argon (Pureshield, BOC) and at a temperature of $20 \pm 2\ ^{o}C$ (unless stated otherwise).

3.2.3. Formation of Paired Gold Junction Electrodes

Platinum wire (100 μm diameter, ca. 10 cm long) was fed into two glass capillaries and then placed into a 5 mm outer diameter glass tube (ca. 8 cm long). This assembly was heat sealed at one end and, by carefully twisting the hot glass, the two platinum wires were

brought into close proximity. After cooling, cutting, and polishing the two platinum disc electrodes are obtained with approximately 50 μm separation (see Figure 3.1).

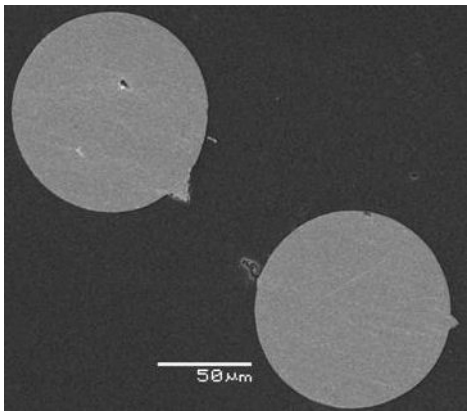

Figure 3.1 SEM image showing clean and polished paired platinum disc electrode.

The bipotentiostatic electrodeposition cell was based on two working electrodes attached to the two platinum discs, a gold wire counter electrode and SCE reference electrode. The plating solution was based on an alkaline cyanide bath ($KAu(CN)_2$, KCN, K_2HPO_4, K_2CO_3; in 10 mL demineralised water [20]), with 60 μL of 0.35 wt% poly-(diallyldimethylammonium chloride) PDDAC, added to suppress dendritic gold growth. During deposition, the gold plating bath was continuously agitated and held at a constant temperature of 55 ºC.

Three methods, voltammetric simultaneous deposition, repetitive connection and chronoamperometric simultaneous deposition of bipotentiostatic growth were investigated, using both cyclic voltammetric and chronoamperometric methods (Autolab GPES, EcoChemie).

Voltammetric simultaneous deposition was the only method to use cyclic voltammetry experimentation to deposit the gold junctions. The method requires a preliminary gold deposition step upon one platinum disc, forming approximately half the junction. This plated disc is then set to a more positive deposition potential, resulting in slower deposition. The second un-plated disc is set to scan a small range within a potential range of fast deposition. Prior to a connection between the electrodes an overloading current is observed, and deposition is stopped.

Repetitive connection growth requires the pre-plating step described previously, the pre-plated disc is then set to a potential of minimal dissolution, whilst the secondary electrode is deposited upon. An oscillation between a connected junction and a gap junction is observed and deposition can be stopped at any pre-set overlaod value.

Simultaneous deposition was achieved by applying the desired deposition potential to the first platinum disc and a potential of 1 mV more positive was applied to the second electrode at the same time. The difference in deposition potential is necessary to create an overloading current as the electrodes approach a close proximity. The similarity in potential removes variation in deposition rate, and in the appearance of the resulting gold deposits. For the smallest junction gap sizes, increased sensitivity is required for junction growth. Therefore the potential difference between the discs was reduced to 0.5 mV. The automatic cut-off function in the GPES software was introduced to stop the gold deposition process when the current exceeded a pre-set limit of 90 μA.

With all three methods after the cut-off point was reached, (and the gap between the two gold electrodes had been reduced to a minimum), the electrode was removed from the gold plating bath, rinsed with demineralised water, dried, and tested. Conductivity tests with the dry paired gold electrode junction revealed no direct short circuit or tunnelling currents.

3.3. Results and Discussion

3.3.1. Optimising Gold Deposition

Original attempts at junction formation were dendritic in structure, (see Figure 3.2.) this generated problems with reproducibility, optical imaging of junction and mechanical stability resulting in the junction's applications being reduced to an unreliable, irreproducible gas phase sensor.

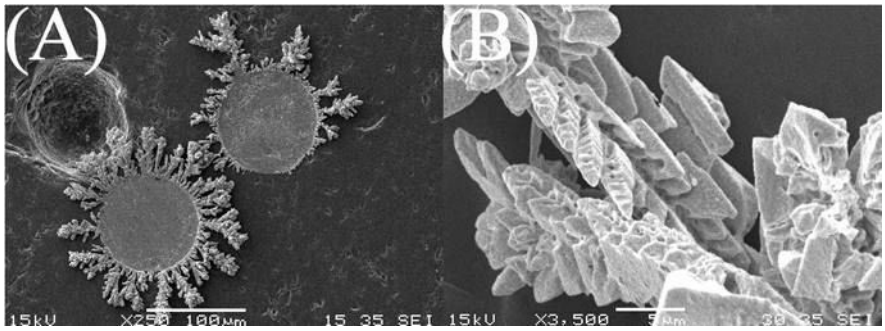

Figure 3.2 Showing original dendritic growth at (A) low magnification (B) high magnification.

To reduce dendritic growth, 60 µl, 0.35 % poly-(diallyldimethylammonium chloride) (PDDAC) (a polycationic binder used as a surfactant) was added to the plating bath and combined with deposition potentials closer to the reversible point (more positive) of gold (III/0) were selected. Figure 3.3 demonstrates the improvements induced. The PDDAC is thought to bind to the gold surface reducing nucleation points and slowing growth improving deposition smoothness.

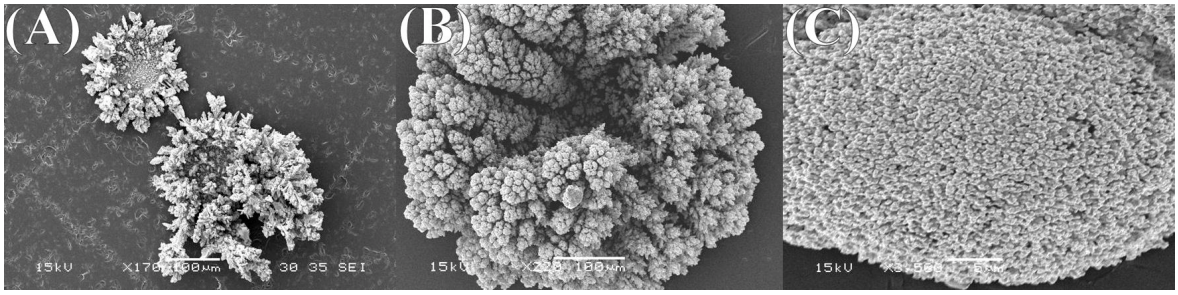

Figure 3.3 Showing gold growth for (A) original gold growth, (B) addition of PDDAC and (C) more positive deposition potentials combined with PDDAC.

3.3.2. Junction Growth via Voltammetric Simultaneous Deposition.

A typical cyclic voltammogram for the deposition process of a 100 µm diameter platinum disc electrode immersed in a stirred deposition solution is shown in Figure 3.4. The gold deposition commences at ca -0.85 V vs. SCE (the reversible potential for Au(III/0) under these conditions [10]). At a potential of ca. -1.20 V vs. SCE an increasing level of noise was detected, which is indicative of mass transport control during turbulent agitation with a magnetic stirring bar.

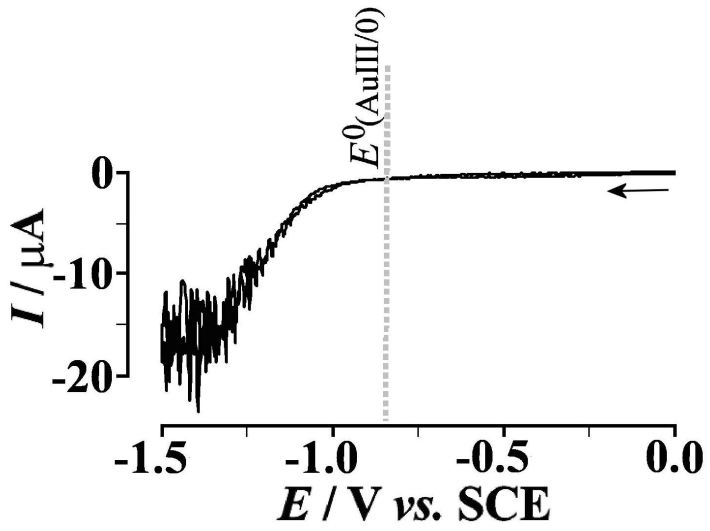

Figure 3.4 Typical CV for gold deposition, from an alkaline cyanide bath, upon a single platinum disc electrode. Plating bath held at constant 55 °C with continuous agitation.

The initial single disc deposition stage was carried out at –1.2 V vs. SCE until the gold deposition covered approximately half the distance between the platinum discs. The electrode was then set at a constant potential of –1.0 V vs. SCE for relatively slow gold growth. The unplated disc was set to scan across a range of faster gold deposition of –1.2 to –1.1 V vs. SCE. Resulting in the secondary electrode 'growing' towards the 'slow growing' primary deposit.

As the dimension between the two discs reduces an overloading current is observed just prior to a bridging connection. By placing an ammeter within the circuit the large current increase can be detected and plating immediately stopped, (see Figure 3.5 at 3 seconds). The junction can then be removed from solution and washed with distilled water.

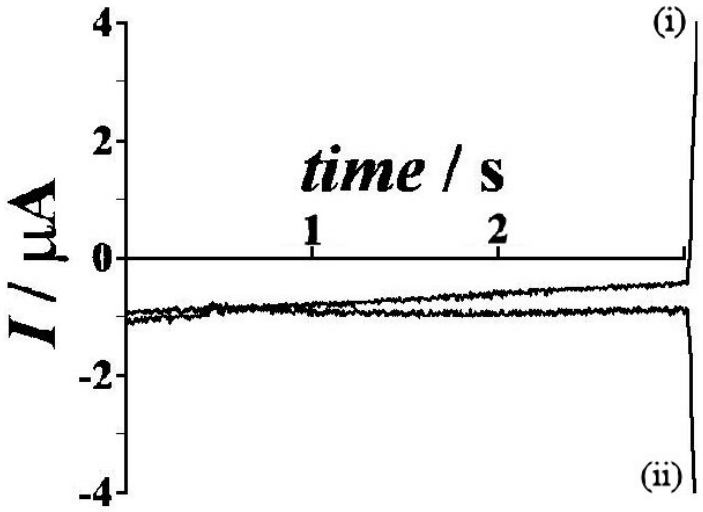

Figure 3.5 Voltammetry showing just prior and during overload for voltammetric simultaneous growth, from alkaline cyanide bath, potential has been converted to time. (i) working electrode one, (ii) working electrode two.

Although effective this method of growth has several disadvantages. The first being the pre-plating stage, adding extra stages of deposition and creating large variation between paired gold deposits generating unwanted asymmetry. Secondly the use of an ammeter to gauge the cut of point for deposition relies upon human interactions where slow reactions result in a connected junction.

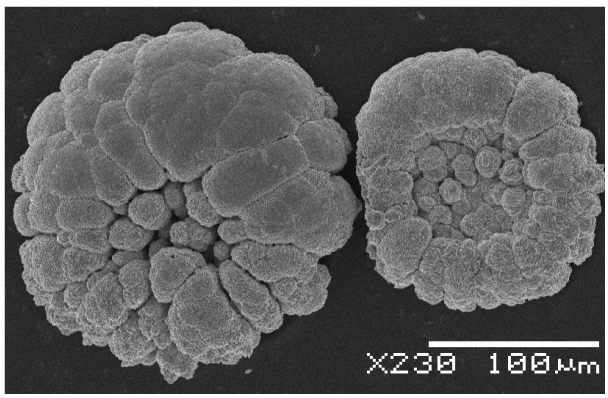

Figure 3.6 Junction formed via voltammetric simultaneous deposition methodology. Image shows improved surface smoothness, however demonstrates junction asymmetry.

3.3.3. Junction Growth via Repetitive Connections.

The initial pre-plating step was carried out as explained previously. The plated electrode is then set to a potential of slight dissolution, 0 V vs. SCE and the secondary electrode set to plate gold at –1.2 V vs. SCE. The secondary electrode grows towards the 'retreating' primary.

Upon a connection between the discs an overloading current occurs (see Figure 3.7 area B) the potential collapses to that of the primary electrode and the gold connection undergoes electrodissolution. Once the connection has dissolved, the electrodes revert to their pre-set condition and the plating stage repeats itself (area C Figure 3.7), if left the electrode will oscillate between these two states, at approximately one 'cycle' a second. (see Figure 3.7)

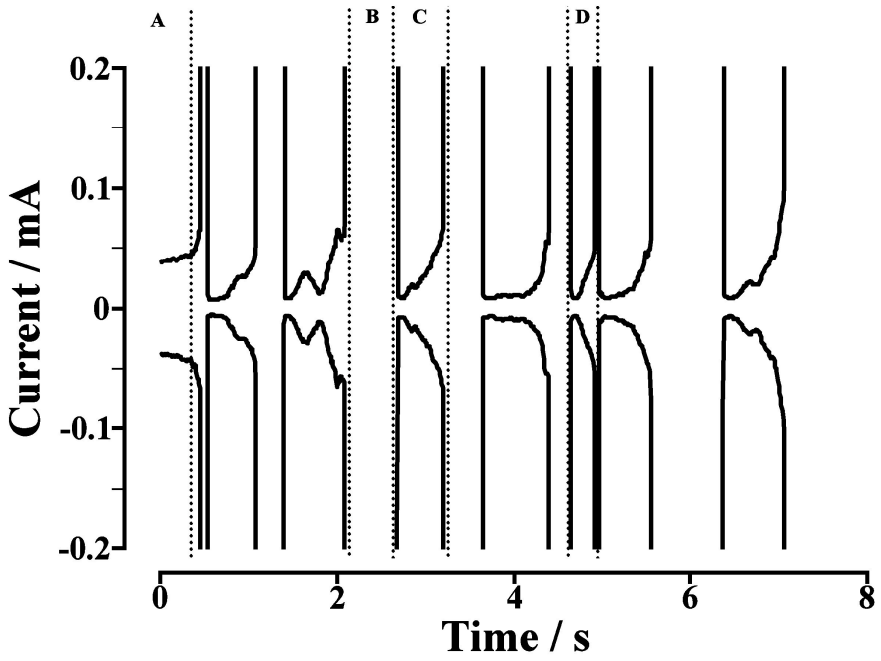

Figure 3.7 Chronoamperometric data showing junction growth via repetitive connection, region A, area of initial growth, region B, junction connected - dissolution occurring, region C, open junction - plating occurring. Region D represents a second repetitive connection occurring.

Figure 3.7 section D represents one cycle occurring out of synchronisation with the other oscillations, this 'cycle' may be assigned to a second connection undergoing oscillation between the connected and open state. This theory is supported by Figure 3.8C which shows several crystalline points bridging between the electrodes.

Although allowing multiple oscillations does not reduce average junction size, only allowing for more crystalline 'bridges', it does offer several chances to stop deposition if the initial opportunity is missed (unlike voltammetric simultaneous growth), however uneven junctions are still problematic.

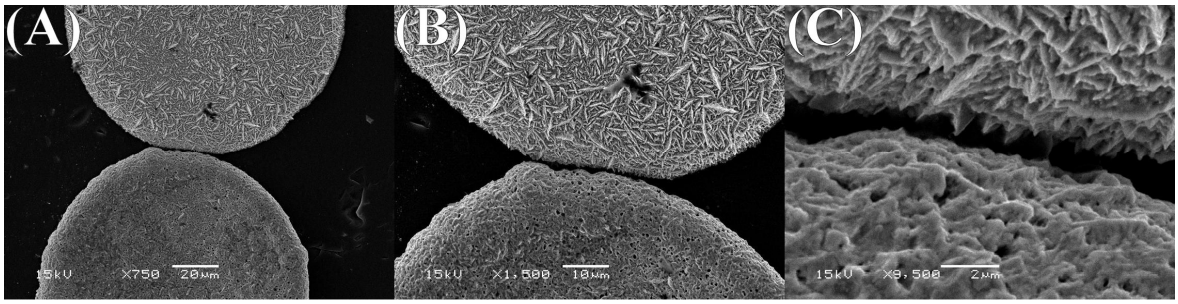

Figure 3.8 SEM of junction formed via repetitive connection method at (A+B) low magnification. (C) High magnification showing uneven surfaces and crystalline bridges between the discs.

3.3.4. Junction Electrode Growth via Simultaneous Electrodeposition

Simultaneous electrodeposition is a combination of the previous two methods, by using chronoamperometric methods, and setting both working electrodes to plate at the same time with a small potential difference between the two discs, symmetric smooth nanojunctions can be formed. In addition, the potentiostats automatic cut off allows reproducible junctions to be produced without human interventions.

In initial larger junctions discussed in Chapters 4, 5, and 6 the difference between the electrodes was set to 1 mV. For the smallest junctions formed, discussed in this chapter, a difference of 0.5 mV was selected, as the potential difference between the discs to ensure a current overload just prior to a connection forming between the discs. The reduced potential difference does not itself affect junction size, however it does increase system sensitivity, which is vital for smaller junction dimensions.

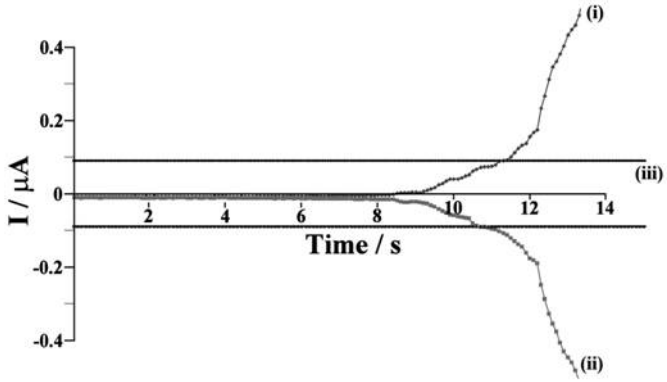

Figure 3.9 Chronoampometry showing growth via simultaneous deposition, (i,ii) represent the working electrodes, (iii) shows autolabs automatic cut of level.

It is tentatively predicted that the overloading current for all junction growth methods described above could be generated by the diffusion of charge carrying gold II between the two discs, and that only in close proximity is the concentration high enough to generate the overloads observed.

3.4. Controlling Junction Gap Size

3.4.1. Overpotential Controlling Gap Sizes

The driving force for the electro-deposition of gold is dependent on the applied overpotential, with the quality (or smoothness) of the deposits improving considerably at a lower overpotential (for a lower rate of deposition at more positive potentials). Figure 3.11A summarises the effect of the deposition potential on the resulting average gap size. In order to estimate the average gap size, SEM images were obtained. SEM images for an approximately 300 nm average gap size gold electrode junction are shown in Figure 3.10.

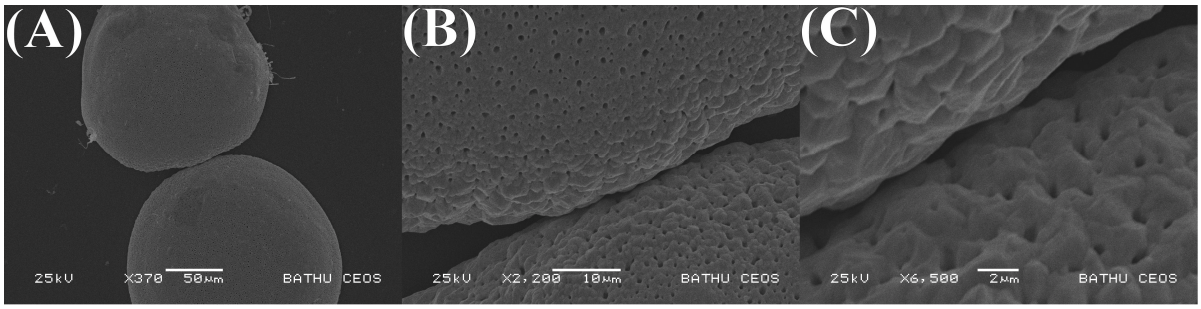

Figure 3.10 SEM images showing a paired gold junction electrode with an estimated average 300 nm gap. The image has been taken at three levels of magnification.

The surface roughness is relatively low and the inter-electrode gap well-defined. However, the gap size clearly varies with position and due to the gold surface curvature only an estimate can be given. The plot in Figure 3.11A demonstrates that the estimated gap size can be conveniently controlled when the deposition potential is changed, with very small gaps being observed for the lowest overpotentials. The deposition time for the small gaps is relatively long (up to 4 hours to automatic cut off), due to the lower deposition current. As previously mentioned, other parameters such as the pre-defined cut-off current, or the bias-voltage difference between the two electrodes did not significantly affect the gap size.

The voltammetric responses obtained for the new paired gold electrode junctions are strongly affected by the gap size (vide infra), but also by the overall junction geometry. The height of the gold growth and the curvature of the gold deposit within the junction zone are key parameters affecting the electrochemical performance. The schematic drawing in Figure 3.11B is indicating how the positioning of the two adjacent platinum disc electrodes and/or the resulting gold electrode diameter are expected to affect the junction zone. For the hypothetical case of gold electro-deposition of gold onto band electrodes (see Figure 3.11Biii) a more uniform junction zone can be predicted.

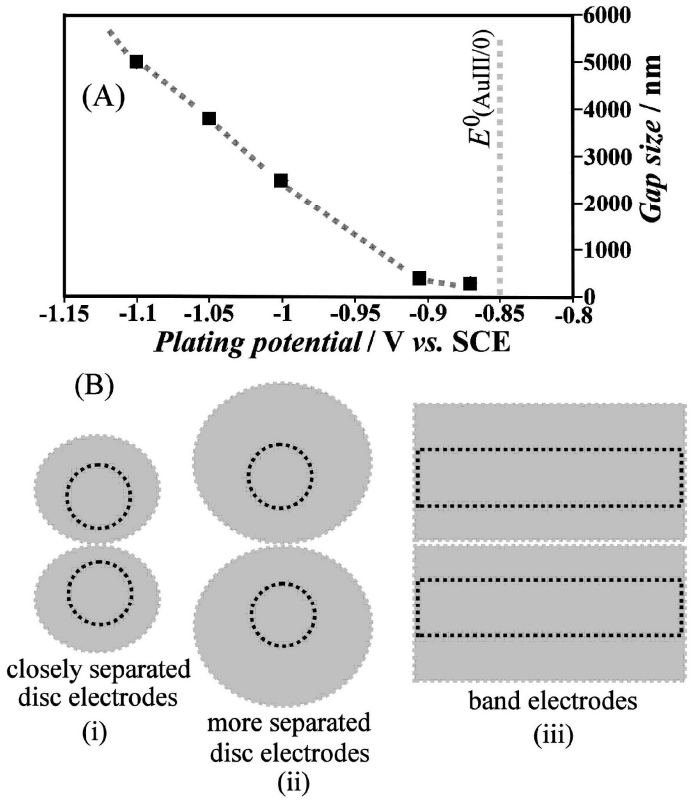

Figure 3.11 (A) Plot of the approximate junction gap for paired gold electrodes (from SEM images) versus the potential applied during electro-deposition. (B) Schematic drawing of the effect of electrode separation and shape on paired junction geometry: (i) for closely spaced disc electrodes less gold is deposited and the effect of curvature and height limit the junction zone; (ii) for more widely spaced disc electrodes the reduced curvature and increased height lead to a more extended junction zone; (iii) for band electrodes a more uniform elongated junction is expected.

3.4.2. Voltammetric Data for the Reduction of Alizarin Red S Obtained with the Paired Gold Junction Electrode: Gap size and Scan Rate Dependencies

In order to quantitatively explore the behaviour of the paired gold junction electrodes, experiments with a well known redox system, alizarin red S, are conducted. Alizarin red S is reduced reversibly in aqueous phosphate buffer solution pH 7 at a potential of -0.53 V vs. SCE (see Figure 3.12 [21]), and the process can be described as a two-electron two-proton reduction [22] with a diffusion coefficient $D_{\text{alizarin red S}} = 0.16 \times 10^{-9}$ m^2s^{-1} [23] (see Equation 3.1).

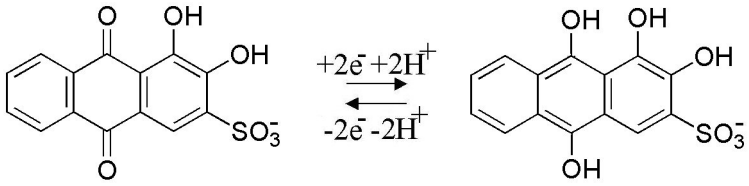

Equation 3.1

Voltammetric experiments were conducted in generator – collector mode with the variable potential applied to one gold electrode (generator) scanned from 0.0 to -0.9 V vs. SCE and the potential of the second electrode (collector) fixed at 0.0 V vs. SCE.

When considering a large junction (4-5 μm), formed using a relatively large overpotential of ca. -0.25 V, the generator current for the reduction of alizarin red S (see Figure 3.12B) shows peak features consistent with those expected from a conventional transient voltammetry at an electrode of approximately 200 μm diameter (see Figure 3.10A). However, the current observed at the collector electrode appears time-independent and is consistent with a steady state experiment. A well-defined limiting current is observed, which remains essentially constant even at scan rates up to 100 mVs^{-1} (see Figure 3.12C). A slight decrease in the limiting current associated with the onset of hysteresis (see Figure 3.12A) is indicative of the diffusion limitations in the gap zone. Due to the non-ideal geometry of the gap between the two gold electrodes, the effect will be gradual with zones of close separation still giving a full feedback response, while other regions in the gap already "decouple".

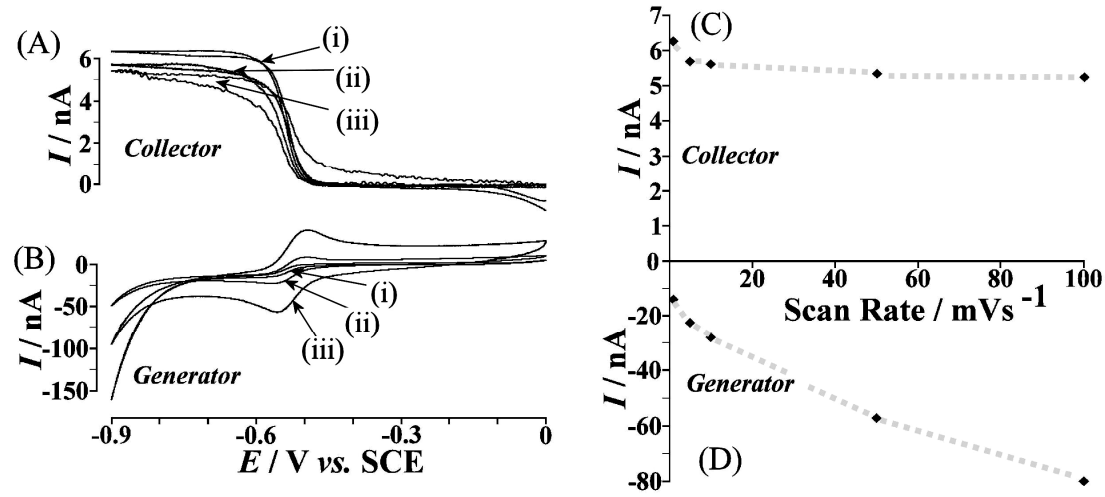

Figure 3.12 Cyclic voltammograms (scan rate (i) 1, (ii) 10, and (iii) 100 mVs^{-1}) for the reduction of 0.2 mM alizarin red S in 0.1 M phosphate buffer pH 7 detected at (A) the collector electrode (potential fixed at 0.0 V vs. SCE) and (B) the generator electrode for a 5 µm gap junction electrode. (C) Plot of the collector current versus the scan rate. (D) Plot of the generator current versus the scan rate.

The shape of the voltammogram in Figure 3.12Ai is consistent with an electrochemically reversible process. Analysis of the shape by plotting $\log\left(\frac{I}{I_{\lim} - I}\right)$ versus potential [24] provides a straight line with a 39 mV slope. This compares to the theoretically expected slope of 59/2 = 29 mV for a fully reversible 2-electron process and therefore only a small contribution from irreversible electron transfer (probably from narrow regions within the gap) appears to be present. Similarly, the analysis via the Tomeš criterion, $E_{3/4} - E_{1/2}$ = 15 mV and $E_{1/2} - E_{1/4}$ = 15 mV is consistent with a close to reversible two-electron transfer. [25] Here, the symbols $E_{1/4}$, $E_{1/2}$, and $E_{3/4}$ denote the potentials at ¼, ½, and ¾ of the limiting current, respectively.

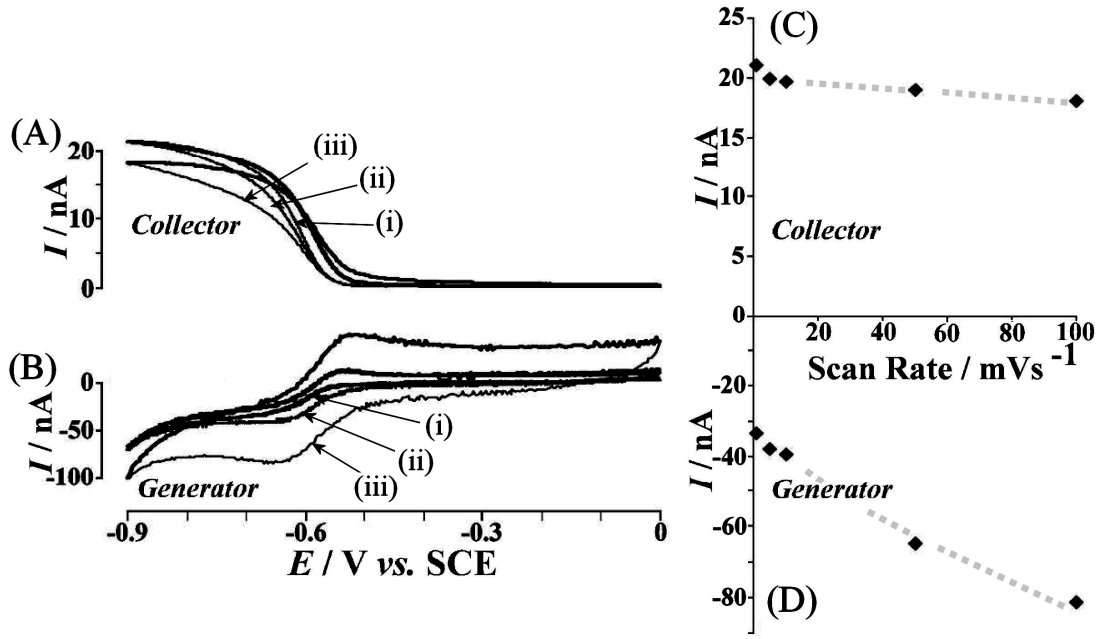

Figure 3.13 Cyclic voltammograms (scan rate (i) 1, (ii) 10, and (iii) 100 mVs^{-1}) for the reduction of 0.2 mM alizarin red S in 0.1 M phosphate buffer pH 7 detected at (A) the collector electrode (potential fixed at 0.0 V vs. SCE) and (B) the generator electrode for a 300 nm gap junction electrode. (C) Plot of the collector current versus the scan rate. (D) Plot of the generator current versus the scan rate.

Figure 3.13 shows voltammetric data obtained with a gold junction electrode with approximately 300 nm average gap size (see Figure 3.10). Generator and collector currents show a similar appearance when compared to the data obtained at a 5 μm gap electrode junction (see Figure 3.12). However, the shape of voltammograms has changed, and a considerable degree of irreversibility in the electron transfer is observed. The plot of $\log\left(\frac{I}{I_{\lim} - I}\right)$ versus potential gives a slightly curved line with a slope of approximately 99 mV suggesting quasi-reversibility (or a combination of irreversible and reversible electron transfer). The Tomeš criterion has changed to $E_{3/4}$-$E_{1/2}$ = 56 mV and $E_{1/2}$-$E_{1/4}$ = 28 mV which suggests irreversibility. With the help of the Mirkin-Bard tables [26] and assuming uniformly accessible electrodes an estimate can be obtained for the standard rate constant for heterogeneous electron transfer $k^o = 4 \times 10^{-4}$ ms^{-1}. However, the accessibility of the gold junction electrodes is highly non-uniform, and the voltammetric response clearly a combination of irreversible and reversible cases. For a more accurate analysis it will be necessary to take the geometry of the electrode junction into consideration.

The magnitude of the collector current, ca. 20 nA, is again relatively independent of scan rate up to 100 mVs^{-1}, but appears only slightly higher compared to that observed for the 5 μm gap electrode (ca. 5.5 nA, see Figure 3.12C). Due to the slower growth of the 300 nm junction, it is possible that the junction width and height are different and therefore, the collector current does not exhibit the simple inverse proportionality predicted by the Nernst diffusion layer model. [27] (Equation 3.2).

Equation 3.2

$$I_{\text{lim}} = \frac{nFDAc}{\delta}$$

In this equation the mass transport controlled limiting current I_{lim} is given by the number of electrons transferred per molecule diffusing to the electrode surface, n, the Faraday constant, F, the diffusion coefficient, D, the electrode area, A, the concentration, c, and the gap size, δ. The area A for the junction employed here is currently not well-defined and clearly affecting the collector currents.

3.4.3. Voltammetric Data for the Reduction of Alizarin Red S Obtained with the Paired Gold Junction Electrode: Concentration Dependencies

The ability of the paired gold junction electrode to provide stable and strongly enhanced collector current responses is of interest in analytical applications. In particular, with the 300 nm gap junction concentration measurements are readily performed down to sub-micro-molar concentration levels. Figure 3.14 shows a typical set of concentration dependent generator – collector voltammograms obtained for a range of alizarin red S concentrations. Good linearity for the collector limiting current is observed (see Figure 3.14C) and concentrations down to 500 nmol dm^{-3} were accessible before the low current signal became indistinguishable from the background response. The sensitivity of this method could be further improved by maintaining the gap size and by extending the width and height of the paired gold electrode junction (extending A in Equation 3.2) for example by employing band electrodes (see Figure 3.11iii).

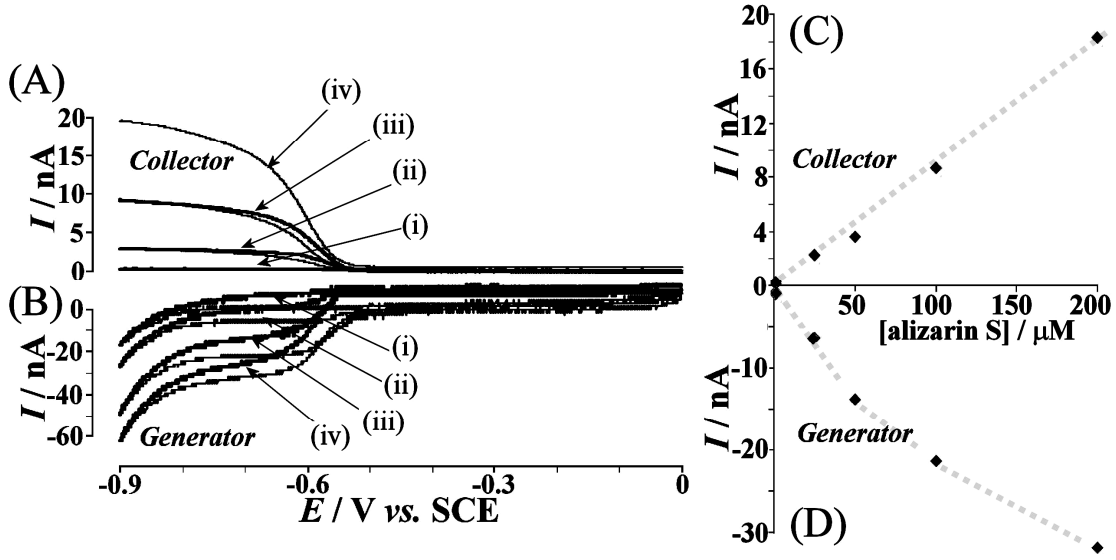

Figure 3.14 Cyclic voltammograms (scan rate 5 mVs^{-1}) for the reduction of (i) 0.001, (ii) 0.025, (iii) 0.1, and (iv) 0.2 mM alizarin red S in 0.1 M phosphate buffer pH 7 detected at (A) the collector electrode (potential fixed at 0.0 V vs. SCE) and (B) the generator electrode for a 300 nm gap junction electrode. (C) Plot of the collector current versus the alizarin red S concentration. (D) Plot of the generator current versus the alizarin red S concentration.

3.5. Conclusions

Paired gold junction electrodes have been prepared in a simple biopotentiostatic electro-deposition process and control of gap size (estimated by SEM) has been demonstrated using overpotentials. The resulting symmetric gold junction electrodes allow well defined collector current free of capacitive background responses to be obtained, and in particular, for the smaller gap junction, very low concentrations of analyte down to sub-micromolar levles (for alizarin red S) can be determined from the limiting current.

The increase in mass transport in the gap between adjacent gold electrodes, upon reducing the gap size, is shown to lead to a transition from reversible electron transfer to irreversible electron transfer (for alizarin red S in 0.1 M phosphate buffer pH 7) and the heterogeneous standard rate constant for electron transfer, $k^o = 4 \times 10^{-4}$ ms^{-1} was estimated. The new junctions formed will now be discussed in the following chapters, with reference to their use as new and novel sensors and analytical tools.

3.6. References

[1] P. Tomcik, S. Jursa, D. Bustin, V. Tvarozek, *Chemicke Listy*, 92, **1998**, 626-632.

[2] K. Eckhard, W. Schuhmann, *Analyst*, 133, **2008**, 1486-1497.

[3] J.D. Porter, A.S. Zinnwarner, *Physics Review Letters*, 73, **1994**, 2879-2882.

[4] W.J. Albery, M.L. Hitchman, "Ring-disc Electrodes", *Oxford University Press*, **1971**.

[5] M. Thompson, E.V. Klymenko, R.G. Compton, *Journal of Electroanalytical Chemistry*, 576, **2005**, 333-338.

[6] C. Amatore, I. Rubinstein (ed.), "Physical Electrochemistry", *Marcel Dekker*, **1995**, p. 131.

[7] K. Aoki, *Electroanalysis*, 5, **1993**, 627-639.

[8] P. Liljeroth, C. Johans, C.J. Slevin, B.M. Quinn, K. Kontturi, *Analytical Chemistry*, 74, **2002**, 1972-1978.

[9] S.L.R. Harvey, K.H. Parker, D. O'Hare, *Journal of Electroanalytical Chemistry*, 610, **2007**, 122-130.

[10] R.L. McCreery, J. Wu, R.P. Kalakodimi, *Physical Chemistry Chemical Physics*, 8, **2006**, 2572-2590.

[11] R. Hölzel, N. Gajovic-Eichelmann, F.F. Bier, *Biosensors and Bioelectronics*, 18, **2003**, 555-564.

[12] S. Carrara, J.D. Riley, V. Bavastrello, E. Stura, C. Nicolini, *Sensors and Actuators B-Chemical*, 105, **2005**, 542-548.

[13] J. Moreland, J.W. Ekin, *Journal of Applied Physics*, 58, **1985**, 3888-3895.

[14] K. O'Neill, E.A. Osorio, H.S.J. van der Zant, *Applied Physics Letters*, 90, **2007**, 133109.

[15] G. Staikov (ed.), "Electrocrystallization in Nanotechnology", *Wiley-VCH*, **2007**.

[16] B. Liu, J. Xiang, J.H. Tian, C. Zhong, B.W. Moa, F.Z. Yang, Z.B. Chen, S.T. Wu, Z.Q. Tian, *Electrochimica Acta*, 50, **2005**, 3041-3047.

[17] C.Z. Li, H.X. He, N.J. Toa, *Applied Physics Letters*, 77, **2000**, 3995-3997.

[18] A.F. Morpurgo, C.M. Marcus, D.B. Robinson, *Applied Physics Letters*, 74, **1999**, 2084-2086.

[19] Y.V. Kervennic, H.S.J. Van der Zant, A.F. Morpurgo, L. Gurevich, L.P. Kouwenhoven, *Applied Physics Letters*, 80, **2002**, 321-323.

[20] M. Schlesinger, M. Paunovic, "Modern Electroplating", *Wiley*, **2000**, p.205.

[21] V.E. Mouchrek, A.L.B. Marques, J.J. Zhang, G.O. Chierice, *Electroanalysis*, 11, **1999**, 1130-1136.

[22] V. Mirceski, M. Lovric, *Electroanalysis*, 9, **1997**, 1283-1287.

[23] R. Abdel-Hamid, M.K. Rabia, H.M. El-Sagher, *Bulletin of the Chemical Society of Japan*, 70, **1997**, 2389-2397.

[24] K.B. Oldham, J.C. Myland, "Fundamentals of Electrochemical Science", *Academic Press*, **1994**, p.290.

[25] A.J. Bard, L.R. Faulkner, "Electrochemical Methods, 2nd ed.", *John Wiley*, **2001**, p. 203.

[26] M.V. Mirkin, A.J. Bard, *Analytical Chemistry*, 64, **1992**, 2293-2302.

[27] A.J. Bard, L.R. Faulkner, "Electrochemical Methods, 2nd ed.", *John Wiley*, **2001**, p. 30.

4. Characterisation of Paired Gold Junction Electrodes I

Contents

Abstract

A 5 μm gap paired gold junction electrode is employed in generator-collector mode to give well defined steady-state feedback currents even for extremely low concentrations of analyte (sub μM) and without any contributions from capacitive charging. Four redox systems are investigated spanning a wide range of diffusion coefficients: (1) the one-electron oxidation of iodide to iodine, (2) the two-electron oxidation of hydroquinone to bezoquinone, (3) the two-electron reduction of alizarin red S and (4) the one-electron oxidation of the redox protein cytochrome *c*. Consistent results for these systems suggest that the junction zone dominates the behaviour of the electrode, it is also suggests how the junction could be calibrated and employed for electroanalysis.

Publication

R.W. French, F. Marken, *Journal of Solid State Electrochemistry*, 13, **2009**, 609-617

Chapter 4: Diffusion Effects Within Generator – Collector Mode

4.1. Introduction

As discussed in the last chapter, paired gold junction electrodes can easily be formed using bipotentiostatic electrodeposition in a simultaneous growth method to form junctions with varying gap sizes. In this chapter a junction with a gap size of approximately 5 μm is employed to gain further insight into the dimensions and characteristics of the electrodes themselves.

This will be done using generator-collector mode electrochemistry, where fast diffusion processes within the junction are driven by opposite potentials applied to the generator and collector terminals of the junctions. Diffusion processes at similar paired microelectrode systems have been investigated and treated theoretically by Oldham [1], Stone [2], Svir [3] and Baur [4], usually for the case of paired inlaid discs or bands and for the case of paired hemisphere electrodes [5]. Generator-Collector experiments are commonly carried out with micro-ring disc [6], rotating [7], or sono-ring-disc electrode systems [8], hydrodynamic double channel electrodes [9], SECM systems [10,11], dual or array band [12] or interdigitated array electrodes [13] as described in Chapter 1.2 and Chapter 1.3. Only for the latter two of these types of electrode systems can a symmetric diffusion field be established. The gap size for dual band or for interdigitated array electrode systems is crucial in determining the magnitude of the feedback current as well as the analytical sensitivity. Smaller gaps enhance the feedback current and are, therefore, more desirable.

The average gap size δ between generator and collector defines the time for the diffusion process to occur and, therefore the limiting current $I_{\mathrm{lim}} = \frac{nFDAc}{\delta}$ (with n, the number of electrons transferred per molecule diffusing to the electrode; F, the Faraday constant; D, the average diffusion coefficient; A, the active electrode area and; c, the concentration of the redox active species).

For a pair of approximately hemispherical electrodes, the average gap size is not well defined, and rather distinct zones are present. A schematic drawing in Figure 4.1 illustrates paired electrode with zones of fast, intermediate and slow diffusion, which also correspond to kinetic zones where fast, intermediate or slow reactions can be investigated. For redox systems with a sufficiently fast standard heterogeneous electron transfer rate constant $K_0 \geq \frac{D}{\delta}$, overall reversible electron transfer conditions are anticipated, and the currents flowing in the "fast-zone" should dominate the overall process.

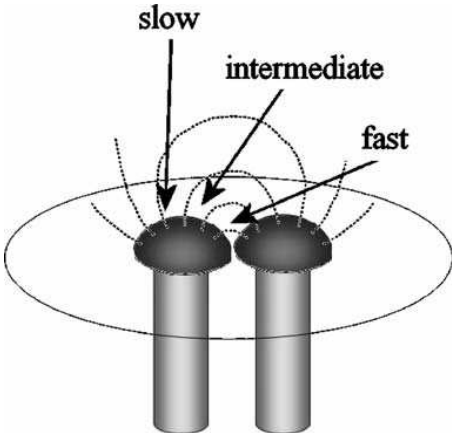

Figure 4.1 Schematic drawing of two approximately hemispherical electrodes, the diffusion field and the kinetic zones reflecting fast, intermediate and slow transport processes.

In this chapter, a set of four redox systems have been investigated to demonstrate that the ratio of the current flowing in the fast junction zone versus the overall current (e.g. the collector efficiency) can depend on the diffusion coefficient of the redox system.

Four redox systems are investigated (I^-/I_2, hydroquinone/benzoquinone, alizarin red S/hydroalizarin and ferri/ferrocytochrome *c*) with sufficiently fast rate for effects from heterogeneous electron transfer to remain insignificant. Reversible electron transfer and fast diffusion within the gold junction are shown to produce highly sensitive collector currents without contributions from capacitive or other background currents. This allows analytically useful steady state voltammograms to be recorded down to sub-micromolar concentrations. The effects of the diffusion coefficient are considered as well as the complete dimensions of the junctions produced.

4.2. Experimental

4.2.1. Reagents

Chemical reagents such as potassium hydroxide, potassium gold (I) dicyanide, potassium cyanide, potassium dihydrogen phosphate, dipotassium hydrogen phosphate, potassium carbonate, poly-(diallyldimethylammonium chloride) or PDDAC, potassium chloride, potassium iodide, sulphuric acid, hydroquinone, 4,4´-bipyridyl disulfide or aldrithiol-4 and alizarin red S were obtained commercially (Sigma-Aldrich) in analytical grade purity and used without further purification. Cytochrome *c* (equine heart, C7752, Sigma, 12384 Dalton) was purified by column chromatography using a PD-10 desalting column (Amersham Biosciences). Demineralised and filtered water was taken from a Vivendi purification unit with not less than 18 MOhm cm resistivity. Pureshield argon (BOC) was employed to de-aerate solutions. Experiments were conducted at 20±2 °C.

4.2.2. Instrumentation

For electrochemical and conductivity measurements a PSTAT30 bipotentiostat system (Autolab, EcoChemie, The Netherlands) was employed. In electrochemical experiments, a conventional three-electrode cell with platinum counter and saturated calomel reference (SCE, Radiometer, Copenhagen) were implemented. Scanning electron microscopy (SEM) images were obtained using a JEOL JSM6480LV system. Samples were gold sputter-coated prior to SEM imaging.

4.2.3. Formation of Paired Gold Electrode Junctions

A 5 μm junction was formed by taking a paired platinum disc electrode with approximately 125 μm separation introduced in Chapter 3. Plating was carried out via the simultaneous growth method as demonstrated in the previous chapter with one platinum disc electrode set to a potential of -1.11 V vs. SCE and, the secondary platinum disc electrode set to a slightly more positive deposition potential of -1.10 V vs. SCE. The difference in deposition potential was chosen minimal to reduce differences in the appearance of the resulting gold deposits. The automatic cut-off function (in the GPES software) was then used to stop the gold deposition process when the current exceeded 90 μA. After the cut-off point was reached, the electrode was removed from the gold plating

bath, rinsed with demineralised water, dried and tested. Conductivity tests with the dry paired gold junction electrode revealed no direct short circuit or tunnel currents. Figure 4.2 shows typical SEM images of the paired gold electrode system. The position of the underlying platinum disc electrodes is indicated with a dotted line.

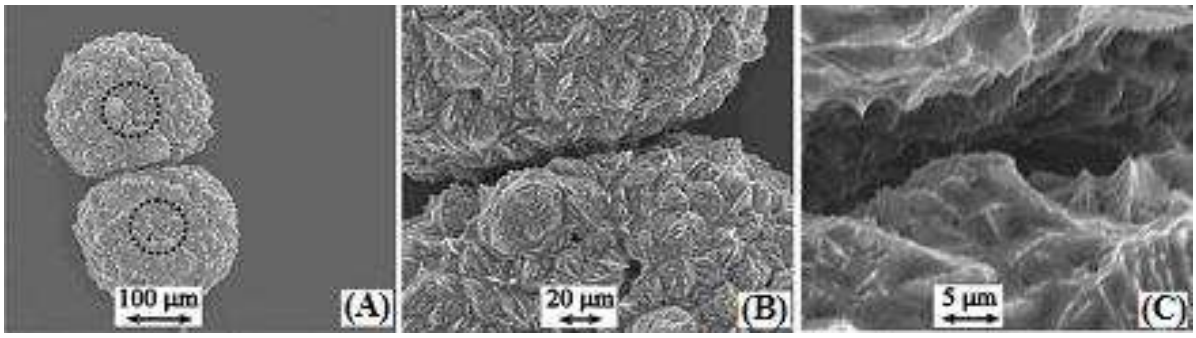

Figure 4.2 Scanning electron micrograph (SEM) images of paired gold junction electrodes. (A) Low magnification view of the two gold deposits and indicated with a dotted line the approximate location of the underlying platinum disc electrodes. Higher magnification images are shown in (B) and in (C) and show a junction with δ ≈ 5 µm average gap

4.3. Results and Discussion

4.3.1. Voltammetric Characterisation of Paired Gold Electrode Junctions I.: Oxidation of Iodide

The oxidation of iodide in aqueous 0.125 M H_2SO_4 occurs as an overall one-electron mechanism (see Equation 4.1 [14]). For this process, intermediates such as the I_3^- ion have been observed, but at sufficiently positive applied potential, a full conversion to I_2 is expected (see Equation 4.1). This process is employed here as a model case for relatively fast diffusion (with $D_{iodide}=1.9\times10^{-9}$ m^2 s^{-1} [15, 16]).

Equation 4.1

$$I^- \rightleftharpoons \tfrac{1}{2} I_2 + e^-$$

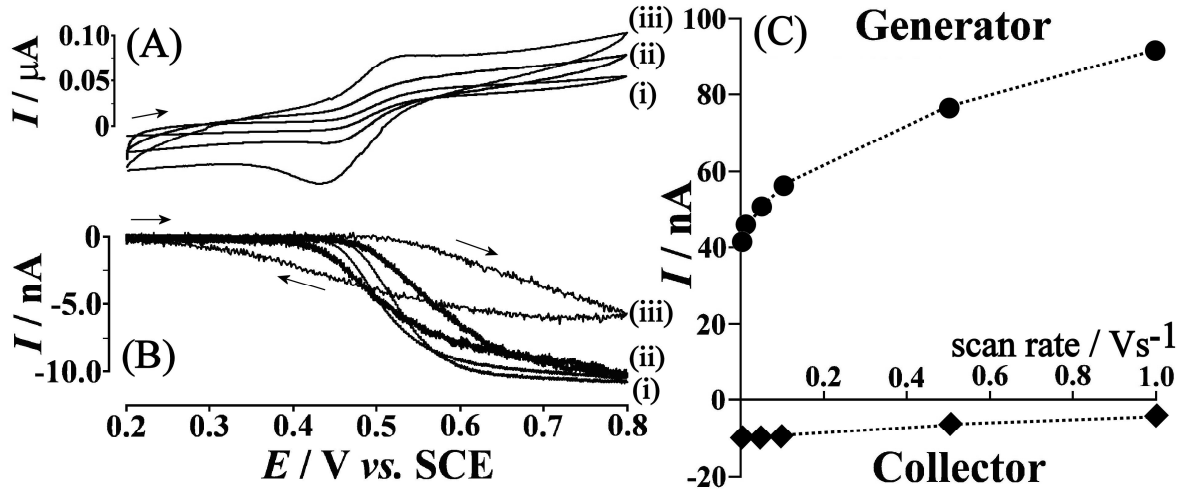

Figure 4.3 (A) Cyclic voltammograms (scan rate (i) 5 mVs^{-1}, (ii) 50 mVs^{-1}, (iii) 500 mVs^{-1}) for the oxidation of 0.2 mM I^- in aqueous 0.125 M H_2SO_4 at a paired gold junction electrode with the collector held at a potential of 0.2 V vs. SCE. The generator current is shown. (B) The collector current is shown. (C) Plot of the peak or limiting currents observed for the generator and the collector electrode versus scan rate.

Figure 4.3A shows typical voltammetric responses for the oxidation of 0.2 mM iodide in aqueous 0.125 M H_2SO_4. The generator electrode current plot shows a peak-shaped reversible response centered at 0.47 V vs. SCE at a scan rate of 0.5 V s^{-1} and a more step-shaped response at slower scan rate. The capacitive background current can be seen to dominate the voltammetric response.

In contrast, the collector current (see Figure 4.3B), which is recorded at a fixed potential of 0.2 V vs. SCE, shows a step-shaped steady state response centered at approximately 0.52 V vs. SCE without any capacitive background current contributions. A clear diffusion-related hysteresis effect is observed to cause a mismatch of forward and backward scan. With increasing scan rate this hysteresis effect also increases. Dimensional analysis allows the average junction gap to be expressed as shown in Equation 4.2

Equation 4.2

$$\delta \approx \sqrt{\frac{DRT}{v_{trans}F}}$$

Where D, the diffusion coefficient; R, the gas constant; T, the absolute temperature; F, the Faraday constant and ν_{trans}, the scan rate where 'decoupling' of generator and collector occurs. With an average junction gap of $\delta \approx 5$ μm (see Figure 4.2), the value for ν_{trans} is approximately 2 V s^{-1} in approximate agreement with the data in Figure 4.3B, where significant 'decoupling' is observed at a scan rate of 0.5 V s^{-1}. The steady state limiting collector current can be obtained reliably up to a scan rate of 100 mV s^{-1} (see Figure 4.3C).

For the iodide or iodine redox system, additional effects may arise from unequal diffusion coefficients ($D_{iodide} \neq D_{iodine}$), and kinetic information about the formation of the tri-iodide intermediate (both beyond the scope of this chapter) may be contained in the fast scan rate collector current responses. Next the voltammetric response is recorded at a constant scan rate of 5 mV s^{-1} and for a range of iodide concentrations (see Figure 4.4). Well-defined voltammetric responses are observed at the collector electrode even for sub-micromolar concentrations and good linearity of the plot of limiting current versus iodide concentration is observed over a range of 200 to 0.2 μM (see Figure 4.4C). The estimated collector efficiency for the iodide/iodine redox system is approximately 30 %.

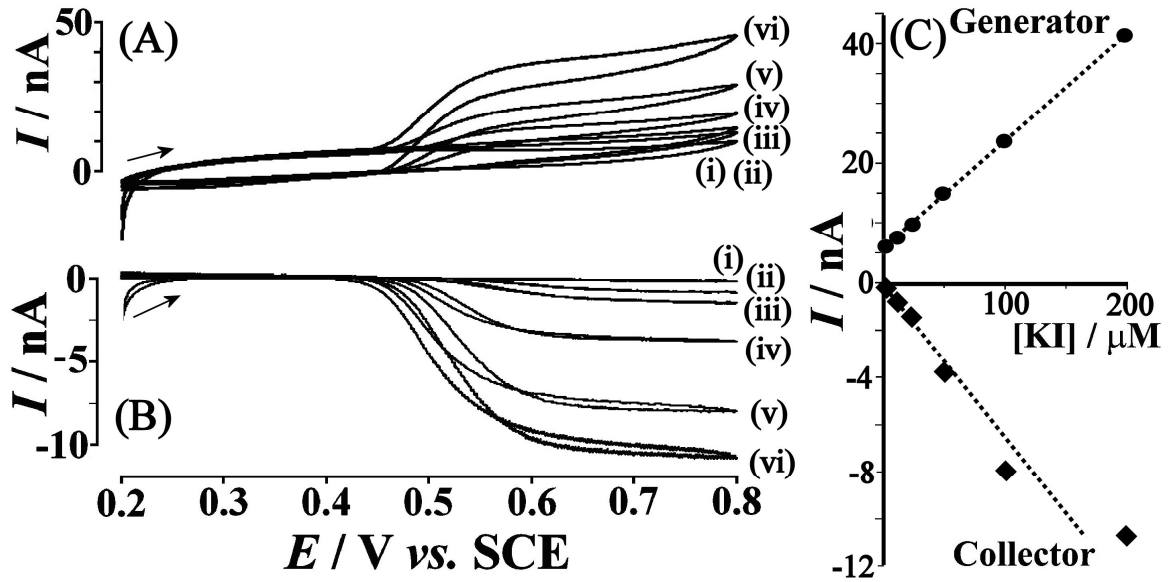

Figure 4.4 (A) Cyclic voltammograms (scan rate 5 mVs^{-1}) for the oxidation (i) 1, (ii) 12, (iii) 25, (iv) 50, (v) 100, and (vi) 200 μM I^- in aqueous 0.125 M H_2SO_4 at a paired gold electrode junction with the collector held at a potential of 0.2 V vs. SCE. The generator current is shown. (B) The collector current is shown. (C) Plot of the limiting currents observed for the generator and the collector electrode versus iodide concentration.

4.3.2. Voltammetric Characterisation of Paired Gold Electrode Junctions II.: Oxidation of Hydroquinone

The oxidation of hydroquinone to benzoquinone is a well-known model redox process with similarity to many naturally occurring quinone/quinol redox processes. [17] In aqueous media the process occurs as a chemically reversible two-electron oxidation (see Equation 4.3) with short-lived semiquinone intermediates. [18]

Equation 4.3

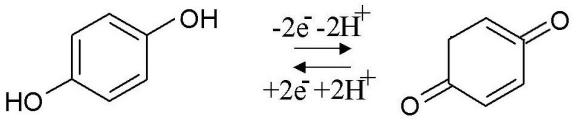

Figure 4.5 shows voltammetric data for the oxidation of 1 mM hydroquinone in aqueous 0.1 M phosphate buffer pH 7. Both, generator and collector electrodes give well-defined current responses, although the limiting current at the collector electrode is virtually constant over a range of scan rates (see Figure 4.5C). The hysteresis effect for the collector current is again observed (vide supra) but the effect is reduced (when compared to that for iodide oxidation). The decrease in hysteresis effect appears to be linked to the slower diffusion coefficient for hydroquinone ($D_{hydroquinone} = 0.85 \times 10^{-9}$ m^2s^{-1} [16]). It is likely that processes for redox systems with a smaller diffusion coefficient are more dominated by gap-diffusion and therefore more confined in the junction gap with reduced hysteresis (vide infra). Due to the symmetry of the generator-collector electrode system, the diffusion coefficients for both hydroquinone and benzoquinone should be taken into account, but these are assumed here to be equal in first approximation.

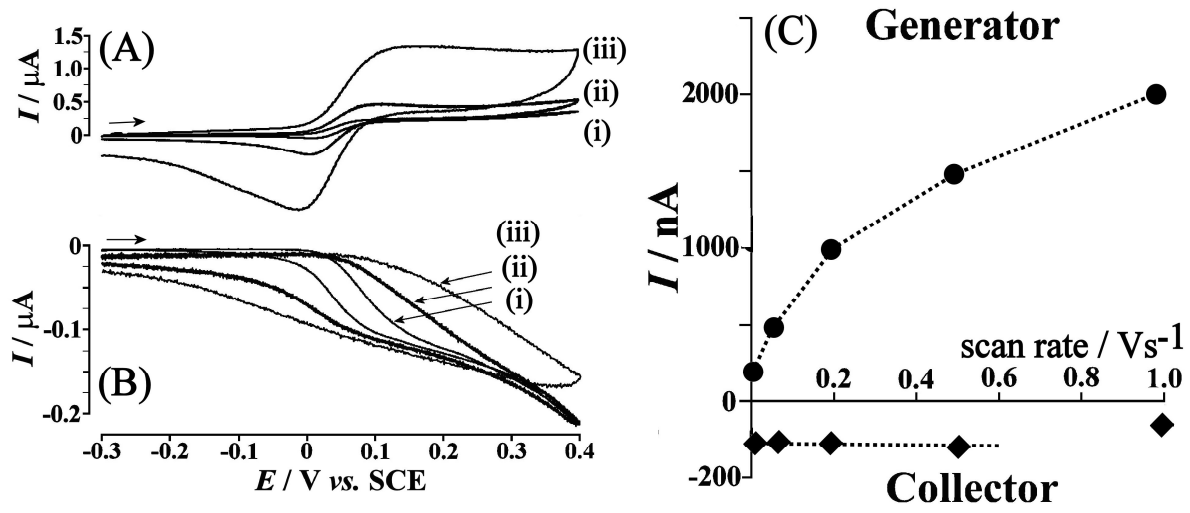

Figure 4.5 (A) Cyclic voltammograms (scan rate (i) 5, (ii) 50, (iii) 500 mVs^{-1}) for the oxidation of 1 mM hydroquinone in aqueous 0.1 M phosphate buffer pH 7 at a paired gold junction electrode with the collector held at a potential of -0.3 V vs. SCE. The generator current is shown. (B) The collector current is shown. (C) Plot of the peak or limiting currents observed for the generator and the collector electrode versus scan rate.

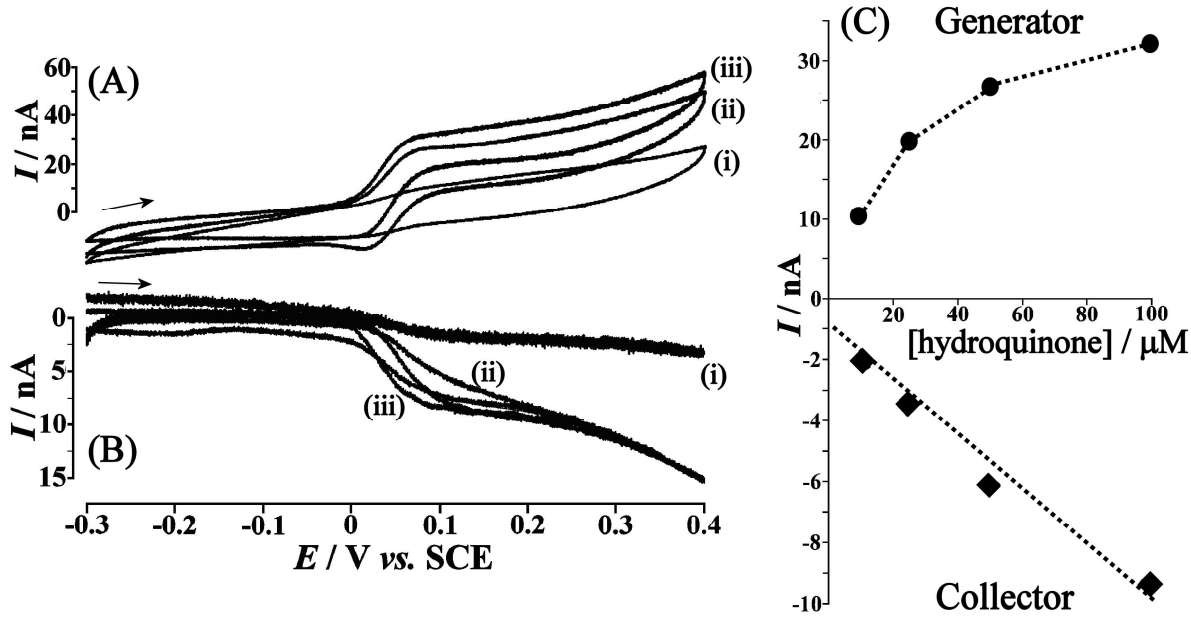

Figure 4.6. (A) Cyclic voltammograms (scan rate 5 mVs^{-1}) for the oxidation of (i) 1, (ii) 10, and (iii) 100 μM hydroquinone in aqueous 0.1 M phosphate buffer pH 7 at a paired gold junction electrode with the collector held at a potential of -0.3 V vs. SCE. The generator current is shown. (B) The collector current is shown. (C) Plot of the peak or limiting currents observed for the generator and the collector electrode versus hydroquinone concentration.

The effect of the hydroquinone concentration on the voltammetric signal is shown in Figure 4.6. The collector response is independent of capacitive background and therefore more reliable measured especially in the low concentration range. The approximate collection efficiency can be estimated as 25 %.

4.3.3. Voltammetric Characterisation of Paired Gold Electrode Junctions III.: Reduction of Alizarin Red S

The alizarin red S redox system has been employed in adsorptive stripping voltammetry for example, boron [19], zirconium [20], vanadium [21] and copper [22,23] and other oxophilic metals have been reported. The interaction of alizarin red S with proteins [24] and with DNA and damaged DNA [25] has been investigated by voltammetry. The mechanism for the reduction of alizarin red S follows a two-electron two-proton pathway [26,27] (see Equation 4.4).

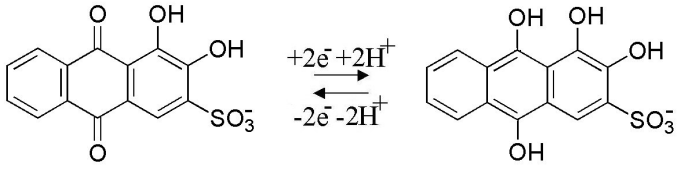

Equation 4.4

Figure 4.7 shows typical voltammetric responses for the reduction of 0.2 mM alizarin red S in aqueous 0.1 M phosphate buffer at pH 7. Both the reversible generator response and the collector signal are observed at ca. -0.55 V vs. SCE. The hysteresis effect is reduced (when compared to voltammograms for iodide and hydroquinone) and this may be attributed to a further reduced diffusion coefficient (with $D_{\text{alizarin red S}} = 0.16 \times 10^{-9}$ m^2s^{-1} [28], vide infra). Stable limiting currents are observed at the collector electrode even at scan rates up to 1 V s^{-1} (see Figure 4.7C).

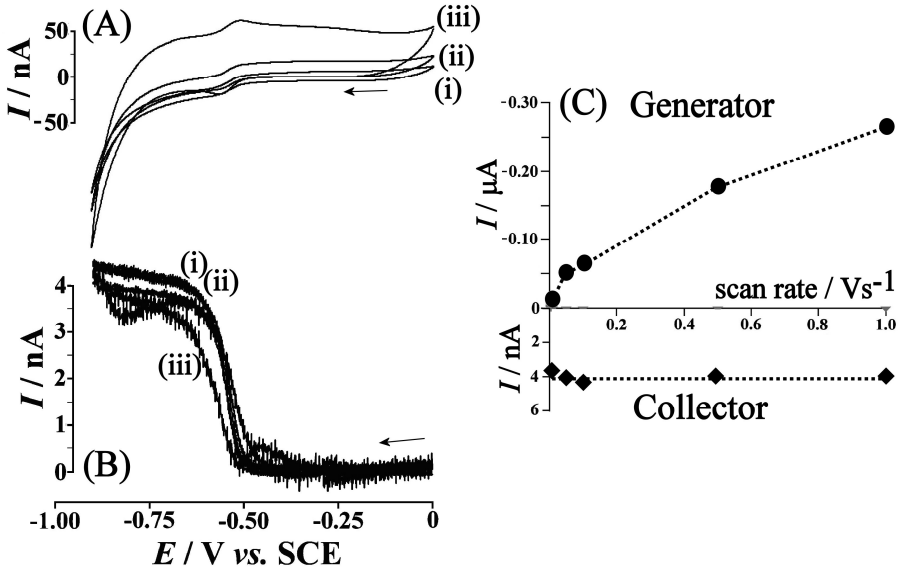

Figure 4.7 (A) Cyclic voltammograms (scan rate (i) 5, (ii) 10, (iii) 100 mVs^{-1}) for the reduction of 0.2 mM alizarin red S in aqueous 0.1 M phosphate buffer pH 7 at a paired gold junction electrode with the collector held at a potential of -0.2 V vs. SCE. The generator current is shown. (B) The collector current is shown. (C) Plot of the peak or limiting currents observed for the generator and the collector electrode versus scan rate.

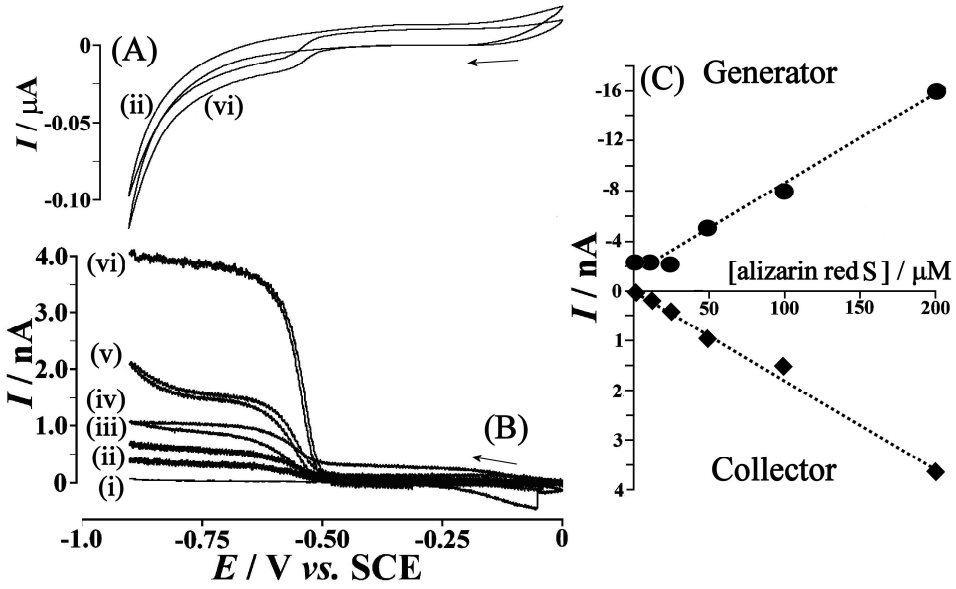

Figure 4.8. (A) Cyclic voltammograms (scan rate 5 mVs^{-1}) for the reduction of (i) 1, (ii) 12.5, (iii) 25, (iv) 50, (v) 100, and (vi) 200 μM alizarin red S in aqueous 0.1 M phosphate buffer pH 7 at a paired gold junction electrode with the collector held at a potential of -0.2 V vs. SCE. The generator current is shown. (B) The collector current is shown. (C) Plot of the peak or limiting currents observed for the generator and the collector electrode versus hydroquinone concentration.

The effect of the alizarin red S concentration on the voltammetric signals is summarized in Figure 4.8. Well-defined collector responses are observed down to sub-micromolar concentrations. The collection efficiency can be estimated as ca. 18 %.

4.3.4. Voltammetric Characterisation of Paired Gold Electrode Junctions IV.: Reduction of Cytochrome c

Fe(III/II) Cytochrome *c* redox system is investigated as an example of an extremely slow diffusion. The diffusion coefficient for Cytochrome *c* in aqueous phosphate buffer media has been reported as ca. 6×10^{-11} m^2s^{-1} [29] consistent with an almost spherical protein of ca. 34 Å diameter. The Cytochrome *c* redox system occurs naturally as an aqueous one-electron redox shuttle connecting cytochrome oxidase and reductase in the respiration process [30].

Cytochrome *c* has been widely used as a model redox protein in electrochemistry [31] following the first observation of direct interfacial electron transfer at surface modified gold electrodes by Hill et al. [32]. The reagent 4,4'-bipyridyl disulfide, when adsorbed onto the gold electrode (from a 1 mM solution in 0.1 M phosphate buffer pH 7) prior to contact with Cytochrome *c*, is effective in preventing interfacial protein de-naturation and it provides a suitable "docking site" for the protein to effectively exchange electrons with the underlying gold surface. This approach is employed here to allow Cytochrome *c* generator – collector experiments with two paired gold electrodes. The covalently attached heme unit within the Cytochrome *c* molecule is responsible for a one-electron transfer (see Equation 4.5 [33]).

Equation 4.5 $$Ferri - Cytochrome\ c \rightleftharpoons Ferri - Cytochrome\ c + e^-$$

Cyclic voltammograms for the oxidation and re-reduction of 25, 100, and 200 μM Cytochrome *c* dissolved in aqueous 0.1 M phosphate buffer pH 7 are shown in Figure 4.9.

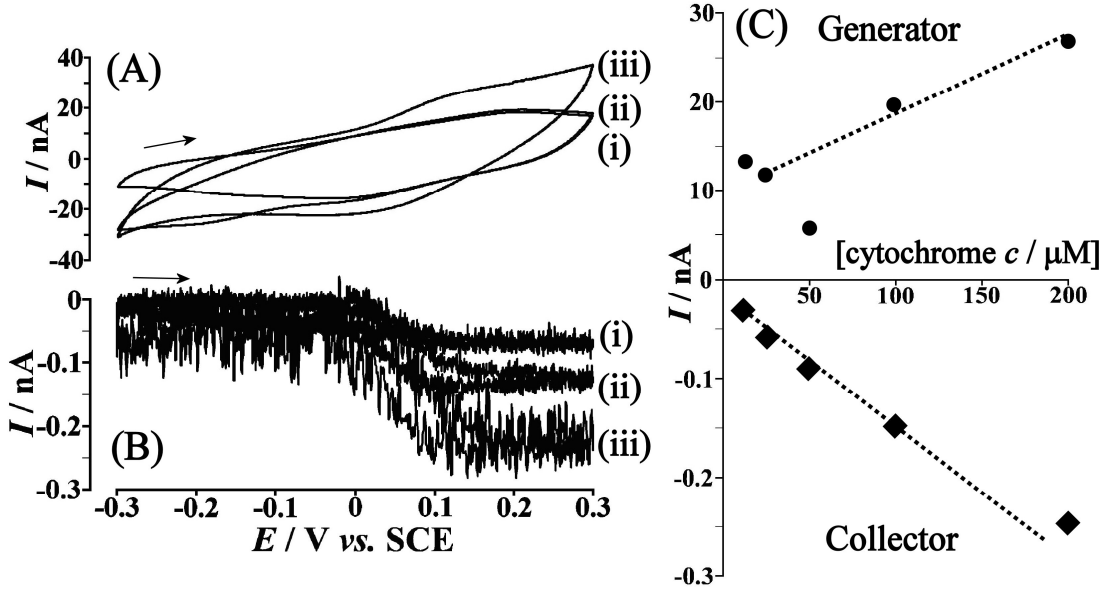

Figure 4.9 (A) Cyclic voltammograms (scan rate 5 mVs^{-1}) for the reduction of (i) 25, (ii) 100, and (iii) 200 μM Cytochrome *c* in aqueous 0.1 M phosphate buffer pH 7 at a paired gold electrode junction (gold surfaces modified by immersion into a solution of 1 mM 4,4'-bipyridyl disulfide) with the collector held at the open circuit potential observed prior to potential scan (typically 0.0 V vs. SCE). The generator current is shown. (B) The collector current (baseline corrected) is shown. (C) Plot of the peak or limiting currents observed for the generator and the collector electrode versus Cytochrome *c* concentration.

Current responses at the generator and at the collector electrode were observed, with a midpoint potential of approximately 0.05 V vs. SCE, which is in good agreement with the literature value for the Cytochrome *c* Fe(III/II) redox system. [34] The responses at the generator electrode are difficult to resolve, in particular, at lower concentrations of Cytochrome *c*. In contrast, well-defined sigmoidally shaped current responses are observed at the collector electrode down to micro-molar concentrations, and, only the increased background noise level at the pico-Ampère current range appears to limit the data quality. However, the clear collector current signals are obtained only after linear baseline correction, which is necessary due to an additional drift current. It was possible to minimize the baseline current drift by starting the experiment at open-circuit conditions. The additional background current component may be due to adsorption of Cytochrome *c*

and/or due to conduction through a monolayer of Cytochrome *c* bound onto the glass surface within the junction.

The approximate collection efficiency for Cytochrome *c* (estimated from Figure 4.9C) is reduced to ca. 1.5 %. For all redox systems studied in this report the magnitude of the collection efficiency appears to be strongly linked to the diffusion coefficient (see the plot in Figure 4.10B). The reason for this correlation may be based on the spatial distribution of the feedback current (see Figure 4.1).

For a redox system with a larger diffusion coefficient, the process within the inter-electrode gap, as well as, considerable parts of the process outside of the gap contribute to the feedback current. In contrast, for a redox system with a very small diffusion coefficient, the inter-gap diffusion appears to dominate the feedback current. This causes a much lower overall collection efficiency. Both, the collection efficiency and the considerable hysteresis effect, observed most clearly for iodide, can be explained based on the same diffusion phenomenon.

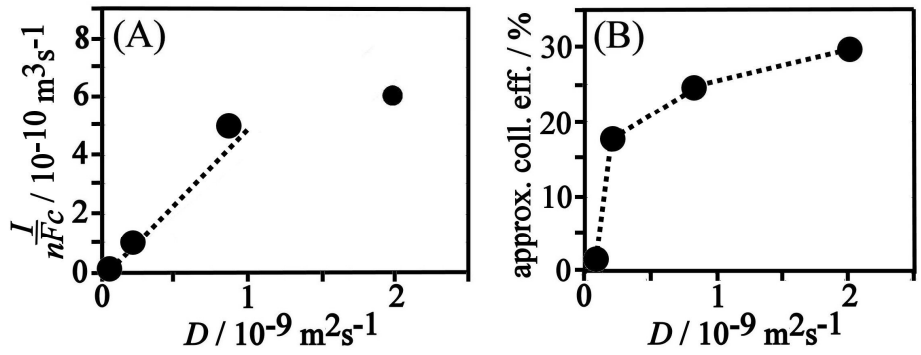

Figure 4.10 (A) Plot of the concentration-normalized limiting current for the collector electrode (see Figure 4.4C, Figure 4.6C, Figure 4.8C, and Figure 4.9C) versus the diffusion coefficients for cytochrome *c*, alizarin red S, hydroquinone, and iodide (see text). (B) Plot of the approximate collection efficiency versus the diffusion coefficient.

Figure 4.10A shows a plot of the slopes of individual current versus concentration plots (see Figure 4.4C, Figure 4.6C, Figure 4.8C, and Figure 4.9C) divided by nF versus the diffusion coefficient. For an electrode system dominated by gap diffusion a straight line

plot is expected with a slope $\frac{I/nFc}{D} = \frac{A}{\delta}$. It can be seen that for systems with fast rate of diffusion such as iodide, the apparent slope $\frac{A}{\delta}$ is too low and therefore δ is too high. For this system diffusion outside of the inter-electrode junction is significantly contributing to the current. If only the data points for the redox systems with lower rate of diffusion are considered, the slope can be estimated as $\frac{A}{\delta} = \frac{h \times l}{\delta} \approx 0.5$. The average gap size δ ≈ 5 μm and the gap length l ≈ 140 μm can be obtained from the SEM shown in Figure 4.2. Therefore an approximate of junction height is determined as ca. h ≈ 18 μm.

4.4. Conclusions

The paired junction electrode system has been characterised with four redox systems, selected to provide data for a wide range of diffusion coefficients. For all four redox systems, measurements at very low concentrations were feasible, due to the extremely low background currents observed for the steady state collector currents. Data analysis shows that for redox systems with sufficiently low diffusion coefficients, gap diffusion dominates and the gap dimensions can be estimated.

4.5. References

[1] K.B. Oldham, *Journal of Electroanalytical Chemistry*, 323, **1992**, 53-76.

[2] C.G. Philips, H.A. Stone, *Journal of Electroanalytical Chemistry*, 437, **1997**, 157-165.

[3] I.B. Svir, A.I. Oleinick, R.G. Compton, *Journal of Electroanalytical Chemistry*, 560, **2003**, 117-126.

[4] J.E. Baur, P.N. Motsegoog, *Journal of Electroanalytical Chemsitry*, 572, **2004**, 29-40.

[5] L.C.R. Alfred, K.B. Oldham, *Journal of Electroanalytical Chemistry*, 396, **1995**, 257-263.

[6] S.L.R. Harvey, K.H. Parker, D. O'Hare, *Journal of Electroanalytical Chemistry*, 610, **2007**, 122-130.

[7] Y.V. Pleskov, V.Y. Filinovskii, "The Rotating Disc Electrode, Plenum", *Plenum*, **1976**.

[8] L.B. Nei, F. Marken, Q. Hong, R.G. Compton, *Journal of the Electrochemical Society*, 144, **1997**, 3019-3026.

[9] M. Thompson, O.V. Klymenko, R.G. Compton, *Journal of Electroanalytical Chemistry*, 576, **2005**, 333-338.

[10] G. Nagy, L. Nagy, *Fresenius Journal of Analytical Chemistry*, 366, **2000**, 735-744.

[11] P. Liljeroth, C. Johans, C.J. Slevin, B.M. Quinn, K. Kontturi, *Analytical Chemistry*, 74, **2002**, 1972-1978.

[12] I. Streeter, N. Fietkau, J. Del Campo, R. Mas, F.X. Munoz, R.G. Compton, *Journal of Physical Chemistry C*, 111, **2007**, 12058-12066.

[13] K. Aoki, *Electroanalysis*, 5, **1993**, 627-639.

[14] R.P. Akkermans, F.L. Qui, S.L. Roberts, M.F. Suarez, R.G. Compton, *Journal of Physical Chemistry B*, 103, **1999**, 8319-8327.

[15] F. Marken, R.P. Akkermans, R.G. Compton, *Journal of Electroanalytical Chemistry*, 415, **1996**, 55-63.

[16] R.N. Adams, "Electrochemistry at Solid Electrodes", *Marcel Dekker*, **1969**, pg. 220.

[17] J.T. Nurmi, P.G. Tratnyek, *Environmental Science and Technology*, 36, **2002**, 617-624.

[18] M. Bauscher, W. Mantele, *Journal of Physical Chemistry*, 96, **1992**, 11101-11108.

[19] I. Sahin, N. Nakiboglu, *Analytica Chimica Acta*, 572, **2006**, 253-258.

[20] Y.H. Li, Q.L. Zhao, M.H. Huang, *Microchimica Acta*, 157, **2007**, 245-249.

[21] Y.H. Li, Y.X. Wang, M.H. Huang, *Electroanalysis*, 20, **2008**, 1440-1444.

[22] K.K. Shiu, F.Y. Song, *Electroanalysis*, 10, **1998**, 256-261.

[23] P.H. Deng, J.J. Fei, J. Zhang, J.N. Li, *Electroanalysis*, 20, **2008**, 1215-1219.

[24] W. Sun, K. Jiao, *Talanta*, 56, **2002**, 1073-1080.

[25] Z.S. Yang, D.P. Zhang, H.Y. Long, G.C. Zhao, *Electroanalysis*, 19, **2007**, 2577-2582.

[26] V.E. Mouchrek, A.L.B. Marques, J.J. Zhang, G.O. Chierice, *Electroanalysis*, 11, **1999**, 1130-1136.

[27] V. Mirceski, M. Lovric, *Electroanalysis*, 9, **1997**, 1283-1287.

[28] R. Abdel-Hamid, M.K. Rabia, H.M. El-Sagher, *Bulletin of the Chemical Society of Japan*, 70, **1997**, 2389-2397.

[29] H.A.O. Hill, Y. Nakagawa, F. Marken, R.G. Compton, *Journal of Physical Chemistry*, 100, **1996**, 17395-17399.

[30] L. Stryer, "Biochemistry. 4th ed", *W.H. Freeman and Co.*, **1995.**

[31] K.J. McKenzie, F. Marken, *Langmuir*, 19, **2003**, 4327-4331.

[32] M.J. Eddowes, H.A.O. Hill, *Journal of the American Chemical Society*, 101, **1979**, 4461-4464.

[33] A.B. Toth, J.Q. Chambers, "Electroanalytical methods for biological materials.", *Marcel Dekker*, **2002.**

[34] M.J. Eddowes, H.A.O. Hill, K. Uosaki, *Journal of the American Chemical Society*, 101, **1979**, 7113-7114.

5. Characterisation of Paired Gold Junction Electrodes II

Contents

Abstract

In this chapter, the use of paired gold junction electrodes as analytical sensing modules will be demonstrated. First, using the chemically reversible oxidation of 1, 1'-ferrocenedimethanol down to sub-micromolar analyte concentrations. Secondly the previously believed chemically irreversible oxidation of nitric oxide is investigated, with evidence for a nitrosonium phosphate intermediate

Publication

R.W. French, A.M. Collins, F. Marken, *Electroanalysis*, 20, **2008**, 2403-2409.

Chapter 5: Chemically Irreversible Processes Within a Paired Gold Junction Electrode.

5.1. Introduction

As demonstrated in the previous chapters, fast mass transport effects can be achieved by bringing two macro-electrodes into close proximity and establishing a generator-collector feedback current. This methodology can commonly be seen applied in interdigitated array electrode systems [1] and in SECM feedback experiments. [2] It has already been shown that by growing the paired gold electrodes into close proximity, a short diffusion path with fast interelectrode diffusion is achieved. The resulting feedback generator-collector currents are high, with the collector signal showing no contributions from capacitive background currents.

Within this chapter, the electrochemical reversible oxidation of 1, 1'- ferrocenedimethanol will be demonstrated, and used to calibrate a new junction electrode as well as supplying information about the gap dimensions. Finally the oxidation of the chemically irreversible nitric oxide, NO, at the gold electrode will be investigated in a phosphate buffer media.

Nitric oxide is a key intermediate in important biological process [3,4], and nitrosonium (NO^+) has also been considered biologically relevant. [5,6] The oxidation of nitric oxide at the gold electrodes has been studied by Vooys et al. [7], and gold nanoparticles [8,9,10] as well as gold-Nafion sensor electrodes [11] have been proposed. All of these reports are consistent with the chemically irreversible oxidation of NO in aqueous media, often proceeding via multielectron pathways and without NO^+ - related intermediates. Here the paired gold junction electrode systems discussed in previous chapters are employed to identify a potential nitrosonium phosphate intermediate.

5.2. Experimental

5.2.1. Reagents

Chemical reagents such as potassium hydroxide, potassium cyanide, potassium dihydrogen phosphate, di-potassium hydrogen phosphate, potassium carbonate, potassium aurocyanide, poly(diallydimethylammonium chloride) or PDDAC, potassium chloride, nitric oxide (lecture steel cylinder), and 1,1′-ferrocenedimethanol were obtained commercially (Sigma-Aldrich) and used without further purification. Demineralized and filtered water was taken from an Elga purification unit with not less than 18 MOhm cm resistivity. Pureshield argon (BOC) was employed to deaerate solutions prior to experiments.

5.2.2. Instrumentation

For electrochemical and conductivity measurements a PGSTAT30 bipotentiostat system (EcoChemie Netherlands) was employed. In electrochemical experiments a conventional three electrode cell with platinum counter and saturated calomel reference (SCE, Radiometer, Copenhagen) were employed. Scanning electron microscopy (SEM) images were obtained using a JEOL JSM6480LV system. All experiments were conducted under argon (Pureshield, BOC) and at a temperature of 20±2 ºC (unless stated otherwise).

5.2.3. Formation of Paired Gold Junction Electrode

Junctions were formed using the simultaneous deposition methodology discussed in Chapter 3. Working electrode one and working electrode two were set to -1.11 V vs. SCE and -1.10 V vs. SCE respectively, with the automatic cut of current set at 90 µA. After the cut-off point was reached, the electrode was removed from the gold plating bath, rinsed with demineralised water, and used for experiments. Conductivity tests with the dry paired gold electrode junction revealed no direct short circuit or tunnel currents. Figure 5.1 shows typical SEM images of the gold plated junction electrode system.

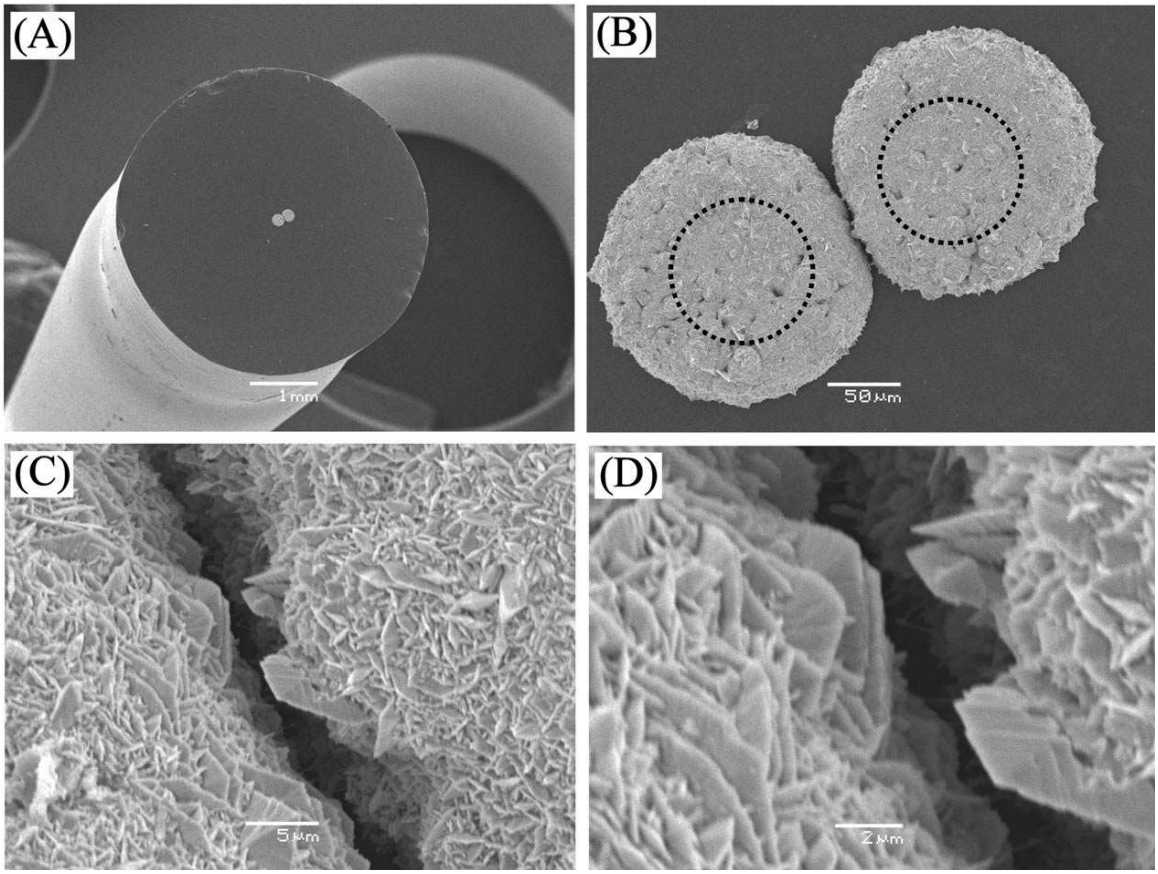

Figure 5.1 Scanning electron micrograph (SEM) images of paired gold junction electrodes, (A) Low magnification view of the glass body. (B) Top view of the gold electrodes and indicated with a dotted line the location of the underlying platinum disc electrodes. Higher magnification images are shown in (C) and in (D) where the micron-sized gap and faceting of individual gold crystallites can be seen.

5.3. Results and Discussion

5.3.1. Voltammetric Characterisation of Paired Gold Junction Electrodes I: Oxidation of 1,1′-Ferrocenedimethanol.

To further establish the voltammetric characteristics and potential applications of the paired gold junction electrodes and to calibrate a junction grown by bipotentiostatic deposition initial voltammetric experiments were conducted with

1,1′ -ferrocenedimethanol model redox system [12], (employed here in 0.1 M KCl), with a highly electrochemically reversible one-electron oxidation mechanism (see Equation 5.1).

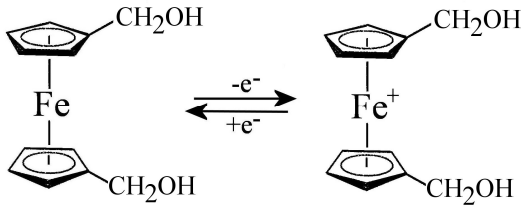

Equation 5.1

Figure 5.2A shows voltammetric responses obtained for the oxidation of 250 μM 1,1'-ferrocenedimethanol. Qualitatively, a sigmoidally shaped response is obtained with a half wave potential approximately $E_{½}$ = 0.45 V vs. SCE. Both gold electrodes contribute to this response due to Faradaic coupling (transfer of the potential from one electrode to the next by the diffusing redox system). The same voltammetric response is observed with only one or with both electrodes connected as working electrode. Next, the collector electrode was set to a potential of 0.0 V vs. SCE and the potential of the generator electrode scanned. The voltammograms, shown in Figure 5.2B, clearly shows a less capacitive current response and a slight increase in the mass transport controlled limiting current, in spite of the electrode size being effectively halved. The corresponding collector current is shown in Figure 5.2C. There is no capacitive current associated with the collector current response, and therefore, (at a sufficiently slow scan rate) the signal perfectly re-traces in the forward and backward potential scans.

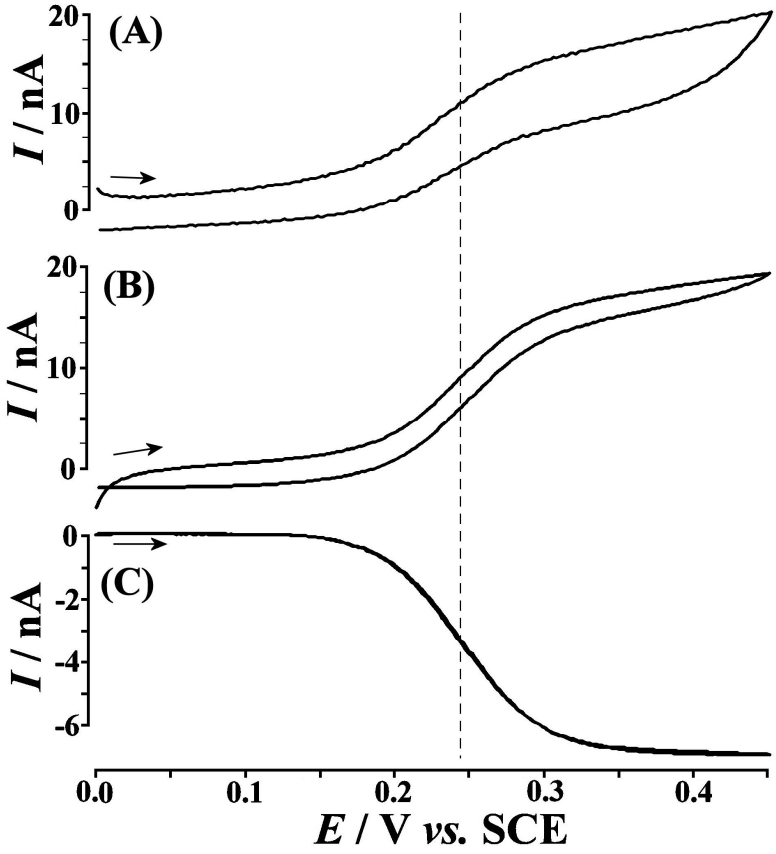

Figure 5.2 Cyclic voltammograms (scan rate 50 mVs^{-1}) for the oxidation of 250 µM 1,1'-ferrocenedimethanol in aqueous 0.1 M KCl at (A) a paired gold electrode (faradaically coupled), (B) the gold generator electrode (collector electrode potential at 0.0 V vs. SCE), and (C) the collector electrode.

Analysis of the current response observed for the collector electrode, by comparison with the theoretically predicted voltammetric response for an electrochemically reversible process [13], shows a perfect match with no indication of quasi-reversibility. The rate of interfacial electron transfer at the gold electrode surface appears to be sufficiently fast and only diffusion is rate limiting. This in turn allows voltammetric responses to be employed to further characterize the gap between the two gold electrodes.

Figure 5.3 summarises voltammetric data obtained for the oxidation of 250 μM 1,1'-ferrocenedimethanol in aqueous 0.1 M KCl as a function of scan rate.

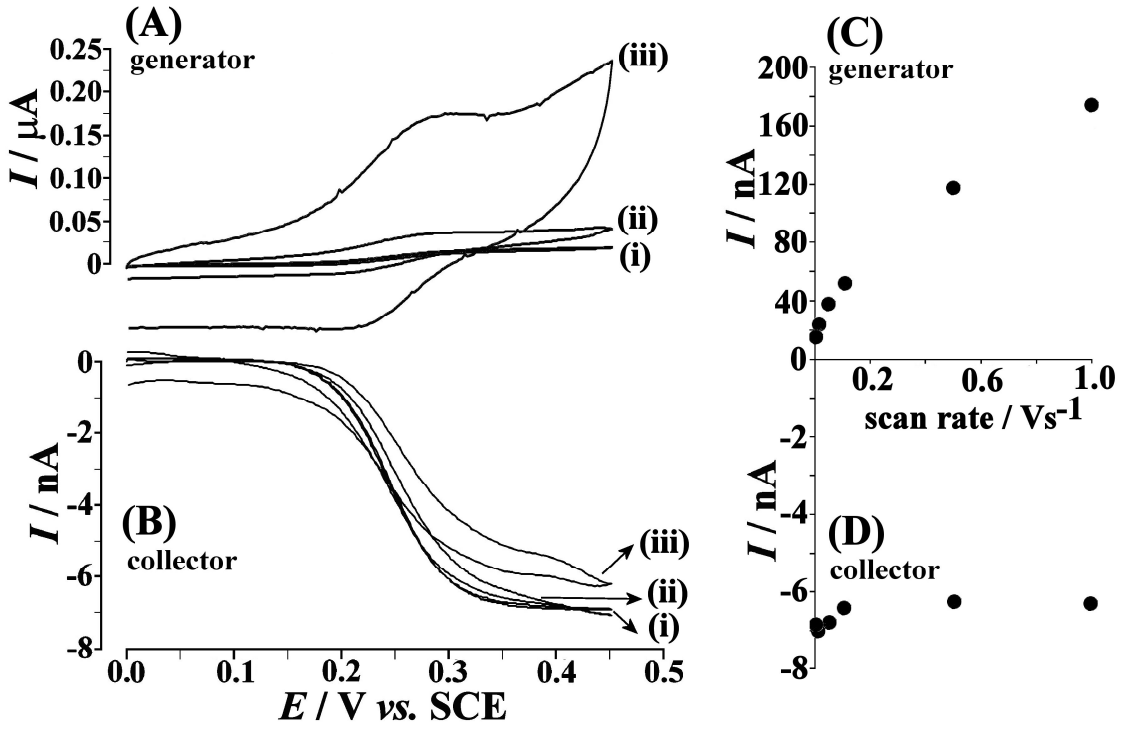

Figure 5.3 Cyclic voltammograms (scan rate (i) 1 mVs^{-1}, (ii) 50 mVs^{-1}, and (iii) 1 Vs^{-1}) for the oxidation of 250 μM 1,1'-ferrocenedimethanol in aqueous 0.1 M KCl obtained at (A) a gold generator electrode and (B) a gold collector electrode (potential 0.0 V vs. SCE). (C,D) Plots showing variation of the peak and limiting current with scan rate for the generator and collector electrodes.

The current response at the generator current clearly increases with scan rate (see Figure 5.3C), and indeed, a more peak-shaped response is observed at higher scan rates. In contrast, at the collector electrode a sigmoidally shaped current signal is observed, which is almost independent of the scan rate (see Figure 5.3D). Interestingly, a non-capacitive hysteresis effect is emerging in the collector current at scan rates higher than ca. 50 mVs^{-1}. This deviation from the steady state current response is due to mass transport delays, and therefore, it contains information about the inter-electrode junction geometry. An estimate of the average junction gap, δ, can be obtained from dimensional analysis with Equation 5.2.

Equation 5.2

$$\delta \approx \sqrt{\frac{DRT}{v_{trans}F}}$$

Giving $\delta \approx 4.2$ μm (assuming a diffusion coefficient for 1,1'-ferrocenedimethanol of $D = 0.7 \times 10^{-9}$ m^2s^{-1} [14] and an estimated transition scan rate of $v_{trans} = 1$ Vs^{-1}). Within the gap (see Figure 5.1) the value of δ is not uniform, but the value estimated here, is in good agreement with the average gap size in SEM images. With the average gap size estimated, it is possible to apply the Nernst diffusion layer model (see Equation 5.3 [15]) to obtain an estimate of the active geometric area within the gap between the two gold electrodes.

Equation 5.3

$$I_{\text{lim}} = \frac{nFDAc}{\delta}$$

In this expression the steady state mass transport controlled limiting current I_{lim} is given by n, the number of electrons per molecule diffusing to the electrode surface, F, the Faraday constant, D, the diffusion coefficient, c, the bulk concentration, and δ, the diffusion layer thickness (which is assumed approximately consistent with the average gap size). With the parameters $\delta = 4.2$ μm, $n = 1$, $F = 96487$ $Cmol^{-1}$, $D = 0.7 \times 10^{-9}$ m^2s^{-1}, $c = 0.25$ mol m^{-3}, and $I_{lim} = 7$ nA (see Figure 4B), the approximate area is $A = 16 \times 10^{-10}$ m^2. This allows the approximate height of the junction (see Figure 5.1B) to be estimated as 16 μm.

Next, the effect of the 1,1'-ferrocenedimethanol solution concentration is studied. Data in Figure 5.4 summarise the generator and collector current responses for lower 1,1'-ferrocenedimethanol concentrations. An excellent linear correlation is observed for both electrodes. The well-defined response at the collector electrode remains clear and quantitative even in the sub-micromolar concentration range (measurements were performed down to 100 nM concentration). This supports data gathered from Chapter 4 and further demonstrates the benefits of the paired gold junction electrodes, in that, the collector current sensitivity reaches very low concentrations of analyte. A further benefit can be observed for chemically highly irreversible redox processes, where short-lived intermediates are generated only very close to the electrode surface.

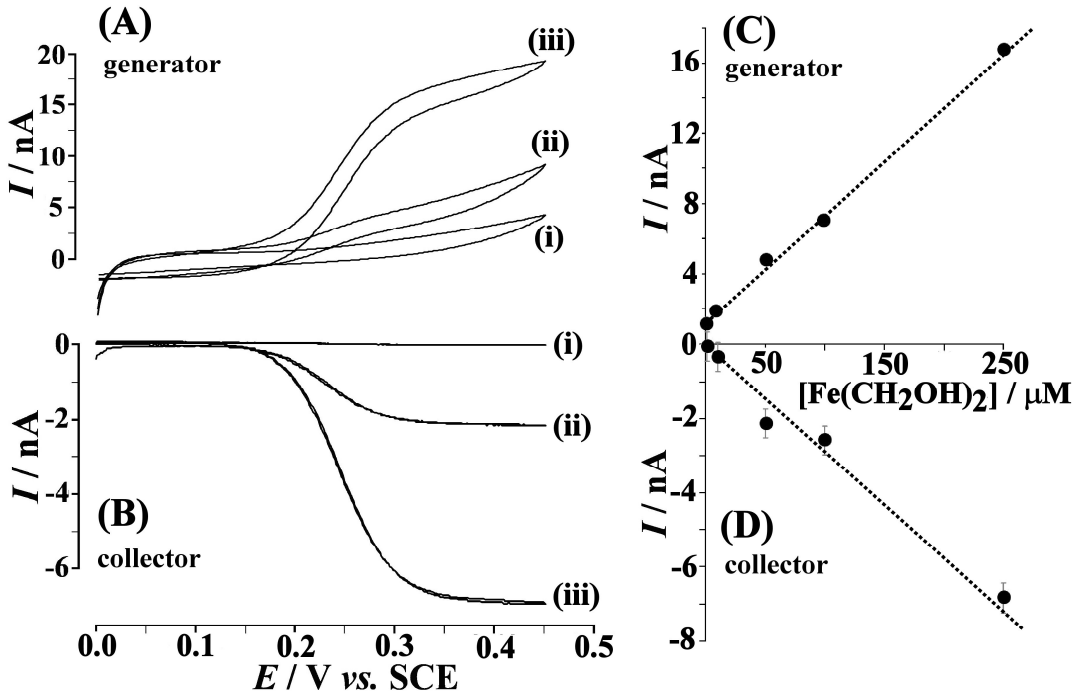

Figure 5.4 Cyclic voltammograms (scan rate 1 mVs^{-1}) for the oxidation of 1,1'-ferrocenedimethanol (concentration (i) 1 μM, (ii) 50 μM, (iii) 250 μM) in aqueous 0.1 M KCl obtained at (A) a gold generator electrode and (B) a gold collector electrode (potential 0.0 V vs. SCE). (C,D) Plots of the peak or limiting current versus 1,1'-ferrocenedimethanol concentration.

5.3.2. Voltammetric Characterisation of Paired Gold Junction Electrodes II: Oxidation of Nitric Oxide

As discussed in the introduction, nitric oxide (NO) is a key intermediate in important biological processes [3,4], and also nitrosonium (NO^+) has been considered biologically relevant. [5,6] This makes it an attractive species to use as a real sensing test for the paired gold junction Electrodes. Electrochemically, the oxidation of NO to NO^+ should proceed as a one-electron process (Equation 5.4).

Equation 5.4 $$NO \rightleftharpoons NO^+ + e^-$$

The hydrolysis of nitrosonium, NO^+, is known to be extremely rapid in liquids [16] (estimated lifetime in water ca. 3×10^{-10} s [17,18]) and somewhat slower in the atmosphere. [19] In some organic solvents NO^+ is stable (sometimes employed as a one electron transfer reagent [20]) and based on this, extremely sensitive sensing methods have been proposed. [21] However, in aqueous media very rapid hydrolysis of nitrosonium occurs (see Equation 5.5) with an equilibrium constant of $K_4 = 3.3 \times 10^6$ M. [22]

Equation 5.5

$$NO^+ + H_2O \rightleftharpoons H^+ + HNO_2$$

Figure 5.5 shows typical cyclic voltammograms for the oxidation of NO in 0.1 M phosphate buffer pH 7 obtained at a paired gold generator-collector electrode system. In Figure 5.5A the oxidation response in the presence of 10 μM NO is clearly observed. This oxidation process is denoted P1 with a second underlying oxidation process P2 (vide infra). This oxidation process at the generator electrode appears chemically irreversible and, only at higher potential scan rates a clear reduction response, P3, is observed.

In spite of the chemically irreversible nature of the anodic process, a clear cathodic signal is detected at the collector electrode (see Figure 5.5B). As previously shown chemically reversible redox systems such as 1,1'-ferrocenedimethanol, the steady state collector current reaches approximately 35 % of the generator current, but here the magnitude of the collector response is only approximately 1 % of the generator response (and dependent on scan rate, vide infra). Therefore, it is likely that a short-lived intermediate such as NO^+ (which is undergoing hydrolysis within the diffusion gap) is responsible for the small collector response.

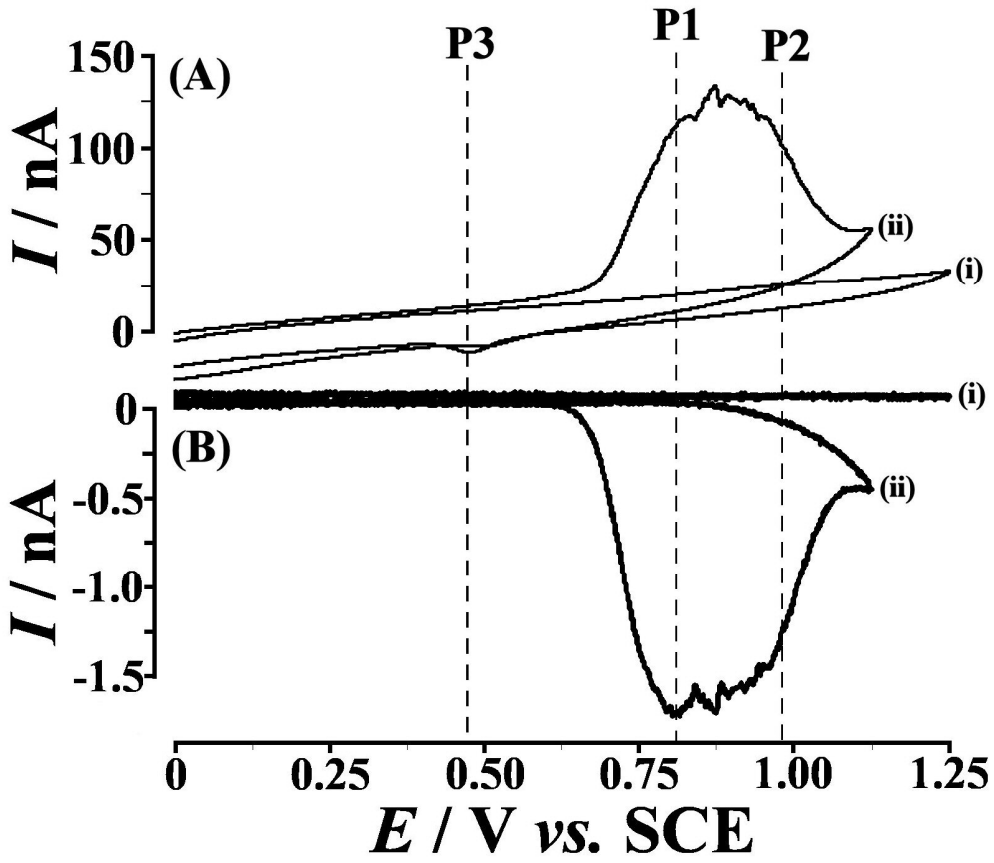

Figure 5.5 Cyclic voltammograms (scan rate 10 mVs^{-1}) for the oxidation of (i) 0 µM and (ii) 10 µM nitric oxide in aqueous 0.1 M phosphate buffer pH 7 obtained at (A) a gold generator electrode and (B) a gold collector electrode (potential 0.0 V vs. SCE). Carried out within an argon atmosphere.

The magnitude of the generator currents, P1 and P2, is considerable when compared to the corresponding response observed for 1,1'-ferrocenedimethanol and therefore a simple one-electron oxidation of NO can be ruled out. The generator current may be associated with (i) a catalytic water oxidation process [10], or (ii) a process involving gold dissolution. The magnitude of the collector current, however, is very similar to that observed for the one-electron oxidation of 1,1'-ferrocenedimethanol (see Figure 5.4).

Next, the effect of the scan rate on the generator and collector currents is investigated. Figure 5.6 shows voltammetric responses obtained over a range of scan rates from 0.01 to 2 Vs^{-1}. It can be seen that the generator current peak follows a trend consistent with a

diffusion controlled response (the peak current increases approximately linear with the square root of scan rate). Perhaps surprisingly, the peak current observed at the collector electrode also increases with scan rate. This suggests that actually a higher concentration of the reactive intermediate is formed with a higher potential scan rate. The predicted limiting collector current based on Equation 5.3 (assuming n = 1, D = 1.9 × 10^{-9} m^2s^{-1} [23], A = 16 × 10^{-10} m^2, and δ = 4.2 μm) is I_{lim} = 3.7 nA, which appears to agree with the low scan rate observation. The feedback current can be explained based on NO^+ (as nitrosonium phosphate) being produced at the generator electrode and causing diffusion controlled feedback to the collector electrode. The upper limit for the dissociation (hydrolysis) rate constant (see Equation 5.6) in 0.1 M phosphate buffer (pH 7) at 293 K is therefore approximately $k_{-5} < \frac{D}{\delta^2} \approx 100\ s^{-1}$.

Equation 5.6 $$NO^+ + H_2PO_4^- \rightleftharpoons (NO)H_2PO_4$$

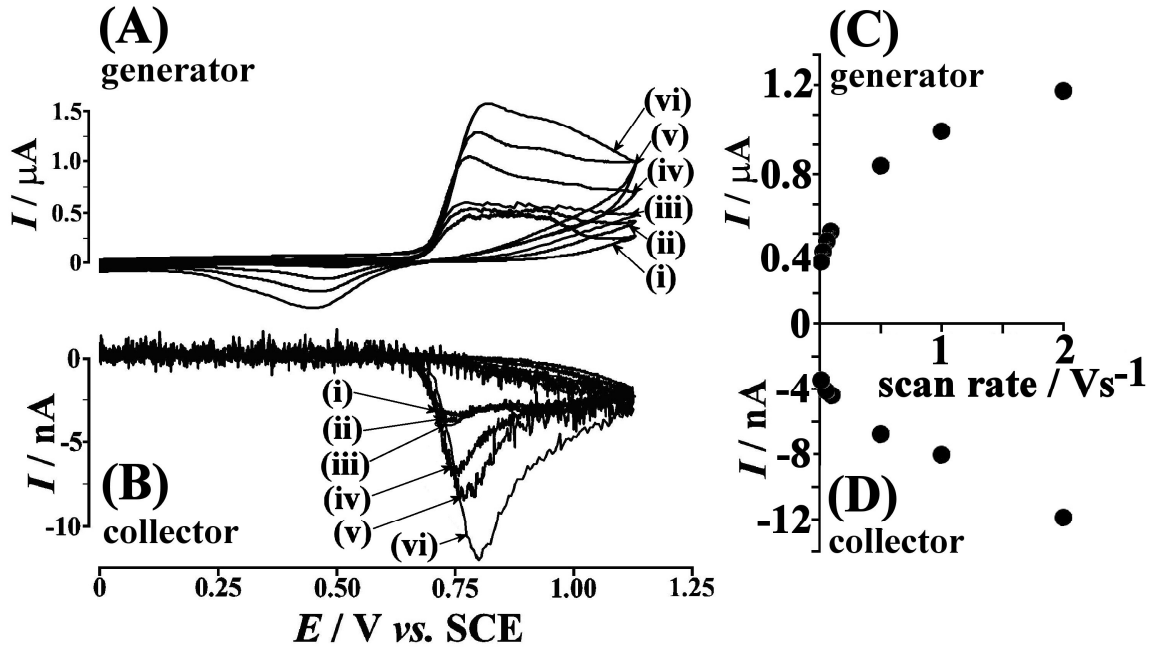

Figure 5.6 Cyclic voltammograms (scan rate (i) 0.01 Vs^{-1}, (ii) 0.05 Vs^{-1}, (iii) 0.1 Vs^{-1}, (iv) 0.5 Vs^{-1}, (v) 1 Vs^{-1}, and (vi) 2 Vs^{-1}) for the oxidation of 50 μM nitric oxide in aqueous 0.1 M phosphate buffer pH 7 and argon atmosphere (A) at a gold generator electrode and (B) at a gold collector electrode (potential 0.0 V vs. SCE). (C,D) Plots of the peak currents versus scan rate observed at generator and collector electrode.

It is interesting to note that P3 (the cathodic current response at 0.5 V vs. SCE Figure 5.6A) is also increasing with scan rate, and therefore, the proposed nitrosonium phosphate intermediate may be at least in part responsible also for P3.

Further experiments employing 1.0 M, 0.1 M, and 0.01 M phosphate buffer pH 7 revealed that the peak current for P3 further increases with phosphate concentration. This further supports the proposed nitrosonium phosphate intermediate. To ensure the signals relate to nitric oxide intermediates and not nitrites and nitrates, both species were tested in the same conditions up to 1 mM with no change to the background signals at either the generator or collector electrodes.

The increase in the collector current at higher scan rates is an indication of added complexity. The adsorption of NO onto gold surfaces is a known process [24] and, it is therefore, speculated that an additional transient current contribution is possible due to NO initially adsorbed onto the gold surface prior to the oxidation process.

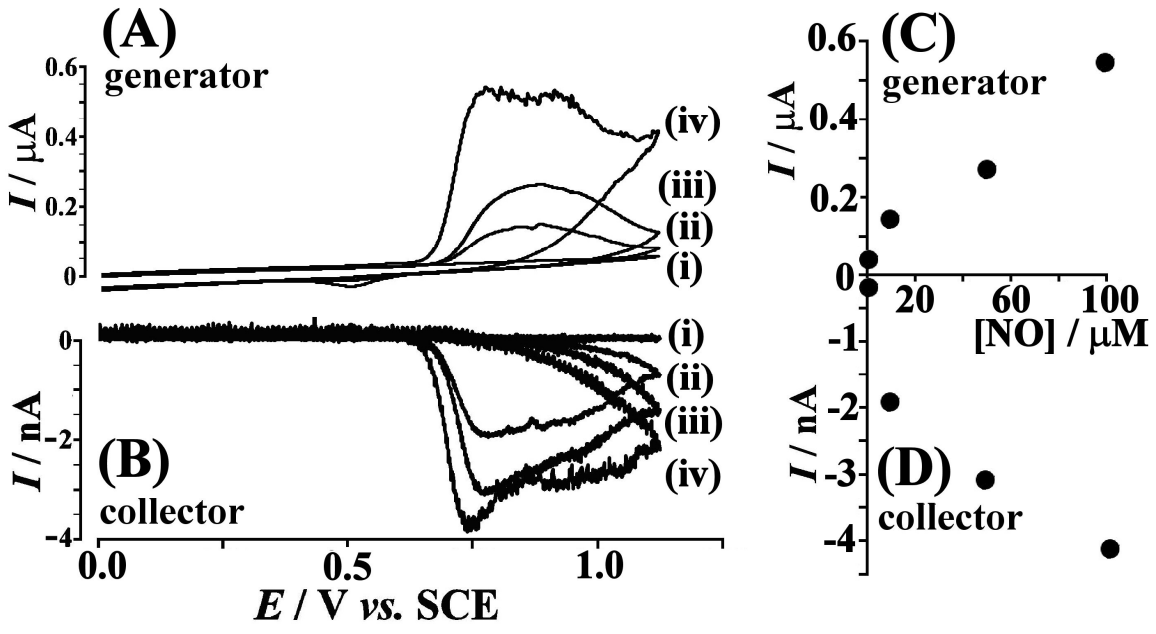

Figure 5.7 Cyclic voltammograms (scan rate 50 mVs^{-1}) for the oxidation of nitric oxide (concentration (i) 1 μM, (ii) 10 μM, (iii) 50 μM, and (iv) 100 μM) in aqueous 0.1 M phosphate buffer pH 7 within an argon atmosphere (A) at a gold generator electrode and (B) at a gold collector electrode (potential 0.0 V vs. SCE). (C,D) Plots of peak current versus nitric oxide concentration for the generator and collector electrode.

The effect of the NO concentration on the generator and collector current was investigated. Figure 5.7 shows voltammetric data as a function of concentration, and for both generator and collector electrode an approximately linear correlation is observed. At low concentrations of less than 10 μM NO, the voltammetric response diminishes non-linearly and analytically useful signals are not observed. In part, this could be due to very low concentrations of NO reacting with traces of oxygen (or alternatively, due to the heterogeneous gold surface based process).

The formation of a nitrosonium phosphate intermediate (see Equation 5.6) provides a chemically realistic mechanism to explain the voltammetric responses observed within a paired gold junction electrode. The approximate rate constant of dissociation for nitrosonium phosphate, $k_{-5} \approx 100\ s^{-1}$, when combined with a typical diffusion controlled association rate constant, $k_5 \approx 10^9\ M^{-1}s^{-1}$, allows the equilibrium constant for nitrosonium phosphate formation $K_5 \approx 10^7\ M^{-1}$ to be estimated. This rough estimate may contain a considerable error, as it is an order of magnitude estimate, and may be out by a factor of ten. However the value is in good agreement with equilibrium constant data for nitrosonium acetate or nitrite. [25] A more accurate determination of the nitrosonium association parameters as a function of pH and phosphate concentration is desirable.

5.4. Conclusions

Paired gold junctions were obtained reproducibly, and voltammetric responses for the reversible 1,1′ -ferrocenedimethanol redox system have been employed to characterise the junction geometry. For the oxidation of nitric oxide, collector currents are observed in agreement with nitrosonium NO^+ cations being produced at the gold anode and stabilised in the form of a phosphate.

This chapter has shown that the paired gold junction electrodes are useful analytical probes with extremely low background currents and high sensitivity even for short lived reaction intermediates.

5.5. References

[1] K. Aoki, *Electroanalysis*, 5, **1993**, 627-639.

[2] G. Nagy, L. Nagy, *Fresenius Journal of Analytical Chemistry*, 366, **2000**, 735-744.

[3] A. Butler, R. Nicholson, "Life, Death and Nitric Oxide," *The Royal Society of Chemistry*, **2003**.

[4] M.N. Hughes, *Methods in Enzymology*, 436, **2008**, 3-19.

[5] A.R. Butler, F.W. Flitney, D.L.H. Williams, *Trends in Pharmacological Sciences*, 16, **1995**, 18-22.

[6] D.R. Arnelle, J.S. Stamler, *Achieves of Biochemistry and Biophysics*, 318, **1995**, 279-285.

[7] A.C.A. de Vooys, G.L. Beltramo, B. van Riet, J.A.R. van Veen, M.T.M. Koper, *Electrochemica Acta*, 49, **2004**, 1307-1314.

[8] A.M. Yu, Z.J. Liang, J.H. Cho, F. Caruso, *Nano Letters*, 3, **2003**, 1203-1207.

[9] J.D. Zhang, M. Oyama, *Analytica Chimica Acta*, 540, **2005**, 299-306.

[10] E.V. Milsom, J. Novak, M. Oyama, F. Marken, *Electrochemistry Communications*, 9, **2007**, 436-442.

[11] M. Zhu, M. Liu, G.Y. Shi, F. Xu, X.Y. Ye, J.S. Chen, L.T. Jin, J.Y. Jin, *Analytica Chimica Acta*, 455, **2002**, 199-206.

[12] S.J. Stott, R.J. Mortimer, K.J. McKenzie, F. Marken, *Analyst*, 130, **2005**, 358-363.

[13] A.J. Bard, L.R. Faulkner, "Electrochemical Methods, 2nd ed.", *Wiley*, **2001**, p183.

[14] W.M. Zhang, I. Gaberman, M. Ciszkowska, *Analytical Chemistry*, 74, **2002**, 1343-1348.

[15] A.C. Fisher, "Electrode Dynamics", *Oxford University Press*, **1996**, p. 18.

[16] S. Goldstein, G. Czapski, *Inorganic Chemistry*, 35, **1996**, 7735-7740.

[17] G. Stedman, *Advances in Inorganic Chemistry and Radiochemistry*, 22, **1979**, 113-170.

[18] D.J. Benton, P. Moore, *Journal of the Chemical Society A*, **1970**, 3179-3182.

[19] R.S. Karlsson, E.B. Ljungstrom, *Environmental Science and Technology*, 30, **1996**, 2008-2013.

[20] S.I. Ajiboye, R.D. Peacock, N. Prouff, G.J. Taylor, J.M. Winfield, X.M. Liu, *Journals of Fluorine Chemistry*, 91, **1998**, 213-218.

[21] T. Gupta, R. Cohen, G. Evmenenko, P. Dutta, M.E. van der Boom, *Journal of Physical Chemistry C*, 111, **2007**, 4655-4660.

[22] N.S. Bayliss, R. Dingle, D.W. Watts, R.G. Wilkie, *Australian Journal of Chemistry*, 16, **1963**, 933-942.

[23] I.G. Zacharia, W.M. Deen, *Annals of Biomedical Engineering*, 33, **2005**, 214-222.

[24] T. Nishimura, K. Hattori, K. Kataoka, Y. Shimamoto, H. Daimon, *Surface Review and Letters*, 13, **2006**, 191-196.

[25] J.H. Ridd, *Advance in Physical Organic Chemistry*, 16, **1978**, 1-49.

6. Liquid | Liquid Ion Transport Junctions

Contents

Abstract

To demonstrate further uses of paired gold junction electrodes simultaneous electrochemically driven double anion transfer across a liquid | liquid interface is presented in this chapter. By immobilising a water insoluble liquid within a junction, anion uptake into the organic phase at the generator and expulsion at the collector is shown, with considerations for the volume of redox liquid and scan rate dependency discussed. Two distinct mechanistic pathways for ion transport are discussed in the context of micro-electrophoretic processes.

Publication

R.W. French, Y.H. Chan, P.C. Bulman-Page, F. Marken, *Electrophoresis*, 30, **2009**, 3361-3365.

Chapter 6: Liquid | Liquid Ion Transport Junctions.

Paired Triple Phase Boundary Processes

6.1. Introduction

Ion transfer at liquid | liquid interfaces is a well-known process studied with electrochemical methods for many decades [1] and with constantly emerging new applications. [2,3] The electrochemically driven transfer of ions into non-ion conducting organic media at the triple phase boundary organic liquid | aqueous electrolyte | electrode is a more recent experimental approach [4,5], based on micro-droplet deposits [6], macro-droplets [7], micro-fluidic two-phase systems [8], or punctured droplet electrodes. [9] A range of triple phase boundary systems based on water-immiscible redox liquids have been studied including redox liquids such as N,N,N',N'-tetrahexyl-phenylene-diamine [10], tetraaryl-phenylene-diamine derivatives [11], nitrobenzene and octanol based redox systems [12], as well as 4-(3-phenylpropyl)-pyridine solutions of porphyrin metal complexes. [13,14] A diverse range of triple phase boundary ion transfer processes have been reported including the transfer of drugs [15] and peptides [16], carboxylate [17] and α-hydroxy-carboxylate (facilitated by boronic acids) [18], as well as chromate [19] and phosphate. [20] The liquid | liquid transfer of biologically relevant ions [21] and ion transfer at bio-inspired membranes [22] are particularly important as a fundamental process for the development of novel ion separation and detection systems.

As demonstrated in previous chapters employing a second sensor probe (e.g. in generator-collector mode [23]) adds new information and provides enhanced sensor responses, bipotentiostatically controlled ion transfer experiments at liquid | liquid interfaces have rarely been reported. In this chapter the use of a 5 μm junction in a new and novel generator-collector experiment where a water immiscible liquid (redox liquid) is placed into the junction gap between the two gold electrodes will be given (see Figure 6.1A).

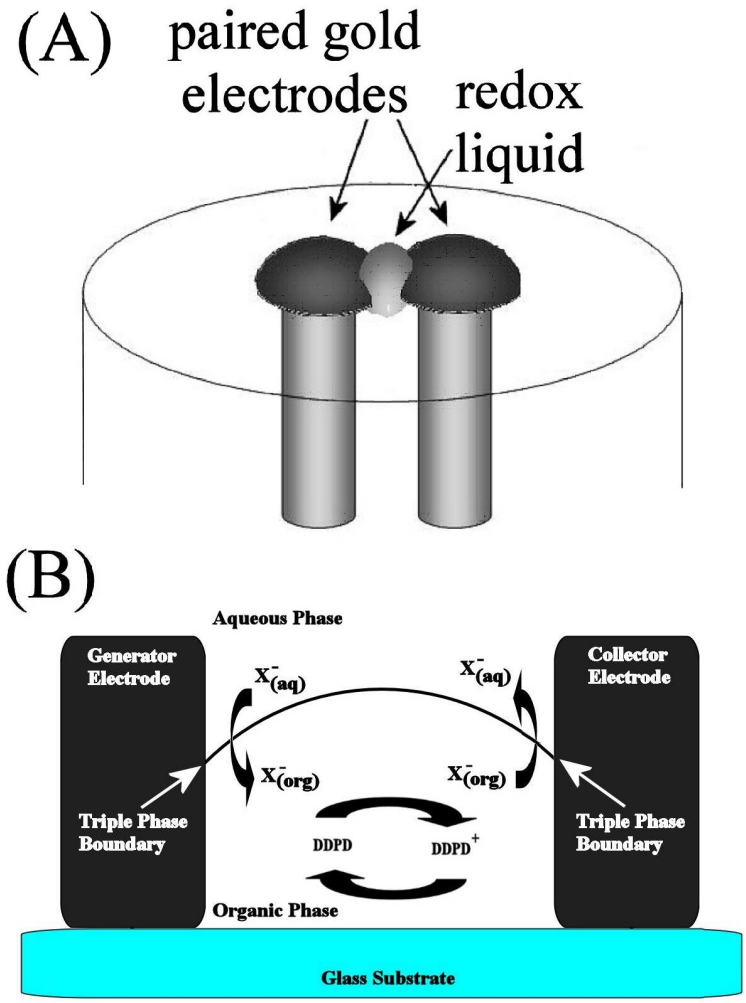

Figure 6.1 Schematic drawing of (A) paired gold junction electrode with small droplet of organic redox liquid immobilized within the gap and (B) the proposed pathway for ion transport (for the anion X^-) along the liquid | liquid interface during generator – collector ion transfer experiments.

The resulting triple phase boundary reaction zones are shown schematically in Figure 6.1B. An oxidation process at the generator electrode will cause the formation of positive charges in the organic phase and the simultaneous transfer of anions from the aqueous into the organic oil phase. Rapid transport of these ions across the liquid | liquid interface will then fuel the re-reduction accompanied by anion expulsion at the collector electrode. Overall, anions are "pumped" between generator and collector (similar to a micro-electrophoresis process) and the current enhancement caused by this feedback mechanism can be measured.

In this chapter the N, N-diethyl-N', N'-didodecyl-phenylene-diamine (DDPD) redox liquid is immobilized into a symmetric paired gold junction electrode and the currents associated with perchlorate anion transfer are measured. New evidence for two distinct transport mechanisms for anions in the organic redox liquid phase is presented.

6.2. Experimental

6.2.1. Reagents

Potassium hydroxide, potassium gold (I) dicyanide, potassium cyanide, potassium dihydrogen phosphate, dipotassium hydrogen phosphate, potassium carbonate, poly-(diallyldimethylammonium chloride) or PDDAC (average molecular weight < 100 kDalton), sodium perchlorate, and potassium chloride were obtained commercially (Sigma - Aldrich). N,N-diethyl-N',N'-didodecyl-phenylene-diamine (DDPD) was synthesized using a published method. [24] Demineralised and filtered water was taken from a Vivendi purification unit with not less than 18 MOhm cm resistivity. Pureshield argon (BOC) was employed to de-aerate solutions. Experiments were conducted at 20±2 ^{o}C.

6.2.2. Instrumentation

For electrochemical measurements an Autolab PSTAT30 biopotentiostat system (EcoChemie, Netherlands) was employed. In electrochemical experiments a conventional three-electrode cell with platinum wire counter and saturated calomel reference (SCE, Radiometer, Copenhagen) were implamented. Scanning electron microscopy (SEM) images were obtained using a JEOL JSM6480LV system. Samples were gold sputter-coated prior to SEM imaging.

6.2.3. Formation of Paired Gold Junction Electrodes

As described in Chapter 3, the paired gold junction electrode was formed via the simultaneous growth method, with the platinum disc electrodes set to potentials of -1.10 and -1.11 V vs. SCE for slow gold growth until automatic cut-off (provided in the GPES software in chronoamperometric mode) when the current exceeded 90 μA. After the

deposition was complete, the electrode was removed from the gold plating bath, rinsed with demineralised water, dried, and tested. Conductivity tests with the dry paired gold electrode junction revealed no direct short circuit or tunnel currents. Figure 6.2 shows typical SEM images of the paired gold electrode system with an average gap size estimated as ca. 5 μm.

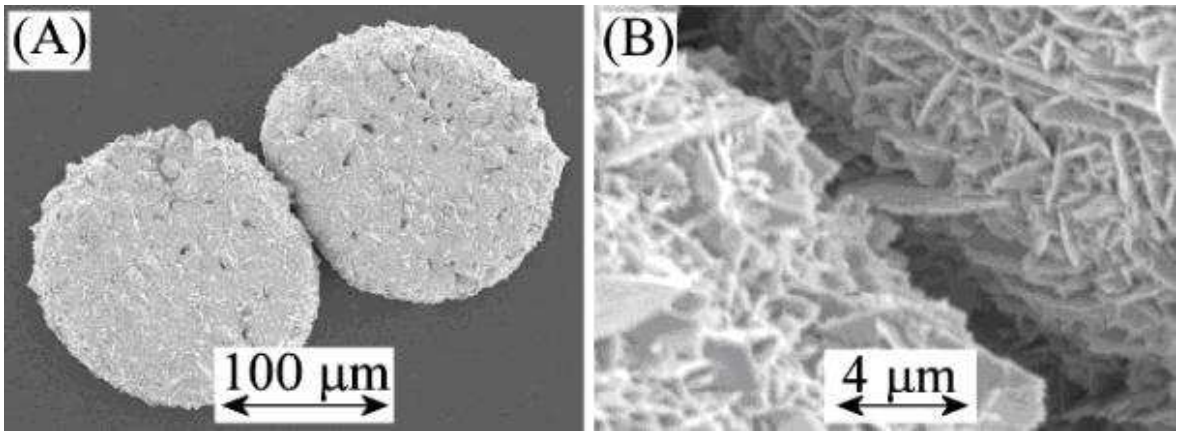

Figure 6.2 Scanning electron micrograph (SEM) images of paired gold junction electrodes. (A) Low magnification view of the two gold deposits. (B) Higher magnification image showing a junction with δ ≈ 5 μm.

6.2.4. Deposition of Redox Liquid into the Paired Gold Electrode Junction

A solution of N, N-diethyl-N', N'-didodecyl-phenylene-diamine (DDPD) in toluene (2 mg in 10 cm^3) is prepared and a volume of 5 μL deposited (equal to one deposition) onto the paired gold electrode. Evaporation of the toluene in an oven at 60 ^oC results in a DDPD deposit of 1 μg distributed over the electrode surface. Using this method, it was possible to deposit the DDPD into the gap to an acceptable reproducibility; however, it was difficult to control the amount of DDPD in direct contact with the paired gold electrode.

6.3. Results and Discussion

6.3.1. Voltammetric Characterisation of DDPD Microdroplets Immobilised in Paired Gold Junction Electrodes I.: Deposition and Perchlorate Anion Transfer

The paired gold electrode immersed into aqueous 0.2 M $NaClO_4$ did not show significant background responses when the potential was scanned between 0.0 and 0.5 V vs. SCE. However, with DDPD redox liquid immobilized at the electrode surface a strong oxidation response is observed at 0.15 V vs. SCE (see Figure 6.3A). This oxidation process is reversible and a corresponding reduction response is detected a 0.10 V vs. SCE. The midpoint potential $E_{mid} = \frac{E_p{}^{ox} + E_p{}^{red}}{2}$ is 0.139 V vs. SCE, which is in good agreement with previous reports for the perchlorate anion transfer across the liquid | liquid interface [25] (see Equation 6.1).

Equation 6.1 $$DDPD[oil] + ClO_4^- \rightleftharpoons DDPD^+[oil] + ClO_4^-[oil] + e^-$$

This perchlorate transfer process is observed irrespective of the process at the collector electrode and therefore feedback processes between generator and collector are relatively small. Holding the potential of the collector electrode at 0.0 V vs. SCE, results in a voltammetric response shown in Figure 6.3B. A two stage feedback process occurs with (i) an initial reduction response commencing with only minimal delay when compared to the generator oxidation response and (ii) a much slower steady increase in the reduction current which continues even after the re-reduction of DDPD at the generator has occurred. A literature report [26] proposes a two stage DDPD oxidation under similar conditions with (i) a fast surface transport of ions and (ii) a much slower bulk transport of ions.

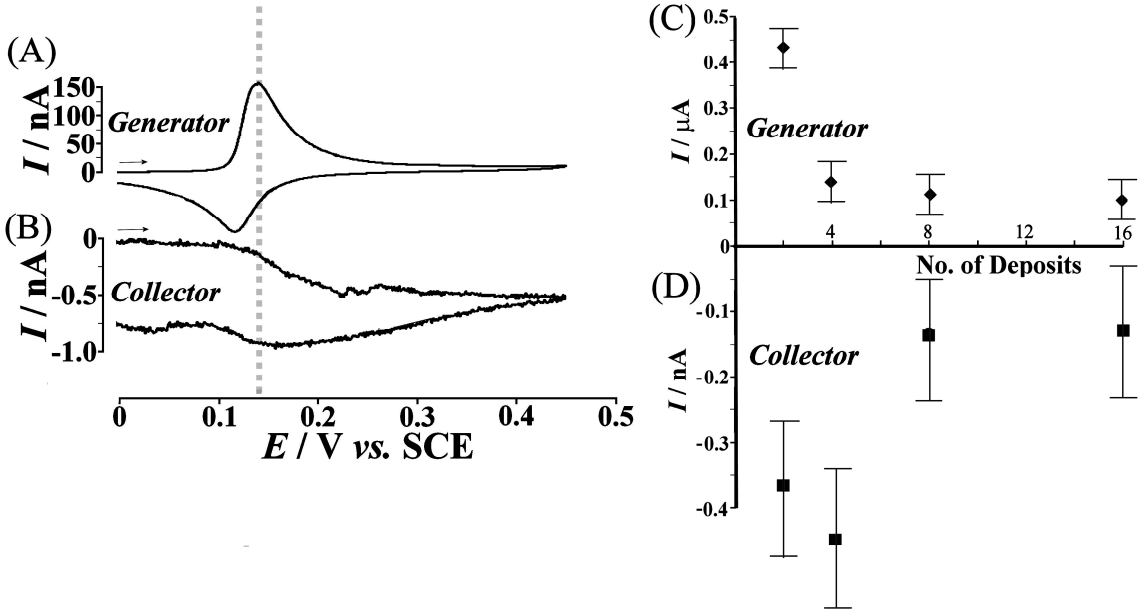

Figure 6.3 Cyclic voltammograms (scan rate 5 mVs^{-1}) for the oxidation and re-reduction of DDPD (4 deposits ≈ 4 μg DDPD deposited as toluene solution onto the electrode surface) when immersed in aqueous 0.2 M $NaClO_4$. (A) Generator current response, (B) collector current response. Plots of the peak currents versus number of deposits (each deposit ≈ 1 μg DDPD) for the generator electrode (C) and for the collector electrode (D) are shown.

The charge under the oxidation peak observed at the generator electrode (see Figure 6.3A) is approximately 2 μC which is much smaller than that expected for a 4 μg deposit of DDPD (ca. 770 μC), and therefore, only a very small fraction of DDPD in close contact with the gold electrode is reactive. In order to further explore the effect of the amount of DDPD deposit, consecutive deposition steps are employed with 2 μg DDPD added onto the electrode each time. The plots in Figure 6.3C and D show typical peak currents with estimated errors. The collector currents were variable (in some cases 2 μg deposit also failed to give collector currents) and the DDPD deposition clearly affects the current responses. Increasing the amount of DDPD deposit causes the generator current to decrease whereas, for the collector currents an optimum is observed at approximately 4 μg DDPD (2 deposits). This behaviour can be explained in terms of the triple phase boundary reaction zone [27] reactivity. In Figure 6.4 a schematic drawing is shown indicating the cases of (A) a low, (B) a medium, and (C) a high amount of redox liquid deposit. A low amount of deposit will create an extended triple phase boundary zone but may lead to poor reproducibility (depending on the surface tension of the deposit). For a medium amount of

deposit the triple phase boundary zone is effective and the diffusion path from generator to collector short. Finally, for a high amount of deposit the triple phase boundary is significantly reduced and the path from generator to collector electrode extended. Therefore, a medium amount of redox liquid placed into the gap should provide the most reliable voltammetric responses.

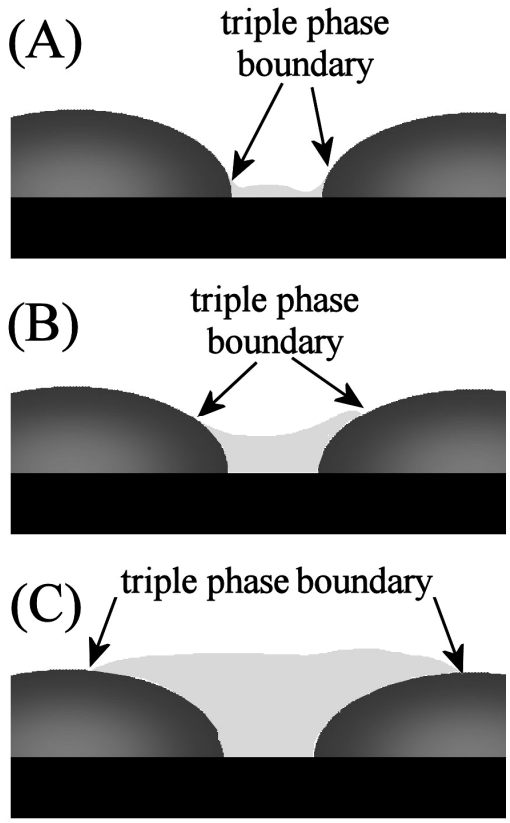

Figure 6.4 Schematic drawing of (A) small, (B) medium, (C) high, amount of redox liquid deposited into the gap of a paired gold junction electrode.

6.3.2. Voltammetric Characterisation of DDPD Microdroplets Immobilised in Paired Gold Electrode Junctions II.: Scan Rate Effects and Mechanism

The tetra-alkyl-phenylene-diamine redox liquid system is known to be relatively complex with surface tension driven convection effects [28] and phase separation processes [10] contributing to ion transport. It is therefore interesting to explore this system further by investigating the effect of the scan rate on the appearance of cyclic voltammograms. Figure 6.5A and Figure 6.5B show typical voltammograms for the oxidation and re-reduction of a 4 µg DDPD deposit. For scan rates faster than ca. 20 mVs^{-1} the generator response is

observed as a well-defined reversible process but the collector response remains insignificant (see (ii) in Figure 6.5B). For the generator electrode, the non-linear increase in the peak current for the generator (see Figure 6.5C) confirms incomplete conversion of the DDPD redox liquid (vide supra). However, for the collector current a clear trend to increased current responses at slower scan rate is observed (see Figure 6.5D).

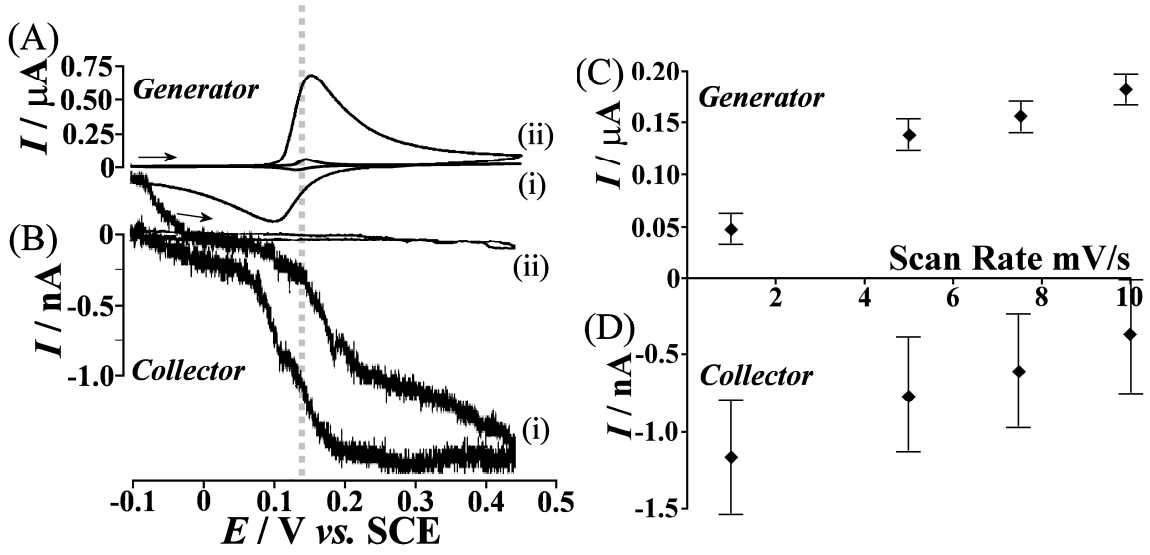

Figure 6.5 Cyclic voltammograms (scan rate (i) 1 mVs^{-1} and (ii) 50 mVs^{-1}) for the oxidation and re-reduction of DDPD (2 deposits ≈ 4 µg DDPD deposited as toluene solution onto the electrode surface) when immersed in aqueous 0.2 M $NaClO_4$. (A) Generator current response, (B) collector current response. Plots of the peak currents versus scan rate for the generator electrode (C) and for the collector electrode (D) are shown.

The appearance of the collector current response can be explained based on the recently proposed mechanisms of surface ion transport versus bulk ion transport. [26] Upon oxidation of the DDPD oil at the generator electrode, initially, the transport of $DDPD^+[oil]ClO_4^-[oil]$ at the liquid | liquid interface occurs rapidly (see Figure 6.6A). The corresponding collector response is observed up to ca. 20 mVs^{-1} suggesting approximately 10 seconds transit time over a 5 µm gap size. The second, much more slowly occurring process merges with the first collector response at approximately 1 mVs^{-1} scan rate (see Figure 6.5B) and therefore this process appears ca. 20 times slower over a 5 µm gap size (see Figure 6.6B).

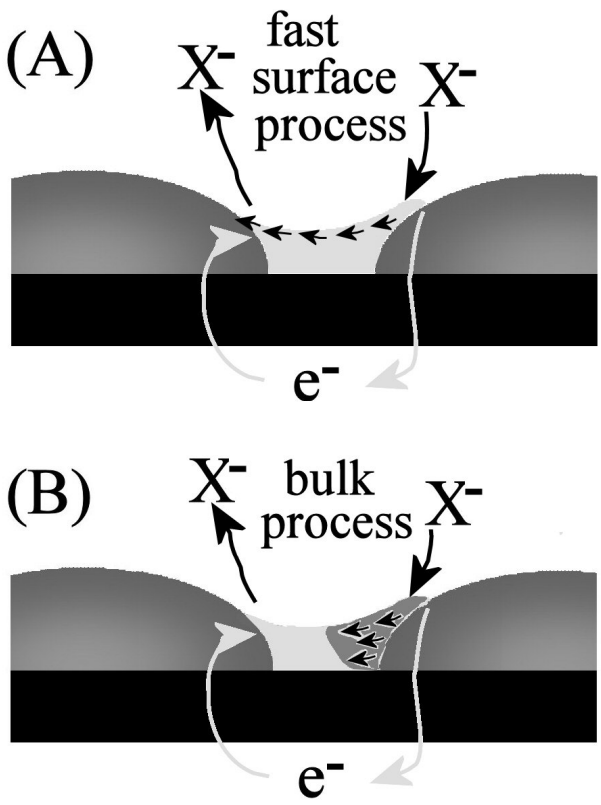

Figure 6.6 Schematic drawing of electrochemically driven ion transport processes (A) at the liquid | liquid interface and (B) in the bulk organic phase.

Data presented in this chapter are preliminary in nature and important experimental parameters, such as, effects introduced by the gap size remain to be studied. However, the possibility of "double ion transfer" at liquid | liquid interfaces based on generator – collector electrode systems has been demonstrated and this methodology could provide a versatile tool for a wider range of ion transfer/transport systems. Sensors for many biological ions could be envisaged exploiting both the potential-dependent selectivity for the transferred ion and the time dependence (time-of-flight) for the transfer across the liquid | liquid interface. Selective binder molecules in the organic phase could be introduced to slow down ion transport or to react and result in a new ion-specific redox response at a different potential.

6.4. Conclusions

The use of paired gold junction electrodes for the study of anion transfer processes at the interface of two immiscible liquids has been demonstrated. By placing an appropriate amount of DDPD redox liquid into the gap between the symmetric gold electrode pair generator – collector experiments were carried out. Simultaneous anion transfer into the organic phase during oxidation (at the generator) and expulsion back into the aqueous phase during reduction (at the collector) occurred for perchlorate anions and, by varying the scan rate new evidence for two transport pathways for anions has been obtained.

In future, the new methodology could be improved by (i) reducing the gap size between generator and collector electrode, (ii) by selecting organic liquid redox systems dominated either by surface or by bulk transport processes, and (iii) by introducing facilitators (such as boronic acids) for specific biologically relevant anions or poly-anions to be transferred.

6.5. References

[1] F. Reymond, H.H. Girault, R.A. Meyers (ed.), "Encyclopaedia of Analytical Chemistry", *Wiley*, **2000**.

[2] J. Strutwolf, M.D. Scanlon, D.W.M. Arrigan, *Analyst,* 134, **2009**, 148-158.

[3] S. Senthilkumar, A. Adisa, R. Saraswathi, R.A.W. Dryfe, *Electrochemistry Communications*, 10, **2008**, 141-145.

[4] C.E. Banks, T.J. Davies, R.G. Evans, G. Hignett, A.J. Wain, N.S. Lawrence, J.D. Wadhawan, F. Marken, R.G. Compton, *Physical Chemistry Chemical Physics*, 5, **2003**, 4053-4069.

[5] F. Scholz, U. Schröder, R. Gulaboski, "Electrochemistry of Immobilized Particles and Droplets", *Springer*, **2005**.

[6] U. Schröder, R.G. Compton, F. Marken, S.D. Bull, S.G. Davies, S. Gilmour, *Journal of Physical Chemistry B,* 105, **2001**, 1344-1350.

[7] J.Y. Chen, M. Sato, *Journal of Electroanalytical Chemistry*, 572, **2004**, 153-159.

[8] S.M. MacDonald, J.D. Watkins, S.D. Bull, I.R. Davies, Y. Gu, K. Yunus, A.C. Fisher, P.C.B. Page, Y. Chan, C. Elliott, F. Marken, *Journal of Physical Organic Chemistry*, 22, **2009**, 52-58.

[9] E. Bak, M. Donten, Z. Stojek, F. Scholz, *Electrochemical Communications,* 9, **2007**, 386-392.

[10] F. Marken, R.D. Webster, S.D. Bull, S.G. Davies, *Journal of Electroanalytical Chemistry,* 437, **1997**, 209-218.

[11] J.D. Wadhawan, A.J. Wain, A.N. Kirkham, D.J. Walton, B. Wood, R.R. France, S.D. Bull, R.G. Compton, *Journal of American Chemical Society,* 125, **2003**, 11418-11429.

[12] F. Scholz, R. Gulaboski, *ChemPhsChem,* 6, **2005**, 16-28.

[13] F. Marken, K.J. McKenzie, G. Shul, M. Opallo, *Faraday Discussion*, 129, **2005**, 219-229.

[14] M.A. Ghanem, F. Marken, *Electrochemical Communications*, 7, **2005**, 1333-1339.

[15] G. Bouchard, A. Galland, P.A. Carrupt, R. Gulaboski, V. Mirceski, F. Scholz, H.H. Girault, *Physical Chemistry Chemical Physics*, 5, **2003**, 3748-3751.

[16] M.Y. Vagin, S.A. Trashin, G.P. Karpachova, N.L. Klyachko, A.A. Karyakin, *Journal of Electroanalytical Chemistry*, 623, **2008**, 68-74.

[17] S.M. MacDonald, M. Opallo, A. Klamt, F. Eckert, F. Marken, *Physical Chemistry Chemical Physics*, 10, **2008**, 3925-3933.

[18] N. Katif, R.A. Harries, A.M. Kelly, J.S. Fossey, T.D. James, F. Marken, *Journal of Solid State Electrochemistry,* 13, **2009**, 1475-1482.

[19] F. Marken, C.M. Hayman, P.C.B. Page, *Electroanalysis*, 14, **2002**, 172-176.

[20] F. Marken, C.M. Hayman, P.C.B. Page, *Electrochemical Communication*, 4, **2002**, 462-467.

[21] S. Pedersen-Bjergaard, K.E. Rasmussen, *TRAC-Trends in Analytical Chemistry*, 27, **2008**, 934-941.

[22] O.D. Uitto, H.S. White, K. Aoki, *Analytical Chemistry*, 74, **2002**, 4577-4582.

[23] W.J. Albery, M.L. Hitchman, "Ring-disc Electrodes", *Oxford University Press: Oxford*, **1971**.

[24] S.J. Stott, K.J. McKenzie, R.J. Mortimer, C.M. Hayman, B.R. Buckley, P.C.B. Page, F. Marken, G. Shul, M. Opallo, *Analytical Chemistry*, 76, **2004**, 5364-5369.

[25] G. Shul, K.J. McKenzie, J. Niedziolka, E. Rozniecka, B. Palys, F. Marken, C.M. Hayman, B.R. Buckley, P.C.B. Page, M. Opallo, *Journal of Electroanalytical Chemistry*, 582, **2005**, 202-208.

[26] D. Rayner, N. Fietkau, I. Streeter, F. Marken, B.R. Buckley, P.C.B. Page, J. Del Campo, R. Mas, F.X. Munoz, R.G. Compton, *Journal of Physical Chemistry C,* 111, **2007**, 9992-10002.

[27] F. Marken, R.G. Compton, C.H. Goeting, J.S. Foord, S.D. Bull, S.G. Davies, *Journal of Solid State Electrochemistry*, 5, **2001**, 88-93.

[28] J.C. Ball, F. Marken, F.L. Qiu, J.D. Wadhawan, A.N. Blythe, U. Schröder, R.G. Compton, S.D. Bull, S.G. Davies, *Electroanalysis*, 12, **2000**, 1017-1025.

7. Conclusion and Summary

Contents

Abstract

In this chapter a summary of the results found within this thesis will be presented with additional information into further experiments being investigated using the new junction formation methods explained within.

Chapter 7: Conclusions and Summary

The focus of this thesis has been upon nanojunction formation and characterisation, specifically towards robust paired gold junction electrodes working in generator-collector mode for electroanalytical sensing.

A new methodology has been developed and the resulting electrodes produced have been characterised and tested as analytical sensors.

A new simultaneous deposition methodology for producing paired gold junction electrodes was developed, allowing the growth of novel nanojunctions to be formed in a simple one-stage technique with minimal specialised equipment or procedures. Additionally the use of different overpotentials to form junctions of varying gap size, ranging from micrometer to nanometer, has been presented and the enhancements to the sensing system discussed.

Generator-collector mode sensing with the junctions produced show excellent sensing characteristics within the collector signal, including, minimal capacitance and noise levels, allowing for sensitive measurements (nanomolar) to easily be obtained, as well as, the ability to sense short lived intermediates. The junctions have shown their diversity as sensors in both the homogeneous phase, and multi-phase systems.

Work with paired gold junction electrodes is continuing beyond the research carried out within this thesis. This includes studies into further junction improvements by altering shape, size and spacing of initial platinum duel electrodes. For example the used of long rectangular band electrodes, rather than discs, reduces the percentage of variation between electrode lengths. Whilst reducing the gap between original platinum electrode spacing this cuts deposition times and reduces overall variation in junction height. The additional control in junction dimensions, combined with, larger electrode areas allows for more comparison between electrodes as well as improved sensitivity.

Work into alternative metals being deposited may also be considered, as smoother deposited metals may result in smaller average gap sizes.

The junctions produced will be employed in further studies into microwave effects upon solutions within the junction cavity [1] and, novel sensing methods, where one electrode creates a intermediates or pH gradients, with the second electrode acting as an analytical sensor. Future work will also include time dependent and generator-collector impedance methods based on junction electrodes.

Investigations with the paired triple phase boundary processes has also been continued with varying organic oils and transferred ions.

The potentially ultimate advance for the junction growth method would be for junctions to be produced with nanometer spacing allowing for molecular junction experimentation to be employed.

7.2. References

[1] L. Rassaei, R.W. French, R.G. Compton, F. Marken, *Analyst*, 5, **2009**, 887-892.